The functional role of the cell adhesion molecule L1 in mitochondrial metabolism and dynamics and the functional consequences of L1´s interaction with nuclear receptors in the murine central nervous system

DISSERTATION

Dissertation with the aim of achieving a doctoral degree at the Faculty of Mathematics, Informatics and Natural Sciences Department of Biology of Universität Hamburg

Submitted by
KRISTINA KRAUS

Hamburg, 2017

The thesis was performed in the Institute for Biosynthesis of Neuronal Structures of the Centre for Molecular Neurobiology Hamburg (ZMNH).

The following evaluators recommended the admission of the dissertation:

Prof. Dr. Dr. h. c. Melitta Schachner

Prof. Dr. Christian Lohr

Day of oral defense: November 10th, 2017

TABLE OF CONTENT

1 INTRODUCTION

1.1 The cell adhesion molecule L1

Cell adhesion molecules (CAM) are surface glycoproteins grouped into several classes: cadherins, the immunoglobulin(Ig)-like superfamily, selectins, mucins and integrins (Fields and Itoh, 1996). CAMs play key roles in many aspects of neural development, such as axon-guidance, synapse formation, regulation of synaptic structure and astrocyte-synapse contacts (Togashi et al., 2009). They are essential for proper brain development and highly coordinated brain functions, such as memory and learning (Sanes and Yamagata, 1999, Yamagata et al., 2003, Washbourne et al., 2004). Neurons migrate in early development of the nervous systems and elongate their axons toward target areas. Initial contacts of axons and neurites, and signaling through homophilic and heterophilic interactions are mediated by CAMs (Togashi et al., 2009). L1 belongs to Ig-like superfamily and is a member of the L1 subfamily which includes also the close homolog of L1 (CHL1), neuron-glia CAM-related cell adhesion molecule and neurofascin (Herron et al., 2009, Wei and Ryu, 2012). L1 mediates cell-cell adhesion to activate various signaling pathways by homophilic interaction or heterophilic binding to other neural cell adhesion molecules and to extracellular matrix proteins (Maness and Schachner, 2007, Colombo and Meldolesi, 2015). L1 is a 200-220 kDa membrane glycoprotein and consists of an extracellular part with six Ig-like domains and five fibronectin type III homologous repeats, followed by a transmembrane region and a cytoplasmic tail (Figure 1.1) (Moos et al., 1988).

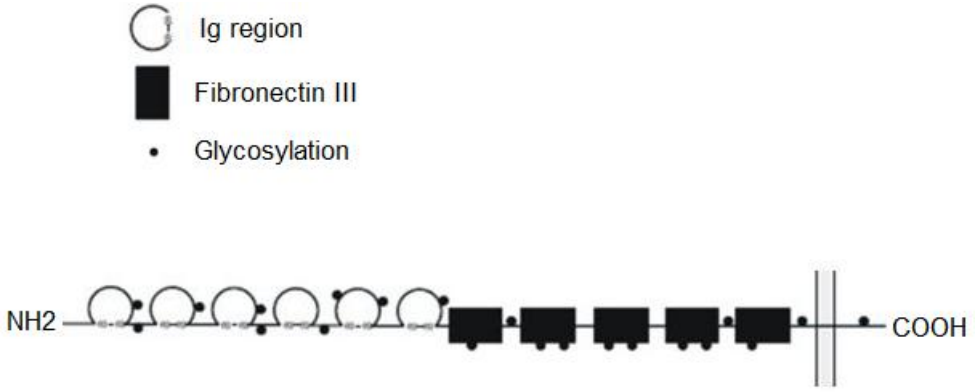

Figure 1.1: Protein domain structure of the cell adhesion molecule L1. L1 is a 200-220 kDa glycoprotein with six Ig-like domains at the amino terminal end followed by five fibronectin type III homologous repeats, a single transmembrane region and an intracellular tail at the C-terminal end (figure was modified from Fields and Itoh, 1996).

L1 is preferantially expressed in the developing peripheral nervous system by neurons as well as by non-myelinating Schwann cells and in the central nervous system it is present on non-myelinated axons and growth cones of differentiating neurons (Hortsch, 1996, Dahme et al., 1997, Kamiguchi and Lemmon, 1998, Kenwrick et al., 2000, Wang et al., 2012). Furthermore, L1 is expressed by leukocytes and epithelial cells of the intestine and urogenital tract (Probstmeier et al., 1990, Kowitz et al., 1992, Kujat et al., 1995). L1 has various functions in the nervous system: it plays important roles in neuronal cell migration and survival, neurite outgrowth, axonal fasciculation (Lindner et al., 1983, Kruse et al., 1984, Fischer et al., 1986, Martini and Schachner, 1986, Moos et al., 1988, Seilheimer et al., 1989, Appel et al., 1993), myelination and synaptic plasticity (Wood et al., 1990, Lüthl et al., 1994). Mutations in the L1 gene on the X chromosome have been related to L1 syndrome comprising a spectrum of X-linked disorders, such as hydrocephalus with stenosis of the Sylvius aqueduct, mental retardation, aphasia, spastic paraplegia, adducted thumbs, complicated hereditary spastic paraplegia, and agenesis of the corpus callosum (Basel-Vanagaite et al., 2006). Moreover, L1 deficiency was observed in some cases of Hirschprung's disease and schizophrenia (Kurumaji et al., 2001) and overexpression of L1 is often associated with tumor progression and metastasis (Raveh et al., 2009).

Full-length L1 can be proteolytically processed within the third fibronectin type III domain by trypsin (Sadoul et al., 1988), proprotein convertase 5a (Kalus et al., 2003) or plasmin (Nayeem et al., 1999, Silletti et al., 2000, Mechtersheimer et al., 2001) resulting in a 140 kDa extracellular fragment and a 80 kDa transmembrane fragment. Members of the disintegrin and metalloprotease family (Mechtersheimer et al., 2001, Maretzky et al., 2005, Riedle et al., 2009) or neuropsin (Matsumoto-Miyai et al., 2003) cleave full-length L1 or the 80 kDa transmembrane fragment generating a soluble 180 or 50 kDa fragment and a 32 kDa transmembrane fragment. The 32 kDa fragment is cleaved by ɣ-secretase and the resulting 28 kDa intracellular fragment is transported to the nucleus (Riedle et al., 2009). Recently, cleavage of full-length L1 in its extracellular domain at arginine 687 (Arg^{687}) in the first fibronectin type III domain by the serine protease myelin basic protein (MBP) was described (Lutz et al., 2014a). Stimulation with an antibody that triggers L1-specific signaling leads to the following mechanism: attachment of one sumo molecule to full-length L1, generation of a

fusion protein between MBP containing the exon II-encoded domain and the C-terminal part of dynamin, sumoylation of the MBP-dynamin fusion protein and release of this sumoylated fusion protein into the extracellular space. Sumoylated full-length L1 is cleaved by the extracellular MBP-dynamin fusion protein at Arg^{687} yielding a 70 kDa transmembrane fragment (L1-70) comprising the intracellular, the transmembrane domain and part of the extracellular moiety. L1-70 is transported into the nucleus and might function in nuclear signaling and transcription (Lutz et al., 2014a). L1-70 can be proteolytically processed by cathepsin E leading to the generation of a sumoylated 30 kDa fragment (Lutz et al., 2014b).

1.2 Mitochondria

1.2.1 Mitochondrial structure and import machinery

Mitochondria are the powerhouses of the cell being the main source of adenosine triphosphate (ATP). Mitochondria contain their own genome, the double-stranded, circular mitochondrial deoxyribonucleic acid (DNA) coding for a few ribosomal ribonucleic acids, transfer ribonucleic acids and mitochondrial proteins. The mitochondrial DNA is transmitted only through the female germ line (Hutchison et al., 1974, Hayashi et al., 1978, Kroon et al., 1978, Giles et al., 1980, Taanman, 1999). Mitochondria have a double membrane, the outer membrane which represents the outer shell of the mitochondria and forms a semi-permeable barrier to the cytosol and the inner membrane that forms invaginations, the so-called cristae. The inner membrane separates the intermembrane space from the lumen which is called matrix. The proton gradient between the intermembrane space (pH 7.2-7.4) and the matrix (pH 7.9-8.0) drives the ATP production by the ATP synthase in the membranes of the cristae (Taanman, 1999, Friedman and Nunnari, 2014).

The mitochondrial genome encodes only a handful of mitochondrial proteins. Mitochondrial proteins are encoded to 99% by nuclear DNA, synthesized on cytosolic ribosomes and imported into mitochondria (Schmidt et al., 2010, Dudek et al., 2013, Ferramosca and Zara, 2013). To transport proteins in mitochondria, different pathways are utilized: the presequence pathway, the carrier pathway, the β-barrel pathway, mitochondrial intermembrane space assembly (MIA) pathway and mitochondrial import protein 1 (Mim1) pathway (Figure 1.2). The first steps of transport of nuclear-encoded mitochondrial precursor proteins into mitochondria are

mediated by the translocase of the outer mitochondrial membrane (TOM) complex, which recognizes import signals within these precursor proteins at the surface of the outer membrane and then selectively distributes them to specific transport routes to mitochondrial subcompartments (Figure 1.2) (Dudek et al., 2013). The TOM complex comprises the proteins TOM20, TOM70, TOM71 which is a homolog of TOM70, TOM40, TOM22, TOM5, TOM6 and TOM7. TOM20/TOM22 are the initial receptors for preproteins with a presequence, while TOM70 is the initial receptor for hydrophobic precursor proteins without presequence or for transmembrane transport proteins with internal targeting signals, so-called carriers. TOM40 represents the channel-forming protein and TOM5 mediates the transfer of preproteins from receptors to the channel and is important for the assembly of the TOM complex. TOM6 contributes to the assembly of the TOM complex, while TOM7 regulates the disassembly and dynamics of the TOM complex (Chacinska et al., 2009).

If precursor proteins have an N-terminal import signal consisting of an amphipathic α-helical segment with a net positive charge and a length of 15 to 55 amino acids, they are imported into mitochondria through the presequence pathway. These proteins with a presequence at the N-terminal end bind to TOM20/TOM22 and TOM40 and are transfered to the protein-conducting pore of the inner mitochondrial membrane (TIM) complex 23 with the help of the translocases TIM50 and TIM21. TIM50 is an intermembrane space receptor responsible for gating of the TIM23 channel, while TIM21 is the modulator of TIM23 and is required for interaction with the TOM complex and the electron transport chain. TIM17 is associated with TIM23 and is involved in lateral sorting of preproteins into the inner membrane (Chacinska et al., 2009). The TIM23 complex is coupled to the electron transport chain and is activated by the mitochondrial membrane potential. Through the presequence pathway precursor proteins can be translocated into the mitochondrial matrix or inserted into the lipid bilayer of the inner mitochondrial membrane. The presequence import pathway into the matrix is completed by the presequence translocase-associated motor (PAM). N-terminal signals of precursors are proteolytically removed by the matrix protein peptidase after import into mitochondria (Becker et al., 2012, Dudek et al., 2013).

If precursor proteins contain an internal targeting signal, they are imported into mitochondria through the carrier pathway. These precursor proteins are recognized by TOM70 and translocated via TOM40 to the TIM22 complex consisting of TIM22, TIM54, TIM18, TIM9, TIM10 and TIM12 (Chacinska et al., 2009). TIM22 is the core of these complexes and forms a channel-forming twin-pore that mediates the membrane potential-dependent membrane insertion of precursor proteins into the inner mitochondrial membrane (Becker et al., 2012). TIM54 is a membrane protein with a domain in the intermembrane space and binds the TIM9-TIM10-TIM12 subunits, while TIM18 is involved in the assembly of the TIM22 complex. TIM9, TIM10 and TIM12 are membrane-bound chaperones which tether precursor proteins to TIM22 (Chacinska et al., 2009).

If precursor proteins have a targeting signal within the last β-strand containing large polar amino acid, such as lysine or glutamine, a glycine and two hydrophobic amino acids, they are imported into mitochondria through the β-barrel pathway (Kutik et al., 2008). It was shown that β-barrel proteins are recognized by TOM20 and are translocated across the TOM complex through the intermembrane space to the sorting and assembly machinery (SAM) of the outer membrane for folding and insertion into the lipid bilayer (Rapaport and Neupert, 1999, Schleiff et al., 1999, Paschen et al., 2003, Wiedemann et al., 2003, Gentle et al., 2004, Kutik et al., 2008, Becker et al., 2012). The SAM complex comprises the proteins SAM50, SAM37 SAM35, mitochondrial morphology protein 10 and Mim1. SAM50 is the central component of the SAM complex, while SAM37 promotes the release of precursor proteins. SAM35 is required for binding of precursor proteins with a β-signal and mitochondrial morphology protein 10 is involved in β-barrel assembly and associates with SAM. Mim1 is required for biogenesis of α-helical proteins and interaction with SAM (Chacinska et al., 2009).

If intermembrane space proteins contain multiple cysteine residues which are implicated in the formation of disulfide bridges, they use the MIA pathway for import into mitochondria. The MIA pathway contains the receptors MIA40, endogenous retroviral element 1 and the zinc-binding protein HOT13. Incoming cysteine-rich precursor proteins are transferred through the TOM complex, but it is so far not clear whether TOM20/TOM22 or TOM70 are responsible for the translocation through the

TOM complex. MIA-dependent precursor proteins may use an alternative pathway to cross the outer mitochondrial membrane which involves TOM40, but not other core components of the TOM complex (Gornicka et al., 2014). Cysteine-rich precursor proteins form transient intermolecular disulfide bonds with the receptor MIA40. MIA40 catalyzes the oxidative folding which leads to substrate release into the intermembrane space and reduction of MIA40 (Chacinska et al., 2004, Grumbt et al., 2007, Milenkovic et al., 2007, Müller et al., 2008). The endogenous retroviral element 1 mediates re-oxidation of MIA40, which is supported by HOT13. Electrons flow from MIA40 via endogenous retroviral element 1 to cytochrome *c* and the cytochrome *c* oxidase of the electron transport chain (Mesecke et al., 2005, Bihlmaier et al., 2007, Dabir et al., 2007, Stojanovski et al., 2008, Banci et al., 2011, Becker et al., 2012).

If precursor proteins have multiple α-helical transmembrane segments, they are imported through the Mim1 pathway. TOM70 recognizes these sequences and with help of Mim1 these proteins are inserted into the membrane lipid layer (Schmidt et al., 2011, Becker et al., 2012).

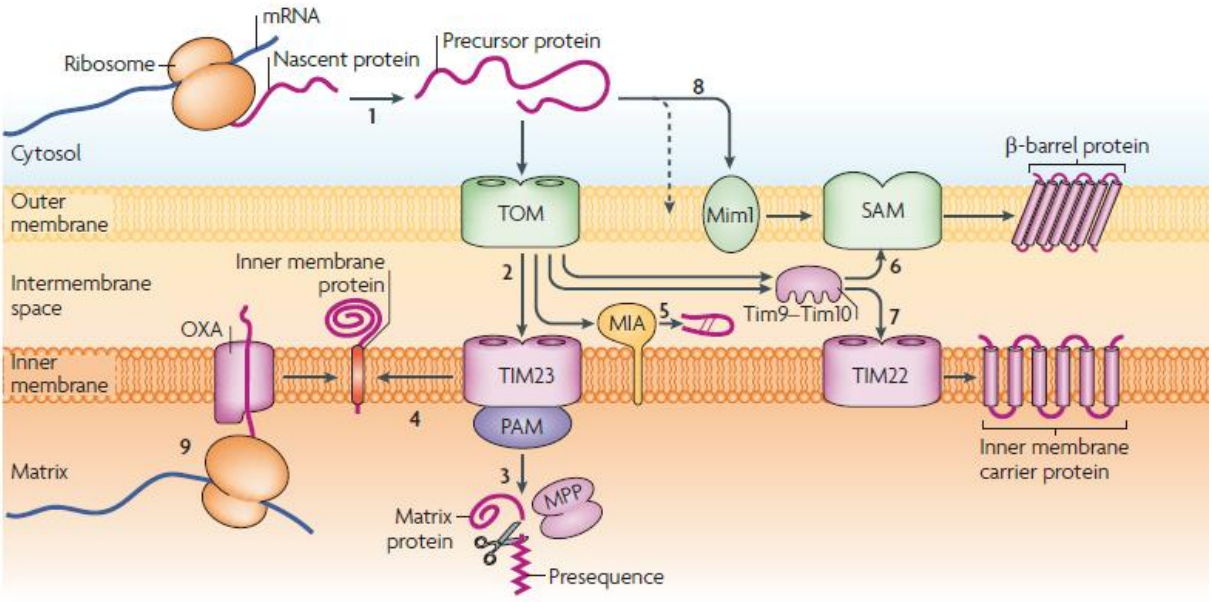

Figure 1.2: Import pathways of mitochondrial proteins. Most mitochondrial proteins are nuclear-encoded and their messenger ribonucleic acid (mRNA) is translated on cytosolic ribosomes to precursor proteins (1). Precursor proteins can have either an amino-terminal targeting signal or an internal targeting signal for import and sorting into mitochondrial compartments. Precursor proteins are translocated through the TOM complex (2) and dependent on their targeting signal they can take different pathways to their final destination. Precursor proteins with an amino-terminal targeting signal

are imported through the TOM complex to the TIM23 complex and PAM into the mitochondrial matrix. The amino-terminal targeting signal is proteolytically cleaved by the mitochondrial processing peptidase (MPP) (3). Precursor proteins with an amino-terminal targeting signal can also be released from the TIM23 complex and inserted into the lipid bilayer of the inner membrane (4). Precursor proteins with multiple cysteine residues are imported through the MIA pathway into the intermembrane space (5). β-barrel precursor proteins are imported through the β-barrel pathway with help of small chaperone proteins (TIM9, TIM10) and inserted into the lipid bilayer of the outer mitochondrial membrane after folding and sorting at the SAM machinery (6). Precursor proteins without an N-terminal presequence can further be imported into mitochondria through the carrier pathway to the TIM22 complex (7). Precursor proteins with multiple α-helical transmembrane segments use the Mim1 pathway to be inserted into the outer mitochondrial membrane (8). Proteins that are inserted into the inner mitochondrial membrane can be further synthesized on mitochondrial matrix ribosomes and are translocated into the inner membrane by the oxidase assembly (OXA) machinery (9) (figure was adapted from Schmidt et al., 2010).

1.2.2 Mitochondrial oxidative phosphorylation complexes

Mitochondria produce ATP via the electron transport chain and oxidative phosphorylation machinery (Figure 1.3). The oxidative phosphorylation machinery contains complex I (nicotinamide adenine dinucleotide (NADH)-dehydrogenase), complex II (succinate dehydrogenase), complex III (ubiquinone, bc_1 complex), complex IV (cytochrome *c* and cytochrome *c* oxidase) and complex V (ATP synthase) (Hüttemann et al., 2007), all embedded in the inner mitochondrial membrane. Basically, the metabolism of glucose, pyruvate, fatty acids or amino acids by glycolysis and the tricarboxylic acid cycle leads to the production of NADH and flavin adenine dinucleotide ($FADH_2$), the substrates for the oxidative phosphorylation machinery (MacAskill and Kittler, 2010). NADH produced by glycolysis and the tricarboxylic acid cycle is bound by complex I and oxided to NAD^+. In a coupled reaction complex I-bound ubiquinone is reduced to ubiquinol (Efremov et al., 2010, Ghezzi and Zeviani, 2012). Reduction of ubiquinone leads to translocation of four protons from the matrix across the inner membrane into the intermembrane space (Baradaran et al., 2013). Complex II is a direct enzymatic component of the tricarboxylic acid cycle catalyzing the oxidation and dehydration of succinate to fumarate and to concomitant reduction of $FADH_2$ (Ghezzi and Zeviani, 2012, Chaban et al., 2014). Oxidation of succinate leads to reduction of ubiquinone to ubiquinol (Chaban et al., 2014). Complex II is not a proton pump like the other complexes of the electron transport chain and does not contribute to proton translocation across the inner membrane. Complex III oxidizes ubiquinol to ubiquinone leading to

generation of two protons and two electrons from ubiquinol. The protons are translocated across the inner membrane from the matrix to the intermembrane space and the electrons are transferred to cytochrome *c* via cytochromes *b* and c_1 of complex III (Rich and Maréchal, 2010). Complex IV catalyzes the transfer of four electrons from cytochrome *c* to molecular oxygen to generate two water molecules. This reaction is coupled to proton pumping of four protons from the intermembrane space back to the matrix (Rich and Maréchal, 2010, Ghezzi and Zeviani, 2012, Chaban et al., 2014). The proton electrochemical gradient created by complex I, III and IV drives complex V to generate ATP from adenosine diphosphate (ADP) and phosphate.

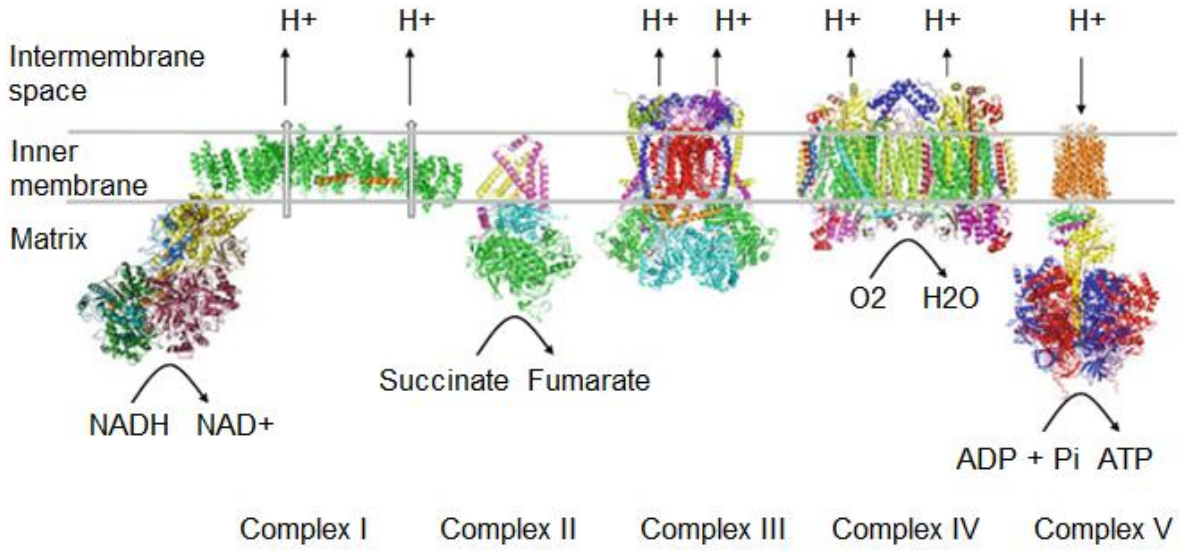

Figure 1.3: Complexes of the oxidative phosphorylation machinery. The electron transport chain comprises four major protein complexes (I–IV). Complex I, III and IV have an enzymatic function to create an electrochemical proton gradient across the intermembrane space that then drives ATP synthesis by the ATP synthase (complex V). Complex I oxidizes NADH to NAD^+ by transfer of two electrons from NADH to ubiquinone. In this reaction, ubiquinol is generated and protons (H^+) are pumped across the inner mitochondrial membrane to the intermembrane space. Complex II catalyzes the oxidation of succinate to fumarate and reduces ubiquinone to ubiquinol. Complex III catalyzes the oxidation of ubiquinol and the reduction of cytochrome *c*. Protons are translocated to the intermembrane space. Complex IV transfers electrons from cytochrome *c* to molecular oxygen and pumps protons across the inner mitochondrial membrane to generate an electrochemical proton gradient whose unbalanced proton gradient is used by complex V to generate ATP from ADP and phosphate (Pi) (figure was modified from Kadenbach, 2012).

1.2.3 Mitochondrial dynamics

Mitochondria are highly dynamic organelles that supply more than 90% of the cellular ATP to support neuronal survival and function (Lin and Sheng, 2015). Since neurons are extremely energy-dependent with many neuronal activities such as synaptic transmission, axonal growth and branching, generation of action potentials and maintenance of calcium homeostasis (Tang and Zucker, 1997, Levy et al., 2003, Rusakov, 2006, Kang et al., 2008), mitochondria must be efficiently delivered to regions of high energy demand in neurons. Mitochondria move on microtubules over long distances and on actin microfilaments for short-range movements with pauses often followed by a reversal of direction (Morris and Hollenbeck, 1995, Chada and Hollenbeck, 2003, Hirokawa and Takemura, 2005, Milone and Benarroch, 2012, Sheng and Cai, 2012). Long-range movement on microtubules requires kinesin and dynein motor proteins (Figure 1.4), whereas short-range movement on actin microfilaments requires myosin motor proteins. Axonal microtubules have a plus-end directed towards the terminals and a minus-end directed towards the cell soma (Milone and Benarroch, 2012). Kinesin is responsible for plus-end directed anterograde transport of neuronal mitochondria. Specific linkage of mitochondria to kinesin requires trafficking protein kinesin-binding (TRAK, also named milton) and mitochondrial rho guanosine triphosphatase (GTPase, Miro). Kinesin contains an N-terminal motor domain, a large tail for dimerization and a C-terminal tail representing the cargo-binding domain (Cai et al., 2005, Cho et al., 2007, MacAskill and Kittler, 2010, Milone and Benarroch, 2012). Miro consists of two N-terminal GTPase domains which flank two calcium-coordinating EF hand domains and a C-terminal transmembrane domain by which it is anchored to the outer mitochondrial membrane (Fransson et al., 2003 and 2006, Tang, 2015). Miro is critical for activity-dependent control of mitochondrial mobility. It binds to the adaptor protein TRAK/milton that is linked to the kinesin heavy chain (Wang and Schwarz, 2009, Sheng and Cai, 2012). Minus-end directed retrograde axonal transport of mitochondria is primarily mediated by dynein motors (Susalka and Pfister, 2000, Hirokawa and Takemura, 2005, Hollenbeck and Saxton, 2005). The cargo binding and regulation of motor activity of dynein is carried out by multiple subunits. Dynactin, a multisubunit complex, binds to dynein and microtubules, and selects between dynein motors and different cargos (Susalka and Pfister, 2000, Schiavo et al., 2013, Lin and Sheng, 2015). Bidirectional axonal transport of mitochondria along actin filaments depends on myosin motors,

such as members of the myosin I, II, V and VI families (Berg et al., 2001, Bridgman, 2004).

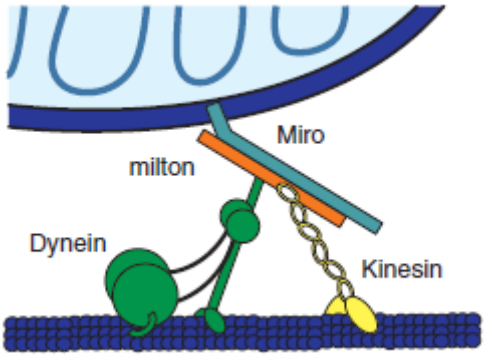

Figure 1.4: Mitochondrial transport. Mitochondria can be transported anterograde (plus-end directed) to axonal terminals of neurons or retrograde (minus-end directed) to the cell soma of neurons. Kinesin, an anterograde motor protein, binds to Miro that is carboxy-terminal anchored to the outer mitochondrial membrane and to the adapter protein milton in the absence of calcium to move mitochondria anterograde on microtubules, whereas dynein, a retrograde motor protein, binds to Miro via the adapter protein milton and transports mitochondria retrograde on microtubules (figure was adapted from Schwarz, 2013).

Mitochondrial morphology depends on the balance of fusion and fission that control the mitochondrial length, shape, and size as well as the number of mitochondria (Milone and Benarroch, 2012). Fusion and fission are regulated by a small number of highly conserved, dynamin-like GTPases (Figure 1.5) (Youle and van der Bliek, 2012, Ishihara et al., 2013). Mitochondrial fusion is mediated by three large GTPase proteins: Mitofusin 1 (Mfn1), Mitofusin 2 (Mfn2), optic atrophy protein 1 (OPA1) (Chan, 2006, Knott et al., 2008). Fusion allows an interconnected mitochondrial network to enhance contact with the endoplasmic reticulum for calcium regulation and further diffusion of the mitochondrial matrix content (Archer, 2013). Mfn1 and Mfn2 contain targeting signals for the outer mitochondrial membrane in their transmembrane and C-terminal domains (Rojo et al., 2002) and form homo-oligomeric or hetero-oligomeric linkages to tether the outer mitochondrial membranes of adjacent mitochondria (Ishihara et al., 2004, Züchner et al., 2004, Liesa et al., 2009). OPA1 comprises eight splice variants, each with different fusion activity and mitochondrial protease function (Zorzano et al., 2010). OPA1 is localized in the intermembrane space and is required for inner mitochondrial membrane fusion. Mitochondrial fusion depends also on the membrane potential across the inner mitochondrial membrane by affecting OPA1 isoform balance (Song et al., 2007,

Milone and Benarroch, 2012). Interestingly, OPA1 needs to interact with Mfn1 for mitochondrial fusion, but not with Mfn2 (Cipolat et al., 2004, Chen et al., 2005). Mitochondria can divide and smaller fragmented mitochondria are created. The fission process requires the recruitment of the dynamin-related protein 1 (Drp1) from the cytosol to the outer mitochondrial membrane (Milone and Benarroch, 2012). Drp1 multimerizes and forms a ring- and spiral-like structure along the mitochondrial surface to encircle and constrict the mitochondrial tubule (Smirnova et al., 2001, Lee et al., 2004, Zhu et al., 2004, Milone and Benarroch, 2012). GTPase receptor proteins such as mitochondrial fission protein 1, mitochondrial fission factor and mitochondrial elongation factor 1 recruit Drp1 to the mitochondrial surface (Lee et al., 2004, Otera et al., 2010, Zhao et al., 2011, Milone and Benarroch, 2012). Especially, mitochondrial fission protein 1, an outer mitochondrial membrane protein is known not only to recruit Drp1 to the mitochondrial surface, but also to modulate the assembly of the fission apparatus that is also regulated by the endoplasmic reticulum, which contacts the mitochondria, creating a microdomain (Otera et al., 2010, Hoppins and Nunnari, 2012, Milone and Benarroch, 2012, Archer, 2013).

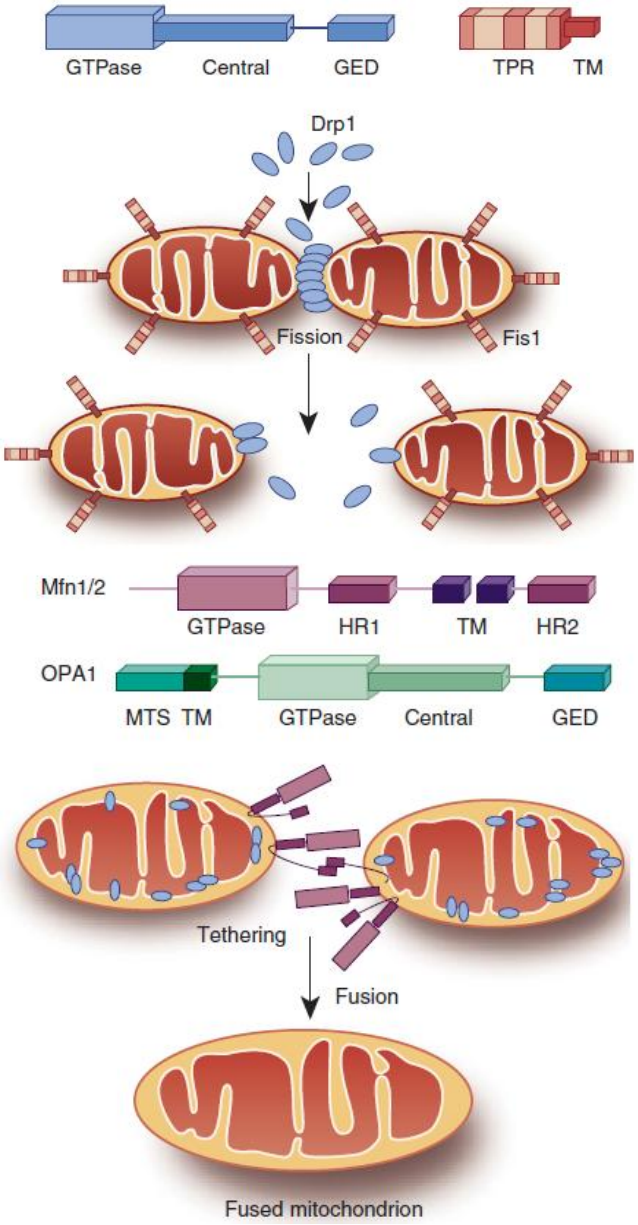

Figure 1.5: Mitochondrial fission and fusion. Fission and fusion of mitochondria are mediated by GTPases such as Drp1, mitochondrial fission protein 1 (Fis1), Mfn1, Mfn2 and OPA1. Drp1 comprises an N-terminal GTPase, a central domain and a C-terminal GTPase effector domain (GED) and forms a ring- and spiral-like structure along the mitochondrial surface to encircle and divide a mitochondrium into two smaller mitochondria. Fis1 contains two central tandem tetratricopeptide repeats (TPRs) and a single C-terminal transmembrane I domain, which is required for anchoring of Fis1 to the outer mitochondrial membrane. Fis1 and Drp1 oligomerize at the outer mitochondrial membrane. Mfn1 and Mfn2 have an N-terminal GTPase domain, two transmembrane domains, and two separating heptad repeat regions (HR1/2). Fusion of the outer mitochondrial membrane is carried out by Mfn1 and Mfn2 through the interaction of adjacent C-terminal HR2 regions. OPA1 contains an N-terminal mitochondrial targeting sequence (MTS), GTPase effector domain at the C-terminus and other functional domains in between and is responsible for the fusion of the inner mitochondrial membrane of adjacent mitochondria (figure was modified from Zhan et al., 2013).

To maintain a healthy mitochondrial population several quality control systems exist. Removal of damaged mitochondria is a selective autophagy process named mitophagy (Ashrafi and Schwarz, 2013). Mitophagy works via a pathway consisting of phosphatase and tensin homolog-induced putative protein kinase 1 (PINK1) and the E3 ubiquitin ligase Parkin (Figure 1.6). PINK1 is a serine/threonine kinase that has a mitochondrial targeting sequence. In polarized mitochondria PINK1 is imported into the inner mitochondrial membrane for cleavage. Mitochondrial degradation of PINK1 is done by several proteases such as mitochondrial processing peptidase and the inner membrane presenilin-associated rhomboid-like protease (Narendra et al., 2010a, Deas et al., 2011, Meissner et al., 2011, Greene et al., 2012). If mitochondria have an impaired membrane potential, PINK1 accumulates at the outer mitochondrial membrane to mediate translocation of cytosolic Parkin to mitochondria (Lazarou et al., 2012, Ashrafi and Schwarz, 2013). Parkin itself is required for polyubiquitination of Mfn1 and Mfn2. Polyubiquitinated Mfn1 and Mfn2 is removed from the outer mitochondrial membrane for subsequent proteosomal degradation to prevent mitochondrial fusion (Poole et al., 2010, Tanaka et al., 2010, Ziviani et al., 2010, Ashrafi and Schwarz, 2013). Other substrates for Parkin are voltage-dependent anion channel, fission 1 and TOM20 (Narendra et al., 2010b, Chan et al., 2011, Glauser et al., 2011). Furthermore, mitochondrial depolarization causes phosphorylation of the adapter protein Miro by PINK1 followed by proteosomal degradation of Miro and disruption of the binding between kinesin motors and mitochondria. In this case, mitochondria are not able to fuse anymore and are rendered immobile, and the damaged mitochondria are engulfed by double-membrane-bound vesicles called autophagosomes (Rambold and Lippincott-Schwartz, 2011, Ashrafi and Schwarz, 2013). In addition, ubiquitin-binding adaptors, such as the nuclear pore glycoprotein 62 (p62), recognize the hyper-ubiquitination of the outer mitochondrial membrane by Parkin and mediate mitophagy through the ubiquitin fold-containing microtubule-associated protein light chain 3 (MAPLC3) (also called LC3 or LC3B) (Tanida, 2011, Ashrafi and Schwarz, 2013).

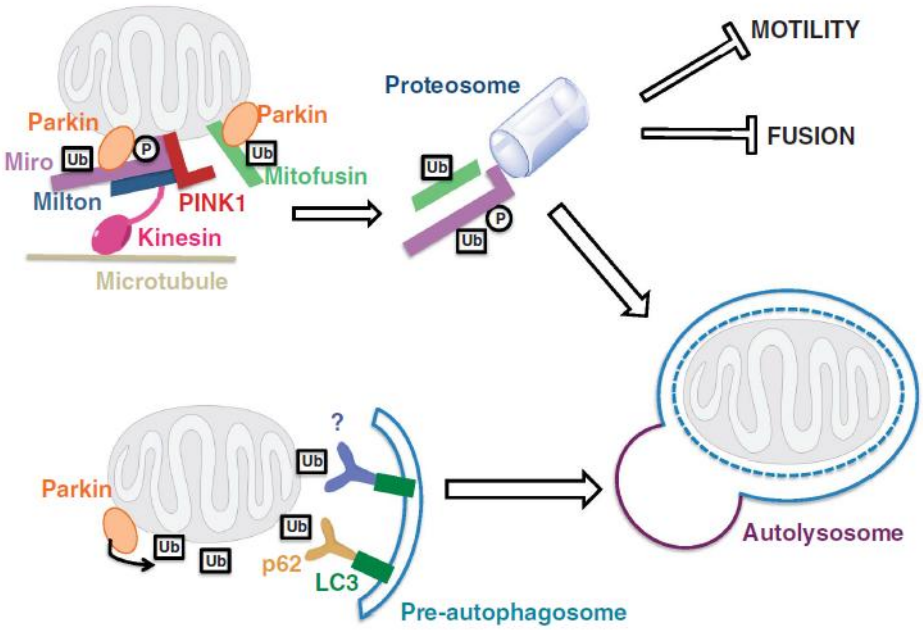

Figure 1.6: PINK1/Parkin pathway of mitophagy. Depolarization of mitochondria leads to an unhealthy mitochondrial pool and prevents cleavage of PINK1. PINK1 accumulates at the outer mitochondrial membrane, recruits Parkin and enhances the ubiquitination activity function of Parkin. Parkin modifies Mitofusin by ubiquitination in order to stop fusion of unhealthy mitochondria. Moreover, PINK1 phosphorylates Miro and milton, and thereby disrupts the association of kinesin via the adapter protein complex of Miro and milton to mitochondria. Parkin polyubiquitinates Mfn1 and Mfn2 and subsequently, mitochondria are engulfed by autophagosomes for degradation. On the other hand, the hyper-ubiquitination of proteins at the outer mitochondrial membrane by Parkin recruits ubiquitin-binding adaptors, such as p62 and other unknown adaptors, which interact with MAPLC3 or LC3 to create pre-autophagosomes, mature autophagosomes and this leads subsequently to mitochondrial degradation (figure was modified from Ashrafi and Schwarz, 2013).

1.3 Nuclear receptors

Nuclear receptors are ligand-inducible transcription factors, which regulate gene expression and have functional importance for embryonic development, maintenance of differentiated cellular phenotypes, metabolism and cell death (Tsai and O'Malley, 1994, Mangelsdorf et al., 1995, Gronemeyer et al., 2004). The mammalian nuclear receptor superfamily can be divided in three main classes with more than 45 diverse intracellular transcription factors (Perissi and Rosenfeld, 2005). Class I is the steroid receptor family with the progesterone receptor, estrogen receptor, glucocorticoid receptor, androgen receptor, and mineralocorticoid receptor. Class II is the thyroid/retinoid family with the thyroid receptor, vitamin D receptor, retinoic acid receptor or retinoid X receptor, liver X receptor and peroxisome proliferator activated receptor. Class III of the nuclear receptor family includes so-called orphan receptors

for which the ligands are still not identified (Perissi and Rosenfeld, 2005, Bain et al., 2007). Nuclear receptors comprise at the amino terminus an activation function (AF-1), which differs in length and sequence in the various family members followed by a highly conserved DNA-binding domain (DBD) with two zinc fingers in the central domain and a ligand-binding domain (LBD) with the ligand-induced activation function (AF-2) required for transcriptional coregulator interaction at the C-terminal end (Figure 1.7). The LBD consists of eleven helices with a ligand-binding pocket inside and the AF-2 region as the twelfth helix that represents the entrance of the ligand-binding pocket (Gronemeyer et al., 2004, Bain et al., 2007).

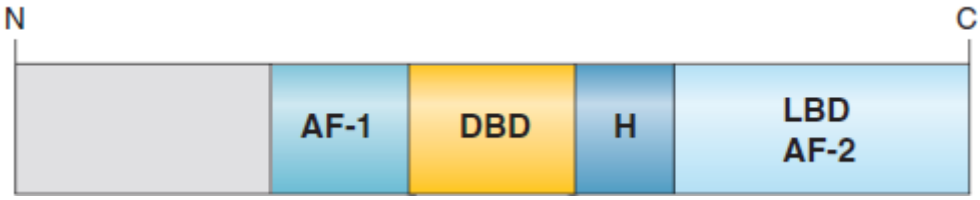

Figure 1.7: Protein domain structure of nuclear receptors. Nuclear receptors consist at the N-terminal end of a AF-1 domain that is important for transactivation of transcription. In the center they have a DBD that is essential for recognition of specific DNA sequences and protein interactions. Next to the hinge (H) region, nuclear receptors have a LBD with an interior binding pocket specific for a ligand at the C-terminal end. The AF-2 domain at the C-terminal part is required to mediate the interaction with chromatin-remodeling proteins and the general transcriptional activation (figure was modified from Bain et al., 2007).

Nuclear receptors can exist as monomers, homodimers or heterodimers in order to activate transcription (Sever and Glass, 2013). The transcription can be repressed by corepressors that contain a region named corepressor nuclear-receptor (CoRNR) box. Corepressors bind with their CoRNR box to a hydrophobic groove in the surface of the LBD of unliganded nuclear receptors to mediate repression of target gene transcription, therefore the initial step in transcriptional activation is the release of corepressor proteins. Binding of ligands to the ligand-binding pocket leads to a conformational change of the AF-2 region in the LBD core followed by disruption of the structure of the hydrophobic groove and a ligand-induced release of corepressors. Nuclear receptors allow coactivators that contain short helical LXXLL (where L is leucine and X is any amino acid) motifs called nuclear-receptor (NR) boxes to bind via hydrophobic interactions to the nuclear receptor groove after release of the corepressor from the nuclear receptor (Gronemeyer et al., 2004, Bain

et al., 2007). Coactivators can contain the NR box with single or multiple copies of the LXXLL motifs. The number and sequence of the NR box varies among the coactivators and amino acid residues nearby the core motif are also important for the recognition of liganded nuclear receptors (Savkur and Burris, 2004). The FXXLF (where F is phenylalanine) motif is a further motif that can be present in coactivators and mediates binding to the AF-2 region in the LBD of liganded nuclear receptors. It stabilizes the ligand-receptor complex and competes with binding of LXXLL motif-containing coactivators to AF-2 (He et al., 2000, 2001, 2002, Dubbink et al., 2006, Askew et al., 2012).

Nuclear receptors and their coregulators are crucial for the development of the central nervous system and are known to regulate cerebellar function. The cerebellum is involved in movement coordination, motor learning and in certain cognitive processes (Chambers and Sprague, 1955, Dow and Moruzzi, 1958, Thach, 1996, Schmahmann, 1997, Ito, 2000). Furthermore, the cerebellum contains nuclear receptors of the steroid receptor family such as estrogens which have regulatory functions during cerebellar development and signaling. Estrogen receptors α/β (ERα/β) are involved in Purkinje cell dendritic growth, spine and synapse formation (Hedges et al., 2012). Activation of ERβ by its ligand estradiol increases the density of parallel fibers to Purkinje cell synapses, whereas it does not affect the density of climbing fiber synapses. Also, estradiol improves cerebellar memory formation by activating ERβ (Andreescu et al., 2007). Recently, it was shown that also the nuclear receptors of the thyroid/retinoid family influence cerebellar functions. The thyroid receptor-mediated gene expression in Purkinje cells plays a critical role in the entire cerebellar development. A transgenic mouse line expressing dominant-negative mutant thyroid receptor β1 showed disrupted cerebellar morphogenesis and disturbed motor coordination (Yu et al., 2015).

Moreover, it was shown that nuclear receptors are involved not only in cerebellar-related functions but also in hippocampal-related functions. The hippocampus is crucial for the formation of new episodic memories and might also have an essential role in their long-term storage. Hippocampus-dependent memory formation and long-term storage is mediated by hippocampal synaptic plasticity (Neves et al., 2008). Steroid receptor coactivator 1 may function with ERα/β in the hippocampus to

modulate estrogen's effects on cognition and stress (Fugger et al., 2000, Isgor et al., 2003, Bodo and Rissman, 2006). Furthermore, retinoic acid receptors functional deletion by mutation in mice results in deficits in synaptic plasticity as well as in deficits in hippocampal-dependent learning and memory tasks (Chiang et al., 1998). Hence, the cerebellar and hippocampal circuitry are of interest for understanding the impacts of nuclear receptors and their coregulators in cerebellar- and hippocampal-related functions.

1.3.1 Cerebellar circuitry

The cerebellum consists of the cerebellar cortex and the deep cerebellar nuclei. The cerebellar cortex itself is divided into the molecular layer, the Purkinje cell layer and the granular layer. The output signals of the cerebellum are controlled by Purkinje cells. Purkinje cells exhibit an extensive dendritic tree that projects from the Purkinje cell layer into the molecular layer and inhibit the deep cerebellar nuclei in the white matter. Two different neuronal fibers send excitatory input to Purkinje cells: mossy fibers and climbing fibers. Mossy fibers that arise from the spinal cord and brain stem make synaptic contacts with granule cells of the granular cell layer and send inputs to parallel fibers and stellate, basket and Golgi interneurons in the molecular layer. Parallel fibers and interneurons form excitatory synapses on the dendritic spines of the Purkinje cells. Climbing fibers that send excitatory signals to Purkinje cells arise from the inferior olivary nucleus of the medulla oblongata (Eccles et al., 1967, Popko, 1999, Purves et al., 2001, Kitazawa and Wolpert, 2005, Ramnani, 2006, Cerminara et al., 2015).

1.3.2 Hippocampal circuitry

The synaptic interaction in the hippocampus is carried out by the trisynaptic pathway from the entorhinal cortex to the hippocampal subfield CA1 (Figure 1.8). Sensory information is send from neurons of the entorhinal cortex through axons of the granule cells of the dentate gyrus. The axons of the granule cells are called mossy fibers. Granule cells of the dentate gyrus provide excitatory synaptic inputs through their axons to neurons in the dentate gyrus hilus and to the proximal apical and basal dendrites of CA3 pyramidal cells. CA3 pyramidal cells make synaptic contacts with CA1 pyramidal cells through Schaffer collaterals and with CA3 and CA1 pyramidal cells through commissural connections (Amaral, 1979, Claiborne et al., 1986,

Frotscher et al., 1991, Acsády et al., 1998, Blaabjerg and Zimmer, 2007, Neves et al., 2008, Galván et al., 2011).

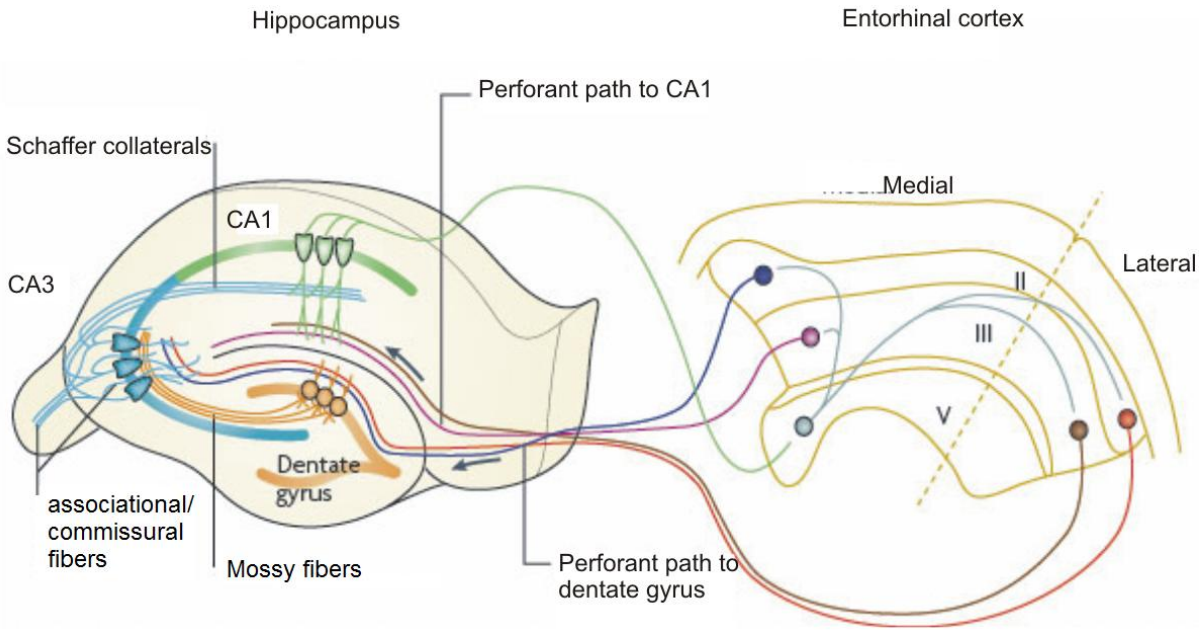

Figure 1.8: Hippocampal circuitry. The dentate gyrus receives the main excitatory inputs through the performant path from axons of the layer II stellate cells of the entorhinal cortex. The terminals of axons of the granule cells of the dentate gyrus are called mossy fibers. Mossy fibers provide inhibitory and excitatory input in the dentate gyrus hilus and the proximal apical and basal dendrites of CA3 pyramidal cells. The CA3 area comprises interneurons such as the associational/commissural fibers that arise from the axon collaterals of CA3 pyramidal cells and the Schaffer collaterals that make synaptic contacts with CA1 pyramidal cells (figure was modified from Neves et al., 2008, Galván et al., 2011).

2 AIMS OF THE STUDY

In previous studies, proteolytic processing of L1 in the first fibronectin type III domain by MBP was shown. The resulting 70 kDa transmembrane fragment, L1-70, is transported to endosomes and released from the endosomes into the cytoplasm and transferred into the nucleus. In independent studies it has been shown that L1 interacts extracellularly with GAPDH, ANT1 and ANT2. Since GAPDH, ANT1 and ANT2 have major functions in mitochondria, the first aim of my study was to investigate whether L1-70 is imported from the cytoplasm into mitochondria to interact with mitochondrial GAPDH, ANT1 and ANT2. With the help of *in vitro* assays the role of translocases of the outer mitochondrial membrane complex for translocation of L1-70 should be analyzed. Furthermore, the influence of L1 on mitochondrial oxidative phosphorylation accomplished by the activities of complex I, II, III, IV and V should be tested. Additionally, the impact of L1 on mitochondrial quality control, mitochondrial fusion and fission mechanisms and mitochondrial motility, and mobility as well as on the direction of mitochondrial transport should be analyzed. Finally, novel binding partners for mitochondrial L1 should be identified.

L1 contains LXXLL and FXXLF motifs which mediate the interaction with nuclear receptors. Since nuclear receptors are associated with essential functions in the central nervous system and affect hippocampal and cerebellar functions like L1, the second aim of my study was to determine if nuclear L1-70 interacts with nuclear receptors such as peroxisome proliferator activated receptor γ, retinoid X receptor β, estrogen receptor α/β, androgen receptor, vitamin D receptor and liver X receptor β via the LXXLL and FXXLF motifs. To examine the functional relevance of the putative interaction of L1 with nuclear receptors, the consequence of mutagenesis of the LXXLL and FXXLF motifs and disruption of the interaction of L1-70 with these nuclear receptors for the functions of the central nervous systems should be analyzed. Effects on neurite outgrowth and synaptic connectivity in the hippocampus and cerebellum should be investigated. To test the possible influence of L1-70 in cerebellum-dependent functions, behavioral tests which give information about defects in motor coordination and learning should be performed.

3 MATERIALS

3.1 Animals

Generation of L1-deficient mice was carried out by insertion of a tetracycline-controlled transactivator into the second exon of the X chromosome-linked L1 gene (Rolf et al., 2001). L1-deficient male mice and their age-matched wild-type male littermates were obtained from heterozygous breeding pairs on a mixed genetic background (129SVJ x C57BL/6J). *Shiverer* mice were maintained on an inbred C57BL/6J background (Mikoshiba et al., 1983).

All animal experiments were approved by the local authorities of the State of Hamburg (animal permit number ORG 679) and conform to the guidelines set by the European Union.

3.2 Chemicals and supplies

All chemicals, reagents and kits were purchased from the following companies: Abcam (Cambridge, UK), Abnova (Taipei, Taiwan), Addgene Inc. (Teddington, UK), Applied Biosystems (Foster City, CA, USA), Biolegend (Fell, Germany), BIOMOL (Hamburg, Germany), Bio-Rad Laboratories (Munich, Germany), Biozol (Eching, Germany), Carl Roth (Karlsruhe, Germany), Corning (Wiesbaden, Germany), Creative BioMart (Shirely, NY, USA), Dako/ Agilent Technologies (Santa Clara, CA, USA), Dianova (Hamburg, Germany), Enzo Life Sciences (Farmingdale, NY, USA), Eppendorf AG (Hamburg, Germany), LifeTechnologies (Darmstadt, Germany), INVIVO BioTech Service (Hennigsdorf, Germany), Jackson ImmunoResearch (West Grove, PA, UK), Macherey-Nagel (Düren, Germany), Merck Chemicals (Darmstadt, Germany), Nunc (Roskilde, Denmark), PAA laboratories (Cölbe, Germany), PAN Biotech (Aidenbach, Germany), Santa Cruz Biotechnologies (Dallas, TX, USA), Sigma-Aldrich (Taufkirchen, Germany), T. H. Geyer (Hamburg, Germany), ThermoFisher Scientific (Waltham, MA, USA), Roche Diagnostics (Mannheim, Germany), VWR International GmbH (Darmstadt, Germany). If not indicated otherwise, all chemicals were used from Sigma-Aldrich.

3.3 Solutions and buffers

Protease inhibitor solution (Complete, EDTA free tablets) *(mitochondrial lysates)*	1 tablet in 2 ml phosphate buffered saline (PBS) (25x stock)
Mitochondrial isolation buffer (MIB) *(mitochondria isolation for affinity chromatography)*	0.32 M sucrose 10 mM Tris-hydrogen chloride (Tris-HCl) 1 mM ethylenediaminetetraacetic acid (EDTA) pH 7.4 1x protease inhibitor solution
Ficoll stock solution *(mitochondria isolation for affinity chromatography)*	20% Ficoll in MIB
Ficoll gradient *(mitochondria isolation for affinity chromatography)*	12% Ficoll solution 7% Ficoll solution dilution of 20% Ficoll stock solution in MIB
Sucrose stock solution *(mitochondria isolation for affinity chromatography)*	1.6 M sucrose 1 mM EDTA 10 mM Tris-HCl pH 7.4
Sucrose gradient *(mitochondria isolation for affinity chromatography)*	1.3 M sucrose 1.0 M sucrose 0.8 M sucrose dilution of 1.6 M sucrose stock solution in dH_2O

TE buffer *(mitochondria isolation for affinity chromatography)*	10 mM Tris-HCl 1 mM EDTA 0.5 mg/ml bovine serum albumine (BSA) pH 7.4
Coupling buffer *(cyanogen bromide (CNBr) activated sepharose)*	100 mM sodium bicarbonate ($NaHCO_3$) 500 mM sodium chloride (NaCl) pH 8.3
Washing buffer/Coupling buffer *(CNBr activated sepharose)*	100 mM $NaHCO_3$ 500 mM NaCl pH 8.3
Blocking buffer *(CNBr activated sepharose)*	0.2 M glycine pH 8.0
Washing buffer *(CNBr activated sepharose)*	100 mM sodium acetate 500 mM NaCl pH 4.0
Neutralization buffer *(affinity chromatography)*	1 M Tris-HCl pH 8.0
Elution buffer *(affinity chromatography)*	0.3 M glycine pH 2.3
Bicinchoninic acid (BCA) protein assay solution *(BCA kit)*	Reagent A Reagent B (50:1)
Sample buffer (5x) *(SDS-PAGE)*	0.35 M Tris-HCl 10% sodium dodecyl sulfate

	(SDS) 50% glycerol 0.13% bromophenol blue 0.5% dithiothreitol (DTT)
SDS 10 % *(SDS-PAGE)*	10 g SDS in 100 ml dH_2O
SDS Running buffer *(SDS-PAGE)*	250 mM Tris-HCl 192 mM glycine 1% SDS
SDS running gel 10 % *(SDS-PAGE)*	1.7 ml dH_2O 2.0 ml 30% acrylamide-bisacrylamide (29:1) 2.3 ml 1 M Tris-HCl, pH 8.8 60 µl 10% SDS 15 µl 10% ammonium persulfate (APS) 6 µl tetramethylethylenediamine (TEMED)
Stacking gel *(SDS-PAGE)*	1.6 ml dH_2O 0.4 ml 30% acrylamide-bisacrylamide (29:1) 0.3 ml 1 M Tris-HCl pH 6.8 30 µl 10% SDS 15 µl 10% APS 6 µl TEMED
Coomassie blue staining solution *(staining of SDS-PAGE gels)*	20% methanol in dH_2O 20% Roti-Blue in dH_2O
Tris-buffered saline (TBS) 10x stock	10 mM Tris-HCl

(Western Blotting)	150 mM NaCl pH 7.5
TBS-T *(Western Blotting)*	0.1% Tween-20 in 1x TBS
Blotting buffer *(Western Blotting)*	25 mM Tris 192 mM glycine 0.01% SDS 20% methanol
Blocking buffer *(Western Blotting)*	4% skim milk powder in 1x TBS-T
Antibody dilution buffer *(Western Blotting)*	4% skim milk powder in 1x TBS-T
Stripping buffer *(Western blots)*	500 mM NaCl 500 mM acetic acid
Mitochondrial lysis buffer *(lysis of mitochondria)*	20 mM Tris-HCl pH 7.5 150 mM NaCl 1 mM disodium ethylenediaminetetraacetate dihydrate (Na_2EDTA) 1 mM ethylene ethylene glycol-bis(β-aminoethyl ether)-N,N,N‘,N‘-tetraacetic acid (EGTA) 1% nonyl phenoxypolyethoxylethanol (NP-40) 1% sodium deoxycholate 2.5 mM sodium pyrophosphate 1 mM β-glycerophosphate

	1 mM sodium vanadate 1x protease inhibitor solution
PBS *(ELISA)*	1x PBS (with or without calcium (Ca^{2+}) and magnesium (Mg^{2+}))
PBS-T *(ELISA)*	0.05% Tween-20 in 1x PBS (with or without Ca^{2+} and Mg^{2+})
Blocking buffer *(ELISA)*	2% BSA in 1x PBS (with or without Ca^{2+} and Mg^{2+})
OPD substrate *(ELISA)*	1 mg/ml o-phenylenediamine dihydrochloride (OPD) substrate in dH_2O mixed with 10x stable peroxide buffer (1:10)
MitoTracker stock solution *(staining of mitochondria)*	MitoTracker® Red CMXRos 1 mM in dimethyl sulfoxide (DMSO)
Paraformaldehyde (PFA) solution *(fixation)*	4% PFA in dH_2O
Cacodylate buffer *(paraffin tissue processing)*	0.2 M sodium cacodylate in dH_2O pH 7.3
PBS 10x stock solution *(Immunohistochemistry for paraffin-embedded tissue sections)*	150 mM NaCl 20 mM trisodium phosphate (Na_3PO_4) pH 7.4
Sodium citrate buffer	100 mM sodium citrate

(Immunohistochemistry for paraffin-embedded tissue sections)	pH 6.0
Blocking solution with normal donkey serum *(Immunohistochemistry for paraffin-embedded tissue sections)*	5% normal donkey serum in 1x PBS 1% Triton X-100 0.02% sodium azide (NaN_3)
Antibody dilution buffer *(Immunohistochemistry for paraffin-embedded tissue sections)*	5% normal donkey serum in 1x PBS 1% Triton X-100 0.02% NaN_3

3.4 Cell lines

Human embryonic kidney cells (HEK293)	ATCC CRL-1573

3.5 Bacterial media and reagents

Lysogeny broth (LB)-medium	10 g/l bacto-tryptone pH 7.4 10 g/l NaCl 5 g/l yeast extract
LB/ampicillin-medium	100 µg/ml ampicillin in LB-medium
LB/ampicillin-plates	20 g/l agar in LB-medium 100 µg/ml ampicillin
LB/kanamycin-medium	50 µg/ml kanamycin in LB-medium
LB/kanamycin-plates	20 g/l agar in LB-medium 50 µg/ml kanamycin

3.6 Cell culture media, buffer and reagents

Poly-L-lysine (PLL) *(coating solution)*	0.01% in dH_2O
HBSS *(cell washing)*	Hank's balanced salt solution without Ca^{2+} and Mg^{2+} containing 0.35 g/l $NaHCO_4$ and phenol red
Trypsin-EDTA *(trypsinization)*	0.05% trypsin/0.02% EDTA in PBS without Ca^{2+} and Mg^{2+}
Medium X-1 *(cerebellar granule cells)*	Neurobasal A containing: 1% penicillin/streptomycin 0.1% BSA 10 µg/ml insulin 4 nM L-thyroxine 100 µg/ml transferrin holo 30 nM sodium-selenite 1x B27 supplement
Medium X-1 with serum *(cerebellar granule cells)*	Medium X-1 5% fetal horse serum
Dnase I solution *(cerebellar granule cells)*	10 mg Dnase I 50 mg glucose 20 ml Neurobasal A
trypsin/Dnase solution *(cerebellar granule cells)*	0.3 g trypsin 30 mg Dnase I 300 µl 80 mM magnesium chloride ($MgCl_2$) 30 ml HBSS

	pH 7.8
RIPA (Radioimmunoprecipitation assay) buffer *(nuclear extract from cerebellar granule cells for Western blot analysis)*	20 mM Tris-HCl 150 mM NaCl 1 mM Na_2EDTA 1 mM EGTA 1% NP-40 10 µM DTT 25 Units/ml benzonase 1x protease inhibitor solution pH 7.4
Urea lysis buffer *(nuclear extract from cerebellar granule cells for Western blot analysis)*	100 mM Tris-HCl 12 mM magnesiumacetate tetrahydrate 6 M urea 2% SDS 10 µM DTT 25 Units/ml benzonase 1x protease inhibitor solution pH 7.4
Staining solution (*neurite outgrowth with cerebellar granule cells)*	1% toluidine blue 1% methylene blue in 1% sodium-tetraborate buffer
Fixing solution *(neurite outgrowth with cerebellar granule cells)*	25% glutaraldehyde
Hippocampal medium *(hippocampal neurons)*	Neurobasal A containing: 2 mM L-glutamine 5 µg/ml gentamycin 12.5 µg/ml b-fibroblast growth

	factor (FGF) 1x B27 supplement
Digestion solution *(hippocampal neurons)*	135 mM NaCl 5 mM potassium chloride (KCl) 7 mM disodium hydrogen phosphate (Na_2HPO_4) 4 mM $NaHCO_3$ 25 mM 4-(2-hydroxyethyl)-1-piperazineethanesulfonic acid (HEPES), pH 7.4
Dissection solution *(hippocampal neurons)*	HBSS 4 mM $NaHCO_3$ 10 mM HEPES 6 mg/ml glucose 5 µg/ml gentamycin 3 mg/ml BSA 12 mM magnesium sulfate ($MgSO_4$)
Dnase I solution *(hippocampal neurons)*	2.5 ml dissection solution 1 mg Dnase I (stock 10 mg/ml)
Trypsin/Dnase solution *(hippocampal neurons)*	1.8 ml digestion solution 1.5 mg DNAse I (stock 10mg/ml) 6 mg trypsin
Trypsin inhibitor *(hippocampal neurons)*	4 ml dissection solution 2.4 mg trypsin inhibitor
DMEM (*HEK cells)*	Dulbecco's modified Eagle Medium (DMEM) with L-glutamine, sodium pyruvate, high glucose (4.5

	g/l) 2% penicillin/streptomycin 10% fetal calf serum
DMEM freezing medium (*HEK cells)*	70% DMEM 20% fetal calf serum 10% DMSO

3.7 Adeno-associated virus 1 (AAV1)

Production of AAV1 coding for wild-type and mutated L1 was performed by Ingke Braren (Universitätsklinikum Hamburg-Eppendorf, Germany).

Virus name	Concentration [vg/ml]
ssAAV1-CMV wild-type L1	6.02E+11
ssAAV1-CMV L1R/A	2.52E+11
ssAAV1-CMV empty control	7.43E+12
ssAAV1-CMV mutant L1 (1046/1136)	1.2E+12

3.8 Plasmids

EGFP-LC3	Addgene Inc., #11546
mito-dendra2	Addgene Inc., #55796

3.9 Recombinant protein constructs

androgen receptor (AR)	Creative BioMart, AR-991H
vitamin D receptor (VDR), 128-427 aa	Creative BioMart, VDR-3659H
estrogen receptor 1 (ESR1), 65-280 aa	Creative BioMart, ESR1-12557H
estrogen receptor 2 (ESR2)	Biozol, ABN-H00002100-P01-2
His-tagged intracellular domain of mouse L1	produced in the lab of M. Schachner
His-tagged intracellular domain of mouse CHL1	produced in the lab of M. Schachner
mouse L1-Fc	custom made; InVivo BioTech Service
NADH:ubiquinone oxidoreductase core subunit V2 (NDUFV2)	Abnova, H00004729-P01
nuclear receptor subfamily 1 group H member 2 (NR1H2) or liver X receptor β (LXRβ)	Biozol, ABN-H00007376-P01-1
peroxisome proliferator activated receptor γ (PPARγ), 209-477aa	Creative BioMart, PPARG-2772H

retinoid X receptor β (RXRβ)	Enzo Life Sciences, BML-SE127-0050

3.10 Antibodies

3.10.1 Primary antibodies

Antigen	Host	Company	Catalog number	Dilution/ Concentration
AR	rabbit	Santa Cruz Biotechnology	sc-816	Immunoprecipitation (IP): 8 µg/ml
Calbindin	mouse	Sigma-Aldrich	C9848	Immunohistochemistry (IHC): 1:100
Calbindin	rabbit	Sigma-Aldrich	C2724	IHC: 1:100
CD171	mouse	Biolegend	838101 (MMS-172R)	Western blot (WB): 1:1,000
Calregulin	goat	Santa Cruz Biotechnology	sc-6467	WB: 1:1,000
Drp1	rabbit	Santa Cruz Biotechnology	sc-32898	WB: 1:500
ERα	rabbit	Santa Cruz Biotechnology	sc-543	IP: 8 µg/ml
Glutamic acid decarboxylase 67 (GAD67)	mouse	Abcam	ab26116	IHC: 1:100

Glyceraldehyde 3-phosphate dehydrogenase (GAPDH)	rabbit	Santa Cruz Biotechnology	sc-25778	IP: 5 µg/ml WB: 1:1,000
Histone H3	rabbit	Santa Cruz Biotechnology	sc-10809	WB:1:1,000
L1-ab 557	rat	INVIVO BioTech Service	custom made	Stimulation: 10-50 µg/ml
L1CAM	rabbit	Abcam	ab123990	IHC:1:100 Enzyme-linked Immunosorbent Assay (ELISA): 1:100 WB: 1:250
L1CAM (D-5)	mouse	Santa Cruz Biotechnology	sc-374046	blocking assay: 30 µg/ml
L1CAM (H200)	rabbit	Santa Cruz Biotechnology	Sc-15326	IP: 5 µg/ml WB: 1:1,000 blocking assay: 30 µg/ml
L1CAM (C-20)	goat	Santa Cruz Biotechnology	sc-1508	WB: 1:1,000
L1CAM (C-2)	mouse	Santa Cruz Biotechnology	sc-514360	WB: 1:1,000
Mfn2	rabbit	Santa Cruz Biotechnology	sc-50331	IP: 5 µg/ml WB: 1:1,000

NDUFV2	mouse	Santa Cruz Biotechnology	sc-271620	IP: 5 µg/ml
Neurogranin	goat	Abcam	ab99269	IHC: 1:100
Normal goat IgG	goat	Santa Cruz Biotechnology	sc-2028	IP: 5 µg/ml
Normal mouse IgG-biotin	mouse	Santa Cruz Biotechnology	sc-2762	IP: 5 µg/ml
PPARγ	rabbit	Santa Cruz Biotechnology	sc-7196	IP: 8 µg/ml
Ras Homolog Family Member A (RhoA)	mouse	Cytoskeleton	ARH04	WB: 1:500
RhoT1	mouse	Santa Cruz Biotechnology	sc-398520	IP: 5 µg/ml WB: 1:1,000
RXRα/β/γ	rabbit	Santa Cruz Biotechnology	sc-831	IP: 8 µg/ml
TOM40	goat	Santa Cruz Biotechnology	sc-11025	blocking assay: 30 µg/ml
TOM70	rabbit	Santa Cruz Biotechnology	sc-366282	blocking assay: 30 µg/ml
VDR	rabbit	Santa Cruz Biotechnology	sc-1008	IP: 8 µg/ml

Vesicular glutamate transporter 1 (Vglut1)	mouse	Synaptic systems	135 311	IHC: 1:100

3.10.2 Secondary antibodies

Conjugate	Host	Specificity	Company	Catalog number	Dilution
Cy2	donkey	mouse	Dianova	715-225-150	IHC: 1:200
Cy3	donkey	rabbit	Dianova	711-165-152	IHC: 1:200
Horse radish peroxidase (HRP)	goat	rabbit	Jackson ImmunoResearch	111-036-144	ELISA: 1:2,000 WB: 1:5,000
HRP	donkey	goat	Jackson ImmunoResearch	705-035-003	WB: 1:5,000
HRP	goat	mouse	Jackson ImmunoResearch	115-035-003	WB: 1:5,000

3.11 Mitochondrial assay kits

Mitochondrial Complex I Activity Assay Kit, 1 Y17	Merck Chemicals AAMT001-1KIT
MitoCheck Complex II/III Activity Assay Kit	BIOMOL Cay-700950

MitoCheck Complex IV Activity Assay Kit	BIOMOL Cay700990-96
MitoCheck Complex V Activity Assay Kit	BIOMOL Cay-701000-96
Mito-ID® Membrane potential detection kit for microscopy and flow cytometry	Enzo Life Sciences ENZ-51018-0025
Mitochondria Isolation Kit for Tissue	Thermo Fisher Scientific 89801

4 METHODS

4.1 Biochemical methods

4.1.1 Isolation of a mitochondrial fraction from mice brains for affinity chromatography

Brains of 40 wild-type mice at the age of four months were used for isolation of mitochondria. All reagents were kept on ice and all steps were carried out on ice or at 4°C. Brains were homogenized in 80 ml MIB using a Potter Elvehjem homogenizer. The homogenate was centrifuged at 1,000 × g for 5 min and the supernatant was kept on ice. The pellet was washed twice with 12 ml MIB at 1,000 × g for 5 min with subsequent collection of the supernatant after every wash. The pellet was then discarded and all collected supernatants were pooled and centrifuged at 1,000 × g for 5 min. The resulting supernatant was directly subjected to the next centrifugation step at 14,000 × g for 15 min. The 14,000 g pellet containing non-synaptic mitochondria, synaptosomes and myelin was resuspended in 12 ml MIB, while the supernatant was discarded. The resuspended pellet was layered on a discontinuous Ficoll (GE Healthcare) gradient containing 12% Ficoll, 7.5% Ficoll and MIB. Each Ficoll gradient layer contained 12 ml for a total volume of 36 ml. The gradient was centrifuged at 73,000 × g for 36 min using the SW 32 Ti rotor (Beckman Coulter). The resulting pellet containing mitochondria was resuspended in 12 ml MIB with 0.5 mg/ml BSA (PAA laboratories) and centrifuged at 12,000 × g for 15 min. The pellet containing the mitochondria was resuspended in 6 ml MIB and applied on a discontinuous sucrose gradient containing 0.8 M, 1.0 M, 1.3 M and 1.6 M sucrose. The volumes for the sucrose gradient were 6 ml/ 6 ml/ 10 ml/ 8 ml, respectively. The sucrose gradient was centrifuged at 50,000 × g for 2 h using the SW 32 Ti rotor (Beckman Coulter). Purified mitochondria were collected at the interface of 1.3 M and 1.6 M sucrose, resuspended in a ratio of 1:3 in TE buffer and centrifuged at 18,000 × g for 15 min. The pellet was washed twice with MIB, first at 12,000 × g for 10 min and then at 8,200 × g for 10 min. Last, the pellets were washed in PBS (PAN Biotech, without Ca^{2+} and Mg^{2+}) at 8,200 × g for 10 min, resuspended in PBS (without Ca^{2+} and Mg^{2+}) by pipetting up and down and stored at -20 °C.

4.1.2 Coupling of ligands to cyanogen bromide-activated sepharose beads

Immobilization of proteins to cyanogen bromide-activated sepharose beads (Sigma-Aldrich) was done according to the protocol of the manufacturer. All steps were carried out on ice or at 4 °C. In brief, 3 mg of his-tagged intracellular domain of mouse L1 or of CHL1 were dissolved in coupling buffer and the required amount of cyanogen-bromide activated resin (1 ml resin per 5-10 mg ligand) was washed and swelled in cold 1 mM HCl for at least 30 min. The resin was washed once with dH_2O and then with coupling buffer. The dissolved ligands were mixed with ~500 µl of the swollen resin and incubated together overnight with constant agitation. After washing the resin was washed with coupling buffer, unreacted groups were quenched by incubation with blocking solution for 2 h at room temperature. The samples were washed with high pH buffer (coupling buffer, pH 8.5) and low pH buffer (0.1 M acetate buffer, pH 4.0). Immediately the resin was incubated overnight with the isolated mitochondrial brain fraction. The next day, the resin (~500 µl) was washed several times with PBS (without Ca^{2+} and Mg^{2+}), PBS (without Ca^{2+} and Mg^{2+}) containing 1% CHAPS (VWR), again with PBS (without Ca^{2+} and Mg^{2+}) and bound proteins were eluted with 0.1 M glycine (pH 2.3) and neutralized with 1 M Tris-HCl (pH 8.0). The protein concentration was measured with the BCA test (ThermoFisher Scientific) and the probes were subjected to protein precipitation. After separation of the proteins by SDS-PAGE and Coomassie blue staining of the proteins, visible bands were excised and subjected to mass spectrometry.

4.1.3 Protein precipitation

Chloroform-methanol precipitation was done according to Wessel and Flügge (1984). Four volumes methanol (T. H. Geyer) were mixed with one volume aqueous protein solution. One volume chloroform (T. H. Geyer) was added, the samples were mixed and three volumes water were added. After mixing, the samples were centrifuged at 12,000 × g for 3 min. The upper phase was discarded and three volumes methanol were added to the inter phase and the lower phase. After mixing, the samples were centrifuged at 12,000 × g for 3 min. The supernatant was discarded and the pellets were boiled in 5x sample buffer for 5 min and subjected for Western blot analysis.

4.1.4 Determination of the protein concentration

The BCA Protein Assay Reagent Kit (ThermoFisher Scientific) was used to determine the protein concentration of the samples. The assay was performed with 10 µl of the samples (dilution of 1:10 and 1:100 in dH_2O), 10 µl BSA standard solutions (50-1,000 µg/ml) and 200 µl of a mixture of Reagent A and Reagent B (50:1). The samples were incubated for 30 min at 37°C and the absorbance was measured at 562 nm with the µQuant™ microplate spectrophotometer (Bio-tek, Germany). The concentrations were calculated using the calibration curve of the BSA standard solutions.

4.1.5 SDS-polyacrylamide gel electrophoresis (PAGE)

For separation of proteins in an electric field the SDS-PAGE was used. The protein samples were boiled in sample buffer at 95°C for 5 min and shortly centrifuged at 16,000 × g. The electrophoresis was performed in the Mini-Protean II system (Bio-Rad Laboratories GmbH, Germany) using 10% gels with a thickness of 1 mm and SDS running buffer. Gel runs were started at a voltage of 80 V for 10 min and continued at 120 V until the bromophenol blue front reached the end of the gel. As a molecular weight standard the ProSieve QuadColor Protein Marker (Biozym) or the Precision Plus Protein Dual Color Standard (Bio-Rad Laboratories GmbH) were used.

4.1.6 Coomassie blue staining of polyacrylamide gels

Protein separation was visualized with the colloidal Coomassie blue staining using the RotiBlue kit (Carl Roth) after the SDS-PAGE. The gels were maintained in Roti-Blue staining solution overnight with constant agitation. The gels were washed several times with dH_2O until the stained protein bands clearly appeared.

4.1.7 Western blot

For identification of proteins, the proteins were transferred from the SDS-PAGE gel onto a 0.45 µm nitrocellulose membrane (GE Healthcare) using the Mini-Protean II blotting system (Bio-Rad Laboratories GmbH, Germany). The blotting sandwich was prepared as described in the manufacturer's manual. The electrophoretic transfer was done in blotting buffer at a constant voltage of 90 V for 120 min on ice. The membrane was placed protein-bound site up in glass vessels and incubated in blocking buffer for 1 h at room temperature. The membrane was incubated overnight with an appropriate primary antibody diluted in blocking buffer. The membrane was

washed three times for 5 min in TBS-T, incubated for 1 h with a HRP-coupled secondary antibody (diluted 1:5,000 in blocking solution) at room temperature and washed again three times for 5 min in TBS-T. Proteins were detected using the ECL select or ECL prime reagents (GE Healthcare) and the LAS 4000 Mini camera (GE Healthcare, UK).

4.1.8 Isolation of mitochondrial fractions for import and enzymatic assays

Mitochondria were isolated from wild-type and L1-deficient mouse brains using male mice at the age of one to three months by the Mitochondria Isolation Kit for Tissue (ThermoFisher Scientific) according to manufacturer's instructions. All steps were performed on ice or at 4°C.

Brains were removed from mice (one brain for each mitochondrial isolation), washed with PBS (without Ca^{2+} and Mg^{2+}), cut into small pieces and homogenized in PBS (without Ca^{2+} and Mg^{2+}). The homogenates were centrifuged at 1,000 × g for 3 min and the supernatant was discarded. The pellet was resuspended in the supplied BSA/Reagent A solution (1,000 µl per brain), mixed for 5 sec and incubated for 2 min on ice. Supplied Reagent B was added (10 µl per brain) and the samples were mixed and incubated for 5 min on ice with mixing every minute. Supplied Reagent C (800 µl per brain) was added and the tube was inverted several times. The samples were centrifuged at 700 × g for 10 min, the pellet was discarded and the supernatant was transferred to a new pre-chilled tube. The supernatant was centrifuged at 8,000 × g for 15 min and the mitochondrial pellet was washed in the supplied Wash Buffer at 12,000 × g for 5 min. After isolation, the mitochondrial pellets were resuspended in PBS (without Ca^{2+} and Mg^{2+}) and used directly for the mitochondrial import assay or they were lysed in the mitochondrial lysis buffer and stored at -20°C.

4.1.9 Isolation of cytoplasmic fractions

Brains from wild-type mice at the age of four weeks were homogenized in PBS (without Ca^{2+} and Mg^{2+}, 1 ml PBS per brain). Homogenates were centrifuged at 1,000 × g for 10 min at 4°C. The pellets containing the nuclear fraction were discarded. The supernatants were centrifuged at 17,000 × g for 20 min at 4°C and afterwards centrifuged at 100,000 × g for 45 min at 4°C. The resulting supernatants were stored at -20°C and then used as cytoplasmic fractions.

4.1.10 Mitochondrial *in vitro* import assay

The *in vitro* import assay was performed with cytoplasmic fractions from wild-type mice and with mitochondrial fractions from L1-deficient mice derived from the same litter. The fractions were mixed and incubated at 37°C under constant agitation for 1 h in absence or presence of antibodies, which were used to block the import or as control antibodies. The antibodies against TOM70, TOM40 or L1 (H200) (Santa Cruz Biotechnology) and non-immune control antibodies (IgGs) were used at a concentration of 30 µg/ml and were directly added to the samples before the incubation started. After the incubation, the samples were centrifuged at 12,000 × g for 10 min to re-isolate the mitochondria, the pellets were resuspended in PBS (without Ca^{2+} and Mg^{2+}) and non-treated or treated with 0.05% trypsin-0.02% EDTA (diluted 1:5 in PBS without Ca^{2+} and Mg^{2+}) to digest proteins on the outside of the mitochondria for 5 min at room temperature in absence or presence of 1% Triton X-100 (T. H. Geyer) to permeabilize the outer mitochondrial membrane followed by an incubation with 1 mg/ml trypsin inhibitor for 5 min at room temperature. The samples which were not incubated with Triton X-100 were centrifuged at 12,000 × g for 10 min. The resulting pellet was resuspended in mitochondrial lysis buffer containing protease inhibitor cocktail (Roche Diagnostics) and centrifuged at 12,000 × g for 10 min. The supernatants containing mitochondrial proteins were stored at -20°C for further analyses.

4.1.11 Mitochondrial enzymatic assays

Mitochondria were isolated from brains (one brain for each isolation) of L1-deficient mice and wild-type littermates at the age of two months with the Mitochondria Isolation Kit for Tissue (ThermoFisher Scientific). All steps were performed on ice or at 4°C and used buffers were provided by the manufacturer. Similar protein concentrations were used for each assay. Before complex II/III, complex IV and the ATP synthase activity assays were performed, mitochondrial lysates underwent two freeze-thaw cycles in liquid nitrogen.

4.1.11.1 Complex I Assay

Measurement of the activity of complex I of the electron transport chain was performed with the Mitochondrial Complex I Activity Assay Kit (Merck Chemicals). The activity of complex I is determined by measuring the oxidation of NADH to NAD^+ in an isolated mitochondrial system. Complex I is immunocaptured within the wells of

a microplate and its activity is determined by following the oxidation of NADH to NAD^+. Proteins from mitochondrial lysates were extracted with the detergent supplied in the kit. The samples were mixed, incubated on ice for 30 min and centrifuged at 12,000 × g for 20 min at 4°C. The supernatant was collected and the samples were diluted to the desired concentration in incubation solution. The samples were added to the wells containing complex I capture antibodies and incubated for 3 h at room temperature. After incubation, the wells were emptied and the strips were washed twice in the supplied washing buffer. The assay solution containing NADH and the 100x dye were added and the generation of NAD^+ was measured at 450 nm with a kinetic program for 30 min using the µQuant™ microplate spectrophotometer.

4.1.11.2 Complex II/III Assay

Activity of Complex II/III of the electron transport chain was measured with the MitoCheck Complex II/III Activity Assay Kit (Biomol). The activity of complex II/III is determined by measuring the complex III-dependent reduction of cytochrome *c* in an isolated mitochondrial system. This reaction depends also on complex II, therefore this assay is also sensitive to complex II inhibitors. The assay solutions A and B were prepared according to the manufacturer's protocol. Solution A containing the Complex III Activity Assay Buffer, 1 mM rotenone, 100 mM potassium cyanide and the isolated mitochondria were mixed with solution B containing Complex III Activity Assay Buffer, Succinate Assay Reagent and Cytochrome *c* Assay Reagent. The reaction was measured at 550 nm in the kinetic read mode for 15 min using the µQuant™ microplate spectrophotometer.

4.1.11.3 Complex IV Assay

Activity of complex IV of the electron transport chain was determined with the MitoCheck Complex IV Activity Assay Kit (Biomol). The complex IV activity is determined by measuring the oxidation rate of reduced cytochrome *c* using an isolated mitochondrial system. The assay solutions A and B were prepared according to the manufacturer's protocol. Solution A containing Complex IV Activity Assay Buffer and the isolated mitochondria were mixed with solution B containing Complex IV Activity Assay Buffer and Reduced Cytochrome *c* Assay Regent. The reaction was measured at 550 nm in the kinetic read mode for 15 min using the µQuant™ microplate spectrophotometer.

4.1.11.4 Complex V assay

Activity of the ATP synthase of the electron transport chain was measured with the MitoCheck Complex V Activity Assay Kit (Biomol). The ATP synthase converts ATP to ADP and ADP is used by pyruvate kinase to convert phosphoenolpyruvate into pyruvate while generating ATP. Pyruvate is reduced by NADH and lactate dehydrogenase. This assay measures the rate of NADH oxidation using an isolated mitochondrial system. The assay solutions A and B were prepared according to the manufacturer's protocol. Solution A containing the Complex V Activity Assay Buffer, 1 mM rotenone and the isolated mitochondria were mixed with solution B containing Complex V Assay Enzyme Mix, Complex V ATP Reagent and Complex V NADH Reagent according to the manufacturer's protocol. The reaction was measured at 340 nm in the kinetic read mode for 15 min using the µQuant^{TM} microplate spectrophotometer.

4.1.12 Immunoprecipitation

Immunoprecipitation was performed with 40 µl Protein A/G plus agarose beads (Santa Cruz Biotechnology) and an antibody amount of 5 µg. All steps were carried out on ice or at 4°C. The mitochondrial lysates (total 2.5 mg/ml, 300 µl per condition) were incubated for 2 hours with the appropriate antibody and incubated overnight with the Protein A/G plus agarose beads. The samples were washed three times with PBS (without Ca^{2+} and Mg^{2+}) by centrifugation at 1,000 × g for 5 min, resuspended in 50 µl 5x SDS sample buffer and boiled at 95°C for 5-10 min. The samples were stored at -20°C or directly applied to SDS-PAGE.

4.1.13 ELISA

Recombinant proteins were diluted in PBS (with or without Ca^{2+} and Mg^{2+}) to a concentration of 5 µg/ml and immobilized in a volume of 25 µl/well on a 384-well high-binding polystyrene plate (Corning) overnight at 4°C. The following steps were all performed at room temperature. To show an interaction of the intracellular domain of L1 and NDUFV2, PBS containing Ca^{2+} and Mg^{2+} was used, whereas PBS without Ca^{2+} and Mg^{2+} was used to show binding of L1 to nuclear receptors. The next day, the plate was washed once for 30 sec with PBS (with or without Ca^{2+} and Mg^{2+}), blocked with 2% BSA in PBS (with or without Ca^{2+} and Mg^{2+}) for 1 h and washed once for 30 sec with PBS (with or without Ca^{2+} and Mg^{2+}). The ligand - either a nuclear extract obtained from cerebellar granule cells (total 800 µg/ml, 15 µl/well) or

the intracellular domains of L1 or CHL1 (total 5-100 µg/ml, 10 µl/well) - was added and the plate was incubated for 1 h. Afterwards the plate was rinsed two times for 10 sec and 3 times for 5 min with PBS-T (with or without Ca^{2+} and Mg^{2+}). The primary antibody (diluted 1:100 in PBS with or without Ca^{2+} and Mg^{2+}) was applied for 1 h, the plate was washed 3 times for 5 min with PBS-T (with or without Ca^{2+} and Mg^{2+}) and incubated for 1 h with a HRP-conjugated secondary antibody (diluted 1:2,000 in PBS with or without Ca^{2+} and Mg^{2+}). The plate was washed again two times for 10 sec and 3 times for 5 min with PBS-T (with or without Ca^{2+} and Mg^{2+}). The HRP-substrate OPD (ThermoFisher Scientific) was added in a concentration of 1 mg/ml and the plate was incubated for 0.5-5 min in the dark. The color reaction was stopped with 2.4 M sulphuric acid and the absorption was measured at 492 nm using the µQuant™ microplate spectrophotometer.

4.2 Molecular biology methods

4.2.1 Streaking a plate from an Addgene stab culture

The plasmids mito-dendra2 and EGFP-LC3 (Addgene Inc.) were sent as transformed bacteria (DH5α) in a stab culture format. Stab cultures were streaked onto a LB agar plate with the appropriate antibiotic (100 µg/ml ampicillin or 50 µg/ml kanamycin). The plate was incubated overnight at 37°C and at the next day a single colony was picked, used to inoculate 400 ml LB medium with the appropriate antibiotic and incubated as an overnight liquid culture under constant agitation (250 rpm) at 37°C. The inoculated culture was used for large scale plasmid isolation at the next day. To create a glycerol stock, a small volume (1-2 ml) of the overnight culture was mixed with 50% glycerol (T.H. Geyer) solution (ratio 1:1) in a cryotube. The 50% glycerol solution was prepared in dH_2O. The glycerol stock was stored at -80°C.

4.2.2 Large scale plasmid isolation (Maxiprep)

To prepare large quantities of plasmid DNA the NucleoBond Xtra kit (Macherey-Nagel) was used. Isolation was done according to the manufacturer's protocol. In brief, bacteria were harvested at 6,000 × g for 15 min at 4°C, resuspended and lysed using the buffers RES and LYS for 5 min at room temperature. The lysate was neutralized with buffer NEU and after equilibration of the filter columns with buffer EQU, lysate was loaded onto the filter columns and cleared by gravity flow. The filter columns were washed with buffer EQU and buffer WASH. The elution step was performed with buffer ELU and the eluted plasmid DNA was precipitated with

isopropanol (T. H. Geyer) at 15,000 × g for 30 min at 4°C. The plasmid DNA was washed with 70% ethanol (T. H. Geyer) by centrifugation at 15,000 × g for 5 min, dried at room temperature and resuspended in Dnase and Rnase free dH_2O. The concentration was determined using the NanoDrop 1000 spectrophotometer (ThermoFisher Scientific, Germany). The pure plasmid DNA was stored at -20°C.

4.3 Cell culture methods and assays

4.3.1 Coating with poly-L-lysine

Sterile plastic cell culture plates (6-, 12-, 24-well, Greiner) or sterile glass coverslips (12 and 22 mm, Carl Roth) were coated with 0.01% PLL and incubated overnight at 4°C with gentle shaking. After incubation, PLL was removed and the surface was dried for 30 min under UV-light.

4.3.2 Primary cell culture

4.3.2.1 Preparation and cultivation of cerebellar granule cells

For preparation of cerebellar granule cells, six to eight days old wild-type and L1-deficient mice derived from the same litter were used. The cerebella were excised and placed in a petri dish with ice-cold HBSS (PAN Biotech). Under the stereomicroscope cerebella were cleaned from blood vessels and moved into a new petri dish with ice-cold HBSS. The following steps were all performed under sterile conditions in a laminar flow hood. For cell separation cerebella were cut into three pieces and washed with ice-cold HBSS. Afterwards trypsin/Dnase solution was added, the cerebella were incubated for 15 min at room temperature or 37°C and then washed three times with ice-cold HBSS. Dnase solution was added and the cerebella were homogenized by pipetting up and down in a fire polished Pasteur pipet and centrifuged for 15 min at 100 × g and 4°C. The cell pellet was resuspended in pre-warmed X1-medium without serum. An aliquot of the cell suspension was mixed in a ratio of 1:2 with 0.4% trypan blue solution to determine the cell number with a hemocytometer. The cells were diluted to a cell number of 1-2 × 10^5 cells/ml (neurite outgrowth) or 1-2 × 10^6 cells/ml (all other experiments), seeded on PLL coated 6-well-plates or glass coverslips and cultured for at least 24 h at 37°C, 5% CO_2 and 90% relative humidity.

4.3.2.2 Preparation and cultivation of hippocampal neurons

For preparation of hippocampal neurons newly born to two days old wild-type or L1-deficient mice derived from the same litter were used. The hippocampi were removed, placed in a petri dish with ice-cold dissection solution and cleaned under the stereomicroscope. The hippocampi were cut into 1 mm big pieces and washed once with ice-cold dissection solution. Digestion solution with trypsin/Dnase was added and the hippocampi were incubated for 5 min at room temperature. The digestion solution with trypsin/Dnase was removed and the hippocampi were washed once with ice-cold dissection solution, and then incubated with the dissection solution containing trypsin inhibitor for 5 min at room temperature. The hippocampi were washed twice with ice-cold dissection solution, homogenized in dissection solution containing Dnase solution and centrifuged for 15 min at 4°C and 100 × g. The cell pellet was dissolved in hippocampal medium without serum and an aliquot of the cell suspension was mixed in a ratio of 1:2 with 0.4% trypan blue solution to determine the cell number with a hemocytometer. The cells were diluted to a cell number of 1-2 × 10^6 cells/ml, seeded on PLL coated 6-well-plates or glass coverslips and cultured at 37°C, 5% CO_2 and 90% relative humidity for up to five days.

4.3.3 Cultures of HEK293 cells

Frozen HEK293 cells from long-term storage were taken out of liquid nitrogen storage, thawed at 37°C and transferred to pre-warmed DMEM (Gibco). The cells were cultured in DMEM supplemented with 5% serum at 37°C, 5% CO_2 and 90% relative humidity. After reaching a confluence of 70-90%, the cells were passaged by washing with pre-warmed HBSS and trypsinized with trypsin-EDTA solution. Cells were taken up in pre-warmed HBSS and cells were centrifuged at 1,000 × g for 5 min at room temperature, resuspended in pre-warmed DMEM and split in a ratio of 1:3 to 1:10 depending on the growth of the cells. To prepare HEK293 cells for long-term storage, cells at a confluence of 70-90% were washed, trypsinized, diluted in DMEM and centrifuged at 1,000 x g for 5 min. The cell pellet was resuspended in freezing solution. The cells were transferred into cryotubes and to cryoboxes containing isopropanol (room temperature warm). The cryoboxes were kept for three to four days at -80°C and then the cryotubes were transferred to a liquid nitrogen tank for long-term storage.

4.3.4 Transduction of cells with AAV1

Cells were immediately transduced after seeding with a multiplicity of infection (MOI) of 1,000 for 1-2 × 10^6 cells/ml. For transduction AAV1 carrying wild-type L1 ($AAV1^{wt\text{-}L1}$), L1 mutated in the MBP cleavage site ($AAV1^{R/A\text{-}L1}$), L1 with a mutation of L_{1136}LILL to A_{1136}LIAA and F_{1046}HILF to Y_{1046}HIAY ($AAV1^{mut\text{-}L1}$) and an empty virus were used. The cells were cultured in the incubator at 37°C, 5% CO_2 and 90% relative humidity.

4.3.5 Transient transfection of HEK293 cells

HEK293 cells were seeded at a density of 1-2 × 10^6 cells/ml on PLL-coated glass coverslips and grown until they reached a density of 70-90%. Transfection was performed according to the manufacturer's manual. 6 µl of Lipofectamine® LTX Reagent (ThermoFisher Scientific) was mixed with serum-free DMEM, incubated for 5 min, then mixed with 5 µg of the appropriate plasmid (EGFP-LC3, mito-dendra2) and 4 µl of PLUS™ Reagent (ThermoFisher Scientific). The mixture was incubated for 30 min at room temperature until it was directly applied in the cell medium. Cells were cultured for at least three days at 37°C, 5% CO_2 and 90% relative humidity.

4.3.6 Isolation of nuclear extracts from cerebellar granule cells for ELISA

Cerebellar granule cells from non-transduced L1-deficient mice and L1-deficient mice transduced with AAV1 carrying wild-type L1 or mutant L1 were cultured for at least 24 h. At the next day, cells were stimulated with mouse L1-Fc (10 µg/ml) for 2 h at 37°C and the nuclear extract was isolated with the subcellular fractionation kit for cultured cells (ThermoFisher Scientific) as described in the manufacturer's protocol. In brief, after stimulation and removal of the medium cells were treated with four different solutions (CEB, MEB, NEB, NEB plus calcium chloride and micrococcol nuclease) containing 1x protease inhibitor. All steps were carried out on ice or at 4°C. First, the cells were incubated with the solution CEB for 10 min with gentle mixing. The cells were scraped off and centrifuged at 500 × g for 10 min. The supernatant was saved at -20°C as the cytoplasmic fraction. The resulting pellet was mixed with MEB solution for 5 sec and the mixture was incubated for 10 min with constant agitation. The samples were centrifuged at 3,000 × g for 10 min and the supernatant containing the membrane extract was saved at -20°C. The resulting pellet was treated with NEB solution, mixed for 15 sec and incubated for 1 h with constant agitation. The samples were centrifuged at 5,000 × g for 10 min and the soluble nuclear extract was kept on ice. In the next step the samples were treated with NEB containing calcium chloride

and micrococcol nuclease, mixed and incubated for 10 min at 37°C. The samples were centrifuged at 16,000 × g for 5 min and the supernatant (chromatin-bound nuclear extract) was pooled with the soluble nuclear extract. The pooled nuclear samples were stored at -20°C and used for further analysis.

4.3.7 Isolation of nuclear extracts from cerebellar granule cells for Western blot analysis

Preparation of nuclear extracts was performed in collaboration with David Lutz (ZMNH, Universitätsklinikum Hamburg-Eppendorf, Germany). Cerebellar granule cells from wild-type or non-transduced L1-deficient mice and L1-deficient mice which were transduced with AAV1 carrying wild-type L1 or mutant L1 were cultured for at least 24 h. The cells were scraped after addition of HBSS to the cells and centrifuged at 3,000 x g for 5 min at 4°C. The pellet was resuspended in RIPA buffer and incubated for 5 min on ice. The solution was centrifuged at 3,000 x g for 5 min at 4°C, the cytoplasmic fraction was stored at -20°C for further analysis and the pellet was resuspended in urea lysis buffer. The resuspended pellet was incubated for 30 min on ice, centrifuged at 20,000 x g for 10 min at 4°C and the supernatant containing the nuclear lysate was directly used for further analysis or stored at -20 °C.

4.3.8 Determination of the energetic status of mitochondria

For monitoring the energetic status of mitochondria, the cell-based assay MITO-ID® Membrane Potential Detection (Enzo Life Sciences) was used. Depending on the functional status of mitochondria, the cationic carbocyanine dye (Detection Reagent) fluoresces either green or orange. In polarized cells, the Detection Reagent accumulates as an orange fluorescent aggregate in mitochondria, whereas it exists also as a green fluorescent monomer in the cytosol. The loss of the mitochondrial membrane potential leads to accumulation of green-fluorescent monomers in the cytosol.

HEK293 cells, which were transduced with AAV1 carrying wild-type L1, mutant L1R/A or an empty virus or cerebellar neurons from wild-type and L1-deficient mice derived from the same litter, which were seeded on glass coverslips with a diameter of 12 mm, were maintained at least for three days at 37°C, 5% CO_2 and a relative humidity of 90%. Reagents were prepared as described in the manufacturer's manual and direct exposure of the reagents to intense light was avoided. For performing the

assay, 1x assay solution was prepared by diluting 10x assay buffer 1 and 50x assay buffer 2 in dH_2O. The cells were washed twice with 1x assay solution and the Dual Detection reagent (1 ml 1x assay solution, 10 µl MITO-ID® MP Detection Reagent) was applied. Cells were incubated for 15 min at room temperature, washed with 1x assay solution and the living cells were observed under a laser scanning confocal microscope with a 60x objective (Olympus FluoView TMFV1000, Germany). For detection of energized mitochondria with high mitochondrial membrane potential a rhodamine filter set was used and for detection of depolarized mitochondria with low mitochondrial membrane potential a fluorescein filter set was used.

4.3.9 Neurite outgrowth assay

Neurite outgrowth assay was performed in collaboration with Hardeep Kataria (ZMNH, Universitätsklinikum Hamburg-Eppendorf, Germany). For measuring the neurite outgrowth, dissociated cerebellar neurons from L1-deficient mice were transduced with AAV1 carrying wild-type L1 or mutant L1 and seeded on PLL-coated coverslips in a density of 1-2.5 x 10^5 and placed in 12-well-plates. The cells were cultured in 1 ml of the appropriate medium for 24 h at 37°C, 5% CO_2 and 90% relative humidity. For fixing, cells were treated with 100 µl 25% glutaraldehyde for 1 h at room temperature. Cells were washed with PBS and stained with 1% toluidine blue and 1% methylene blue in 1% sodium-tetraborate buffer for 2 h at room temperature. After the cells were washed three times with water, the coverslips were placed onto a filter paper and dried at room temperature. Eukitt mounting solution (Fluka) was used to mount the coverslips on objective slides and the mounting solution was allowed to harden overnight. Cells were imaged with a AxioVert microscope (Carl Zeiss, Germany) and their neurite length was measured using the ImageJ software.

4.4 Histological methods

4.4.1 Labeling of mitochondria

Labeling of mitochondria was done with MitoTracker® Red CMXRos (ThermoFisher Scientific). 1 mM MitoTracker stock solution was diluted to the final concentration of 100 nM in the appropriate pre-warmed medium. Adherent cells (density of 1-2 × 10^6 cells/ml, at least three days in culture) on glass coverslips were washed once with HBSS (with phenol red, without Ca^{2+} and Mg^{2+}) or dissection solution and incubated with pre-warmed staining solution containing MitoTracker® Red CMXRos for 30 min at 37°C. The staining solution was replaced by the appropriate amount of pre-

warmed medium. Cells were used either for fixation and staining of nuclei or directly for time-lapse video microscopy of live cells.

4.4.2 Fixation of cells and staining of nuclei

After labeling of mitochondria with MitoTracker® Red CMXRos, the medium was aspirated and the cells were treated with 4% PFA solution (Carl Roth) for 20 min at room temperature. After fixation, cells were washed once in PBS (without Ca^{2+} and Mg^{2+}) and mounted with mounting solution containing the nuclear marker 2-(4-Amidinophenyl)-1H-indole-6-carboxamidine (DAPI, Roti-Mount® FluorCare DAPI, Carl Roth). Fixed cells were kept at 4°C until they were used for mitochondrial analysis.

4.4.3 Paraffin tissue processing

Brains from mice, which were used for behavioral studies were removed, fixed in 4% parafomaldehyde (Carl Roth) solution containing cacodylate (Carl Roth) and incubated for 5 hours in PBS, under gentle agitation at room temperature. For dehydration of the tissue a series of graded ethanol baths was used, starting with an incubation in 70% ethanol overnight and followed by incubation in 80%, 90% and four times in 100% ethanol at room temperature for 1 h each. Afterwards, the tissue was incubated 2 times in xylene (Sigma-Aldrich) for 2 hours. The wax infiltration started with an incubation of the tissue with liquid paraffin wax at 62°C overnight. The liquid paraffin wax was exchanged and the tissue was again incubated at 56°C overnight. After infiltration the tissue was formed into paraffin blocks and stored at room temperature until it was used for section cutting. The cutting of 10 µm thick sections was performed by Ahmed Sharaf (ZMNH, Universitätsklinikum Hamburg-Eppendorf, Germany).

4.4.4 Immunohistochemistry using paraffin-embedded tissue sections

For deparaffinization and rehydration, sections with a thickness of 10 µm were treated three times with xylene for 5 min followed by consecutive treatments for 5 min with 100%, 90% and 70% ethanol. The sections were washed in dH_2O, in a 1:2 mixture of dH_2O and PBS and in PBS alone for 10 min. All steps of deparaffinization, rehydration and washing were performed at room temperature.

For antigen retrieval the sections were boiled in 0.1 M sodium citrate buffer (pH 6.0) for 2-5 min in a microwave and cooled down at room temperature for 20 min. The

following steps were all performed at room temperature. The sections were washed two times in PBS, incubated with methanol (T. H. Geyer) for 15 min and washed again with PBS for 5 min. Permeabilization and blocking was done with blocking solution with normal donkey serum containing 1% Triton X-100 for 1 h. The blocking solution was removed and the primary antibody (diluted 1:100 in blocking solution) was applied overnight at 4°C in a humidified chamber. The sections were washed three times with PBS, the fluorescently labeled secondary antibody (diluted 1:200 in blocking solution) was applied and the sections were incubated for 1 h in the dark at room temperature. Afterwards the sections were washed three times for 10 min with PBS and incubated for 10 min with DAPI solution. The sections were washed once with PBS and mounted with Dako Fluorescent Mounting Medium S3023 (Dako). The sections were kept for 30 min at room temperature and then stored at 4°C. Imaging of the samples was performed by David Lutz (ZMNH, Universitätsklinikum Hamburg-Eppendorf, Germany).

4.5 Microscopy and image analysis

4.5.1 Fluorescence imaging

Fluorescence imaging was performed using the Olympus FluoView TMFV1000 (Olympus, Germany) laser scanning confocal microscope with a 60x objective. For simultaneous double-channel fluorescence, images were taken in a sequential scanning mode. Images were adjusted for brightness and contrast using Adobe Photoshop CS5 software (Adobe Systems Inc.).

4.5.2 Co-localization analysis

Co-localization of mitochondria with EGFP-LC3 was analyzed using the ImageJ software. The co-localization tool JACoP (Just Another Colocalization Plugin) from ImageJ was used to determine the Pearson's Coefficient (PC). This coefficient describes the linear correlation between intensities of each channel in each pixel. Its value can range from 1 to −1, with 1 representing complete positive correlation and −1 negative correlation, with zero representing no correlation (Bolte and Cordelieres, 2006). Pixel grey values of two different channels (green/red) were plotted against each other and a pixel distribution diagram was generated, which was used to calculate the PC.

4.5.3 Cell fluorescence analysis

The level of the fluorescence intensity in a given region of a green or orange channel was analyzed by calculating the corrected total cell fluorescence (CTCF) with the ImageJ software. CTCF was determined with the formula (McCloy et al., 2014):

CTCF = integrated density – (area of selected cell x mean fluorescence of background readings)

The level of the fluorescence intensity was used to quantify the energetic status of mitochondria with the cell-based assay MITO-ID® Membrane Potential Detection (Enzo Life Sciences).

4.5.4 Time-lapse video microscopy

Imaging was carried out with an upright microscope (Nikon Instruments, Netherlands) combined with Spinning Disk (Yokogawa, Germany) live cell confocal technology (Visitron Systems, Germany). For single-channel live imaging a 561 nm laser was used. Images were taken at intervals of 2 seconds for a duration of 5 minutes. For image acquisition, a 60x objective was used. During time-lapse imaging cells were kept in X-1 medium without serum (cerebellar neurons) or dissection solution (hippocampal neurons) with controlled temperature (37°C) and CO_2 concentration (5%). Videos at the microscope stage were acquired using the VisiView software (Visitron Systems).

4.5.5 Kymograph analysis

Mitochondrial dynamic parameters were analyzed using the ImageJ software. Determination of motility, mobility and direction of the transport (anterograde/retrograde) of mitochondria were performed using the kymograph (time space plot) plugin from ImageJ (Rietdorf and Seitz, 2008).

First, a segmented line was drawn in a region of interest in the time-series, where mitochondrial movement was visible. In the next step, grey values along a segmented line for each frame of the time-series were generated using the kymograph plugin to create a new image (kymograph). The kymograph showed a horizontal line on top, which represented the first time point, while later time points were shown below that line. The kymograph is a time space plot, where the x-axis

indicates the distance and the y-axis shows the time. Vertical lines represent no movement, while diagonal lines show dynamic mitochondria. The direction (right/ left) of diagonal lines indicates retrograde or anterograde transport, depending on the position of the cell soma (Marra et al., 2015). To calculate the motility of moving mitochondria, segmented lines were drawn along the diagonal lines of the kymograph and the velocity tool from ImageJ (Rietdorf and Seitz, 2008) was used for quantification of the motility.

4.5.6 Fluorescence recovery after photobleaching (FRAP)

Time-lapse-video microscopy was performed as described before. Additionally a 488 nm laser was used with a very low intensity (1%) to obtain a clear image of the green fluorescent (non-photoconverted) mito-dendra2-expressing cells. Positively transfected cells were chosen and irreversible photoconversion of mito-dendra2 from its green to red fluorescent state was achieved by exposure of a defined region of interest to UV-laser (405 nm) at 2%. During time-lapse video microscopy, frames were captured every 2 sec for 5 min in a green and red channel mode. Images were analyzed with the ImageJ software by determination of the area of fused mitochondria in the defined region of interest.

4.6 Behavioral tests

4.6.1 Rotarod test

Twelve weeks old wild-type or L1-deficient mice and L1-deficient mice, which were transduced with AAV1 carrying wild-type L1 or mutant L1 *in utero* at embryonic day 16, were placed in position on a 3 cm diameter rod (Rota-rod for mice, UGO BASILE S.R.L., Germany), which was set in motion before the mice had to walk. Mice underwent three training trials and five test trials. The training trials were performed on the same day with a slow, constant rotating speed at 4 rpm for a maximum duration of 1 min. After every training trial, the training was stopped for an inter-trial interval of 10 min and then continued with the next training phase. The test trials were performed on five consecutive days every morning and afternoon in an acceleration mode of the rod, starting with 4 rpm up to 40 rpm within 300 sec. At the end the running time (latency) and the instrument rotation speed, at the time the mouse falls off, was recorded.

4.6.2 Pole test

Twelve weeks old wild-type or L1-deficient mice and L1-deficient mice, which were transduced with AAV1 carrying wild-type L1 or mutant L1 *in utero* at embryonic day 16, were placed head-upward on top of a vertical 48.5 cm long pole made of rough wood and the time needed to climb down the vertical pole was measured on five consecutive days. Each day every mouse had to repeat the test trial three times with making a break of 30 sec between each test trail.

4.6.3 Grip strength test

Twelve weeks old wild-type or L1-deficient mice were hold by the tail and the strength of the forelimbs was measured. The strength was measured with a Grip Strength Meter system (TSE Systems, Germany) while the mice grasped to a grip bar attached to a dynamometer. The maximal force the mice needed to hold on the grip bar until the mice released the grip was noted. Mice were tested twice, before and directly after performing the Rotarod and pole test.

4.7 Statistical analysis

All numerical data are presented as group mean values with standard error of the mean (S.E.M.). Statistical tests used for comparisons are indicated in the text and figure legends. Analyses were performed using the SigmaPlot version 12.5 software.

5 RESULTS

5.1 L1-70 is imported into mitochondria and influences mitochondrial characteristics

5.1.1 L1-70 is imported into mitochondria

Previously the interaction of L1 with GAPDH and with ANT1 and ANT2 at the cell surface of neurons was described (Makhina et al., 2009, Loers et al., 2012). GAPDH binds to the Ig-like domains I-VI and the fibronectin type III homologous repeats 4-5 in L1. GAPDH is not only localized at the cell surface of neuronal cells, but also in mitochondria and plays an essential role in mitochondrial function as well as in dysfunction during oxidative stress-induced cell death, pro-apoptotic mitochondrial membrane permeabilization and mitophagy (Tarze et al., 2007, Hwang et al., 2015, Nakajima et al., 2017). Furthermore, ANT1 and ANT2 present in the plasma membrane bind to the fibronectin type III domains of L1. Since GAPDH, ANT1 and ANT2 interact with L1 at the cell surface of neurons and GAPDH as well as ANT1 and ANT2 are present in mitochondria, it was tested whether L1 is imported from the cytoplasm into mitochondria to interact with mitochondrial GAPDH, ANT1 and ANT2. At first, mitochondria were isolated from brains of L1-deficient mice and their age-matched wild-type littermates, lysed and applied to Western blot analysis. Detection with an antibody against the intracellular L1 domain revealed a band of approximately 70 kDa in mitochondrial lysates from wild-type, but not L1-deficient mice (Figure 5.1 A), suggesting that L1-70 is present in brain mitochondria. Next, mitochondrial lysates were analyzed for their degree of purity using antibodies directed against marker proteins associated with the nucleus (histone H3), the endoplasmic reticulum (calregulin) and the cytoplasm (rhoA). In contrast to brain homogenates, the nuclear, endoplasmic and cytoplasmic marker proteins were not detectable in mitochondrial lysates (Figure 5.1 B-D). Thus, one can conclude that the mitochondrial fraction was not contaminated with other organelles, indicating that L1-70 is indeed present in mitochondria.

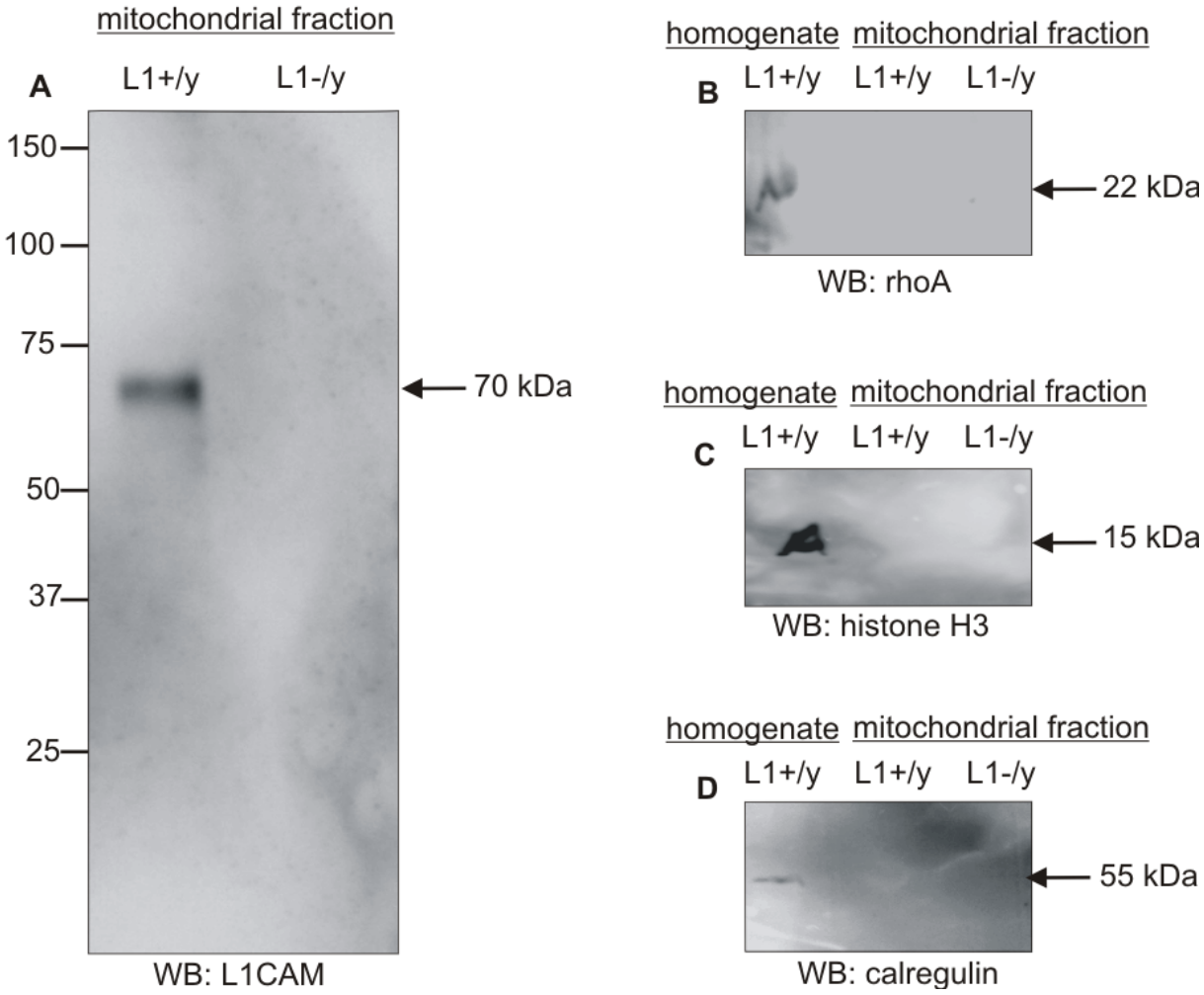

Figure 5.1: A L1 fragment of 70 kDa is localized in mitochondria. ***A***, Mitochondrial lysates were prepared from L1-deficient mice (L1-/y) and their age-matched wild-type (L1+/y) littermates and subjected to Western blot (WB) analysis. L1-70 was detected in mitochondrial lysates of wild-type littermates with the L1-specific antibody L1CAM, which recognizes an epitope (amino acid 1153-1182) within the intracellular L1 domain. A representative blot out of three independent experiments is shown. The arrow indicates L1-70. ***B-D***, Mitochondrial lysates from L1-deficient and wild-type mice and brain homogenates from wild-type mice were tested in WB analysis using specific antibodies recognizing the cytoplasmic marker rhoA (**B**), the nuclear marker histone H3 (***C***) and the endoplasmic marker calregulin (***D***). Representative blots out of three independent experiments are shown. RhoA, histone H3 and calregulin are indicated by arrows.

To examine whether L1-70 is imported from the cytoplasm into mitochondria, an *in vitro* import assay was performed. To this aim, a L1-70-containing cytoplasmic fraction isolated from brains of wild-type mice and a L1-lacking mitochondrial fraction isolated from brains of L1-deficient mice were mixed, mitochondria were re-isolated, non-treated or treated with trypsin in absence or presence of the detergent Triton X-100 and subjected to Western blot analysis. Treatment with trypsin in absence of the

detergent was done to digest proteins that are present outside of re-isolated mitochondria, whereas treatment with trypsin in presence of the detergent was done to permeabilize the mitochondrial membranes and to digest also proteins inside of mitochondria. Mitochondrial lysates from brains of wild-type and L1-deficient mice were used as positive and negative controls. Using an antibody against L1, a band of approximately 70 kDa was detected in the cytoplasmic fraction of wild-type mice, in mitochondrial lysates from wild-type mice and in lysates from the *in vitro* import assay without and with trypsinization (Figure 5.2). This result shows that the transmembrane L1-70 fragment enters mitochondria and confirms the presence of L1-70 inside of mitochondria. L1-70 was not detected in mitochondrial lysates from L1-deficient mice and in lysates from the *in vitro* import assay after trypsinization in the presence of the detergent. This result reveals that L1-70 is present inside of mitochondria and not at the surface of the outer mitochondrial membrane since it is digested by trypsin after permeabilization of the mitochondrial membrane.

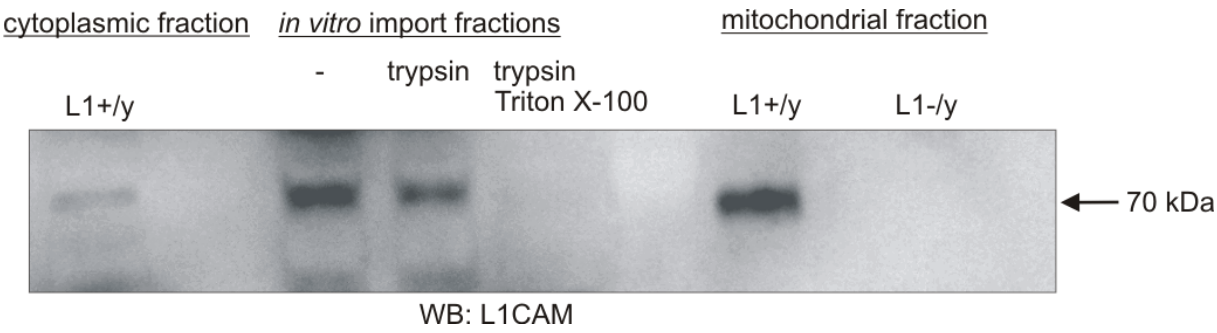

Figure 5.2: L1-70 is imported into mitochondria from the cytoplasm. Mitochondrial lysates were prepared from L1-deficient mice (L1-/y) and wild-type (L1+/y) littermates and used as controls in WB analysis. A cytoplasmic fraction was isolated from wild-type mice and a mitochondrial fraction was isolated from L1-deficient mice. For the *in vitro* import assay the cytoplasmic fraction and the mitochondrial fraction were mixed. The mitochondria were re-isolated and non-treated (-) or treated with trypsin in the absence or presence of Triton X-100. The mitochondria were lysed and subjected to protein precipitation and WB analysis with the antibody L1CAM. A representative blot out of three independent experiments is shown. L1-70 is indicated by an arrow.

Since nuclear-encoded precursor proteins with internal targeting signals for mitochondrial import are recognized at the outer mitochondrial membrane by the receptor TOM70 and TOM40 of the TOM complex (Chacinska et al., 2009), the potential binding of L1 to these receptors during *in vitro* import was analyzed. The *in vitro* import assay was performed in the presence of a TOM70- or TOM40-specific antibody to block the translocase subunit TOM70 and TOM40 and to prevent binding

of the cytoplasmic L1-70 to TOM70 or TOM40, respectively, at the outer mitochondrial membrane. As control, the *in vitro* import was performed without antibodies or with a non-immune control antibody. After incubation mitochondria were re-isolated, lysed and subjected to protein precipitation followed by Western blot analysis with a L1 antibody and a GAPDH antibody to control for loading. The levels of L1-70 and GAPDH were quantified. Western blot analysis and quantification showed that the *in vitro* import of the cytoplasmic L1-70 in mitochondria was reduced by blocking the translocase subunit TOM70, whereas no reduction of the L1-70 level was detected after incubation with a TOM40-specific antibody or a non-immune control antibody (Figure 5.3 A-D). This result suggests that TOM70 interacts with cytoplasmic L1-70 for import into mitochondria. The finding that the TOM40-specific antibody did not impede the import of L1-70 into mitochondria could be due to the fact that TOM40 is not involved in binding and/or transport of L1-70 or that the interaction of L1-70 with TOM40 is not hampered by the TOM40 antibody. In addition, the *in vitro* import was performed with an antibody against an extracellular membrane-proximal epitope in L1 to specifically block the import of L1-70 and without antibodies and/or with a non-immune control antibody. Western blot analysis and quantification of the *in vitro* import assay showed a reduction of mitochondrial L1-70 levels after application of the L1-specific antibody, but no reduction of mitochondrial L1-70 levels was detectable without antibodies and/or with a non-immune control antibody (Figure 5.3 E and F). This finding indicates that binding of the L1 antibody to cytoplasmic L1-70 blocked the import of this fragment, confirming the notion that L1-70 is imported from the cytoplasm into mitochondria.

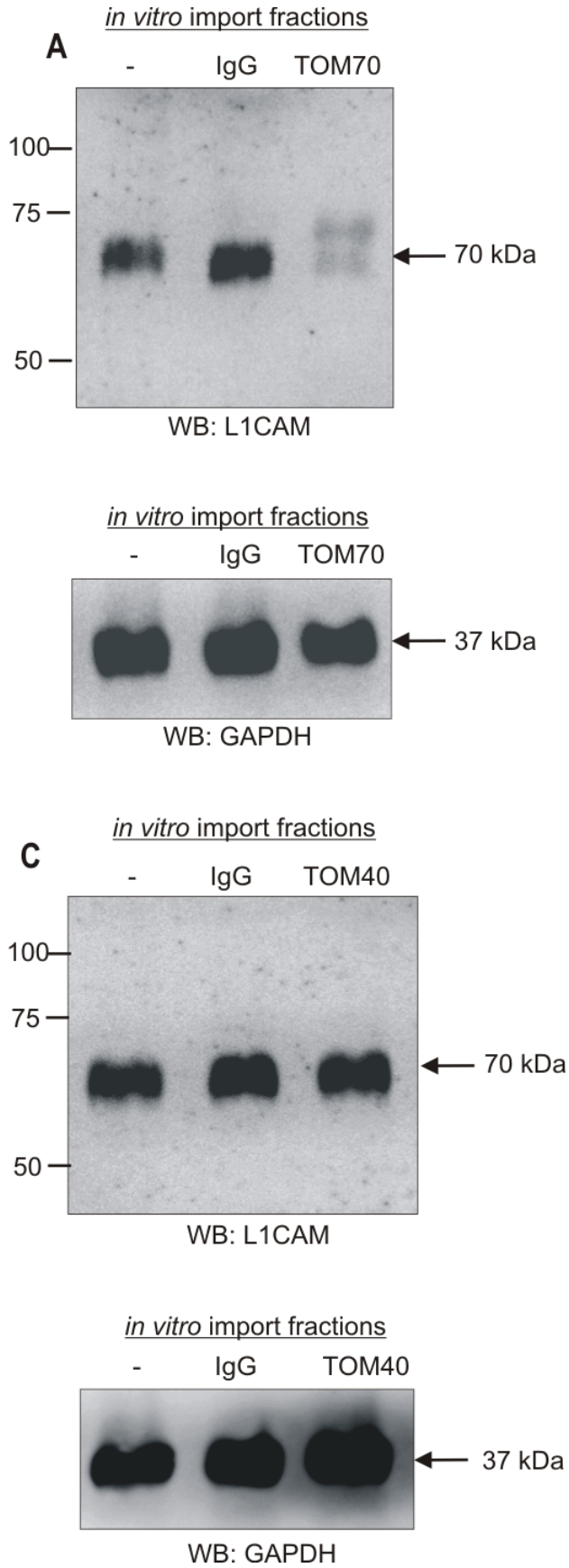
A
in vitro import fractions
-
IgG
TOM70
100
75
50
70 kDa
WB: L1CAM
in vitro import fractions
-
IgG
TOM70
37 kDa
WB: GAPDH
B
***
L1-70 level in mitochondria
1.60
1.40
1.20
1.00
0.80
0.60
0.40
0.20
0.00
-
IgG
TOM70
C
in vitro import fractions
-
IgG
TOM40
100
75
50
70 kDa
WB: L1CAM
in vitro import fractions
-
IgG
TOM40
37 kDa
WB: GAPDH
D
n.s.
L1-70 level in mitochondria
1.60
1.40
1.20
1.00
0.80
0.60
0.40
0.20
0.00
-
IgG
TOM40

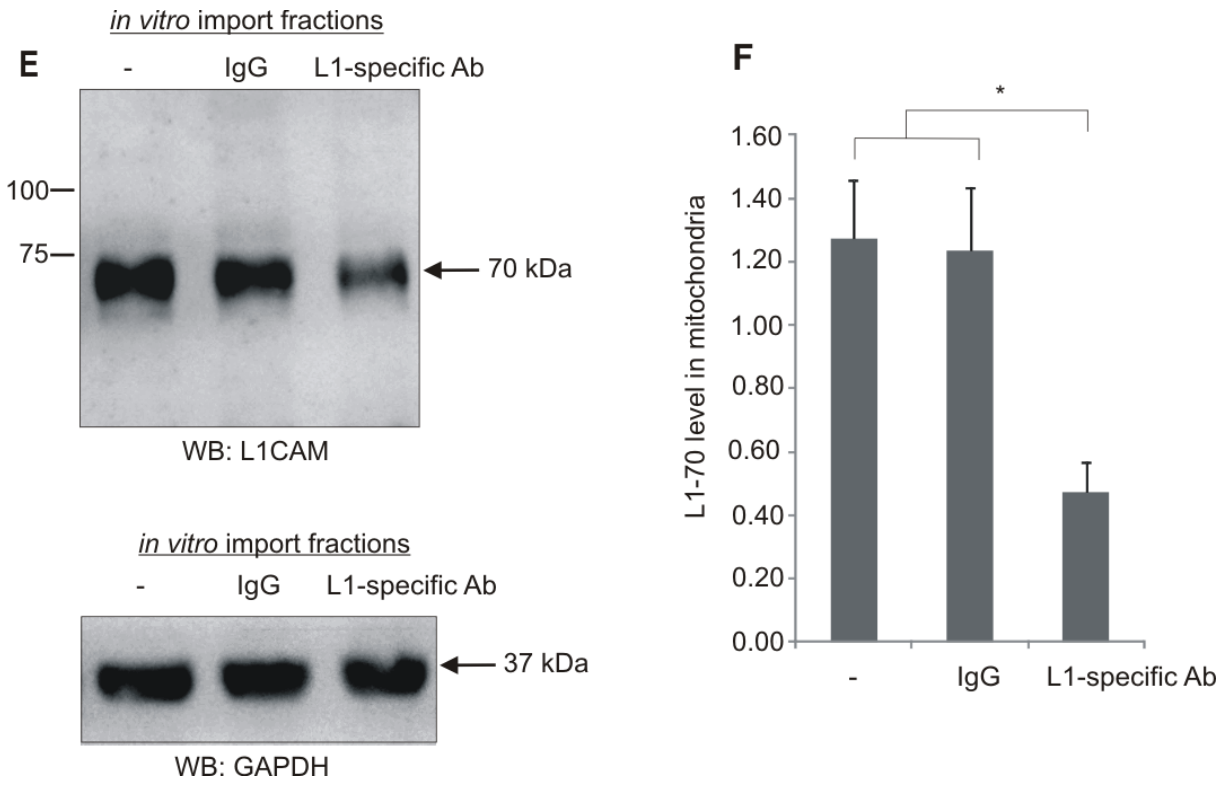

Figure 5.3: Import of L1-70 from the cytoplasm into mitochondria is reduced by application of TOM70- and a L1-specific antibody. ***A-F***, For the *in vitro* import assay, the cytoplasmic fraction from brains of wild-type mice and the mitochondrial fraction from brains of L1-deficient mice were incubated in the absence (-) or presence of a non-immune control antibody (IgG), a TOM40-specific antibody (TOM40), a TOM70-specific antibody (TOM70) or a L1-specific antibody. The mitochondria were then re-isolated and lysed. Proteins were precipitated, subjected to WB analysis and L1-70 was detected with a L1-specific antibody (L1CAM). GAPDH was detected to control for loading. ***A***, ***C*** and ***E***, Representative Western blots are shown from five independent experiments. L1-70 and GAPDH are indicated by arrows. ***B, D*** and ***F***, L1-70 and GAPDH levels were quantified using ImageJ. Mean values + S.E.M. are shown for the mitochondrial L1-70 levels relative to the GAPDH levels from five independent experiments (*** $p<0.001$; one-way ANOVA with Holm-Sidak multiple comparison test).

To verify whether L1 interacts with GAPDH after import into mitochondria, mitochondrial fractions from brains of wild-type mice or L1-deficient mice were used for immunoprecipitation with GAPDH antibody or non-immune control antibody. Western blot analysis with L1CAM antibody showed an immunopositive L1 band of approximately 70 kDa in GAPDH immunoprecipitates from wild-type brain mitochondria, but no visible immunopositive L1 band was detected in GAPDH immunoprecipitates from L1-deficient brain mitochondria nor in non-immune control immunoprecipitates from wild-type and L1-deficient brain mitochondria (Figure 5.4). Immunoprecipitation using ANT1 or ANT2 antibodies or non-immune control antibody was performed, but no L1-positive band was detected in these immunoprecipitates

(data not shown). These results indicate that L1-70 interacts with GAPDH in mitochondria but not with mitochondrial ANT1 or ANT2.

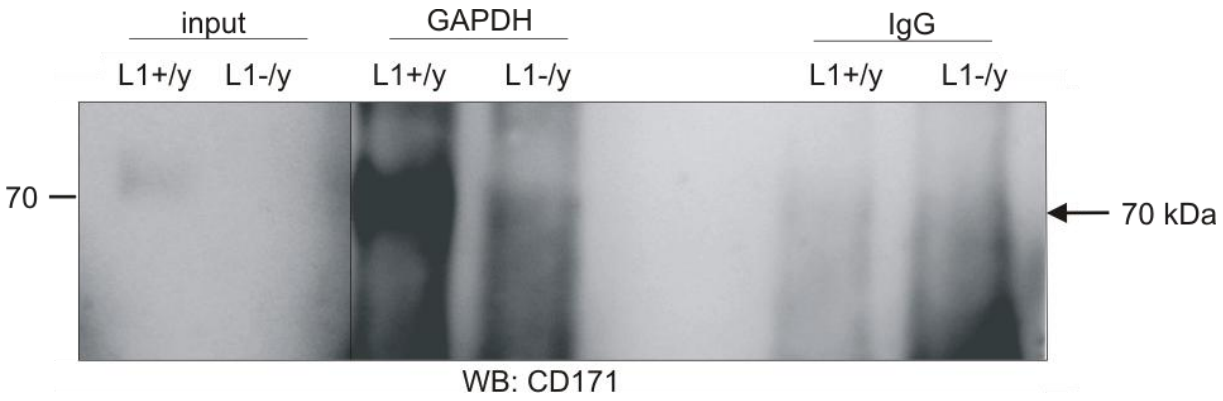

Figure 5.4: L1-70 precipitates with GAPDH. Soluble mitochondrial proteins from brains of L1-deficient (L1-/y) and wild-type (L1+/y) mice were subjected to immunoprecipitation with GAPDH antibody or a non-immune control (IgG) antibody. Mitochondrial lysates (input) and GAPDH and IgG immunoprecipitates were subjected to WB analysis with the L1CAM antibody. A representative blot out of four experiments is shown. L1-70 is indicated by an arrow. Lanes not adjacent to each other but derived from the same blot are indicated by a vertical line.

5.1.2 Ablation of L1-70 affects complex I activity and mitochondrial membrane potential

L1-70 is imported into mitochondria and in mitochondria it binds to mitochondrial GAPDH that has a regulatory function in mitochondrial oxidative phosphorylation (Ramzan et al., 2013). In order to produce ATP, mitochondria use the oxidative phosphorylation machinery that comprises the electron transport chain containing the enzymes of complex I-V of the inner mitochondrial membrane. To test whether mitochondrial L1, like GAPDH, has an influence on mitochondrial metabolism, the activities of complex I-V of the electron transport chain were analyzed. In mitochondria of L1-deficient mice complex I activity was reduced to ~51% compared to the activity in wild-type mitochondria (Figure 5.5 A). This result indicates that L1 affects complex I activity and therefore the inner mitochondrial membrane potential might be impaired. Complex I activity was also determined in mice deficient in CHL1 and NCAM which belong to the Ig superfamily and are functionally and structurally related to L1. The activity in mitochondria of CHL1-deficient and NCAM-deficient mice was not significantly altered compared to the complex I activity in mitochondria of the corresponding wild-type littermate mice (Figure 5.5 B and C).

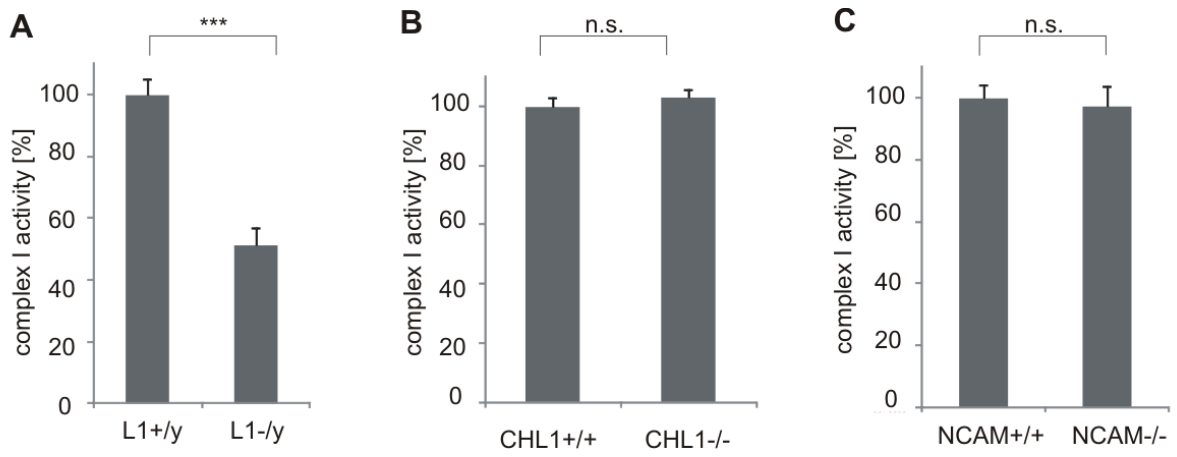

Figure 5.5: Complex I activity is reduced in mitochondria of L1-deficient mice. Mitochondria were isolated from L1-deficient (L1-/y, n=4), CHL1-deficient (CHL1-/-, n=2) and NCAM-deficient (NCAM-/-, n=4) mice and the corresponding wild-type littermates (L1+/y, n=4; CHL1+/+, n=2; NCAM+/+, n=4), the protein concentration was adjusted and the activity was determined separately for each probe by measurement of the oxidation of NADH to NAD^+ at 450 nm. Mean values + S.E.M. are shown (*** $p<0.001$; two-tailed Student's t-test).

Complex I, III and IV generate an electrochemical proton gradient across the inner mitochondrial membrane. The energy of this proton gradient is used by complex V to catalyze synthesis of ATP from ADP and inorganic phosphate (Kucharczyk et al., 2009). Complex II/III and IV activity was not different in mitochondria of L1-deficient and wild-type mice (Figure 5.6 A and D). The same results were obtained after measuring complex II/III and IV activity in mitochondria of CHL1-deficient, NCAM-deficient mice and their corresponding wild-type littermate mice (Figure 5.6 B, C and E, F), indicating that L1, CHL1 and NCAM do not influence the activity of complex II/III and IV. In addition, the results from the enzymatic assay for complex V showed no impairment of the ATP synthase activity in mitochondria of L1-deficient and wild-type mice (Figure 5. 6 G), leading to the conclusion that L1 does not affect production of ATP but complex I activity.

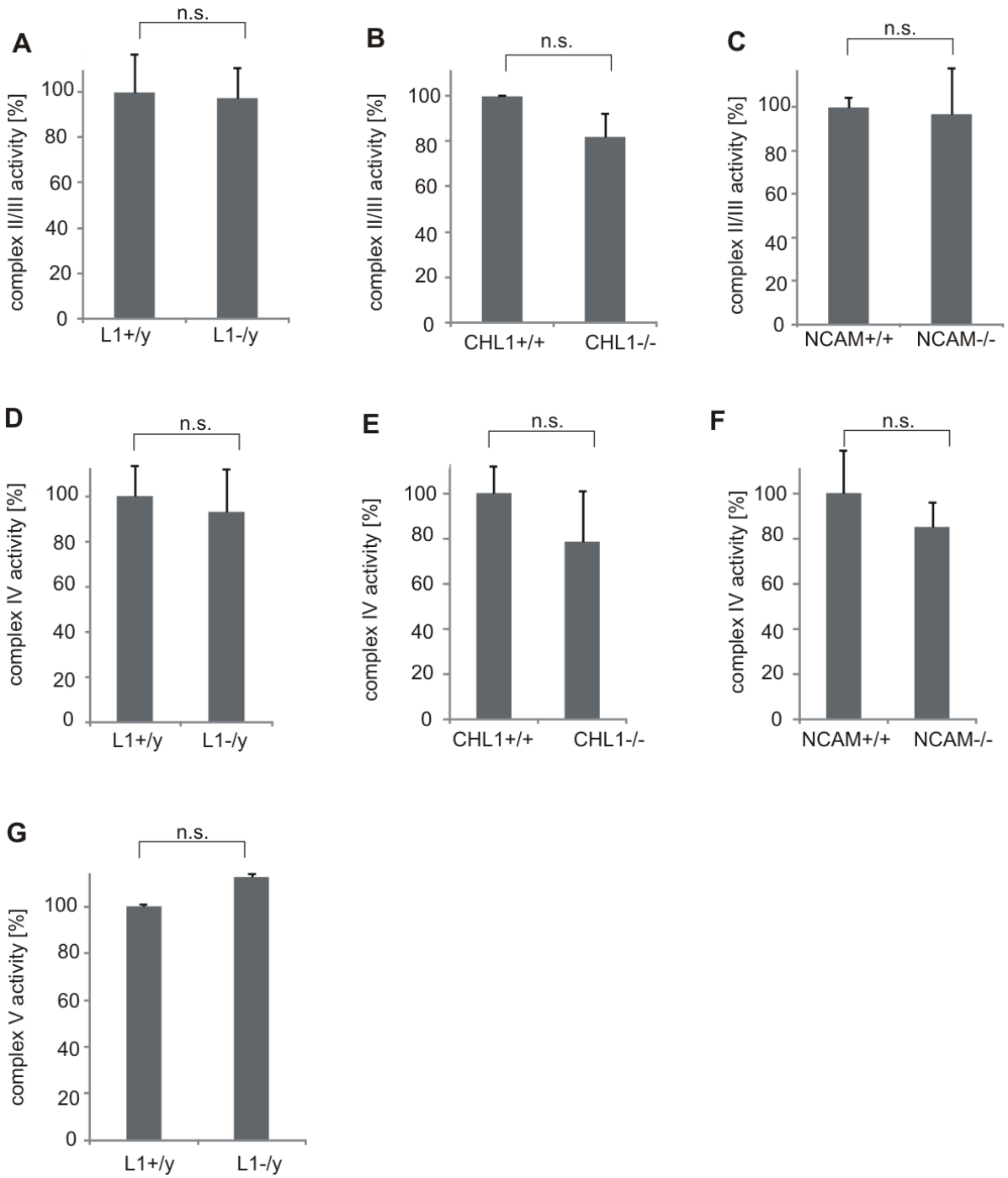

Figure 5.6: Complex II-V activity is not altered in L1-deficient mice. Mitochondria from brains of L1-, CHL1- and NCAM-deficient mice and their respective wild-type littermates at the age of two months were isolated. ***A-C***, Complex II/III activity was determined by measuring the complex III-dependent reduction of cytochrome *c* at 550 nm in isolated mitochondria from brains of L1-deficient (L1-/y, n=5), CHL1-deficient (CHL1-/-, n=4) and NCAM-deficient (NCAM-/-, n=4) mice and the corresponding wild-type littermates (L1+/y, n=5; CHL1+/+, n=4; NCAM+/+, n=4). ***D-F***, Complex IV activity was analyzed by measuring the oxidation rate of reduced cytochrome *c* at 550 nm in isolated mitochondria from brains of L1-deficient (L1-/y, n=5), CHL1-deficient (CHL1-/-, n=4) and NCAM-deficient (NCAM-/-, n=4) mice and wild-type mice (L1+/y, n=5; CHL1+/+, n=4; NCAM+/+, n=4). ***G***, Complex V activity was measured in a reverse functional system by measuring the rate of NADH

oxidation, which reduces pyruvate after ADP was used to generate it and was converted to ATP in isolated mitochondria from brains of L1-deficient mice (L1-/y, n=9) and wild-type littermates (L1+/y, n=9). Mean values + S.E.M. are shown (n. s.; two-tailed Student's t-test).

To test whether the complex I activity depends on the import of L1-70 into mitochondria, an *in vitro* import assay was performed with subsequent measurement of complex I activity. Complex I activity was reduced to ~55% in mitochondrial lysates of L1-deficient mice relative to the complex I activity in mitochondrial lysates from L1-deficient mice after *in vitro* import of L1-70 in mitochondria (Figure 5.7). These findings suggest that import of L1-70 into mitochondria leads to enhanced complex I activity.

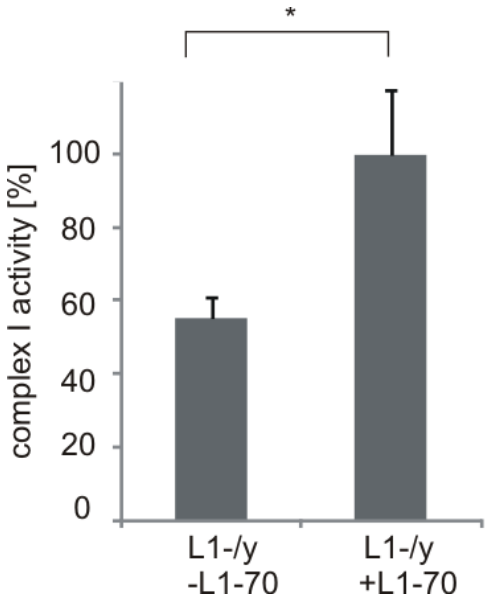

Figure 5.7: Complex I activity is affected by L1-70. *In vitro* import was performed with cytoplasmic fractions from wild-type mice and mitochondrial fractions from L1-deficient (L1-/y) mice. Mitochondria were re-isolated without co-incubation (-L1-70) and with co-incubation of these fractions (+L1-70). Mitochondria were lysed and the complex I activity was determined by measurement of the oxidation of NADH to NAD+ at 450 nm in three independent experiments. Mean values + S.E.M. are shown and differences between the groups are indicated (* $p<0.05$; two-tailed Student's t-test).

To investigate if L1 plays a role in the maintenance of the proper mitochondrial membrane potential, the energetic status of mitochondria was analyzed by measurement of the polarization of the inner membrane of mitochondria from L1-deficient and wild-type mice. To measure the energetic status of mitochondria a cationic carbocyanine dye was used. The cationic carbocyanine dye accumulates as a green-fluorescent monomer in the cytosol if mitochondria have a low membrane potential and accumulates as orange-fluorescent multimer if mitochondria have a

proper membrane potential. Mitochondria of L1-deficient mice were depolarized and showed a lower ratio of orange/green fluorescence intensity compared to mitochondria of wild-type mice (Figure 5.8 A and C). To determine whether MBP-generated L1-70 or full-length L1 is important for a proper mitochondrial membrane potential, the membrane potential reagent was applied to HEK293 cells transduced with empty AAV1 or with AAV1 coding for wild-type L1 or L1R/A. In L1R/A the mutated MBP-cleavage site inhibits the generation of L1-70 containing the intracellular domain and a part of the extracellular moiety (Lutz et al., 2014a). Mitochondria in cells that had been transduced with AAV1 carrying L1R/A or an empty virus, were more depolarized (lower ratio of orange/green fluorescence intensity) than mitochondria in cells that had been transduced with AAV1 carrying wild-type L1 (Figure 5.8 B and D). Apparently, L1-70 has an effect on the membrane potential of mitochondria and absence of this L1 fragment impairs membrane potential in the inner mitochondrial membrane.

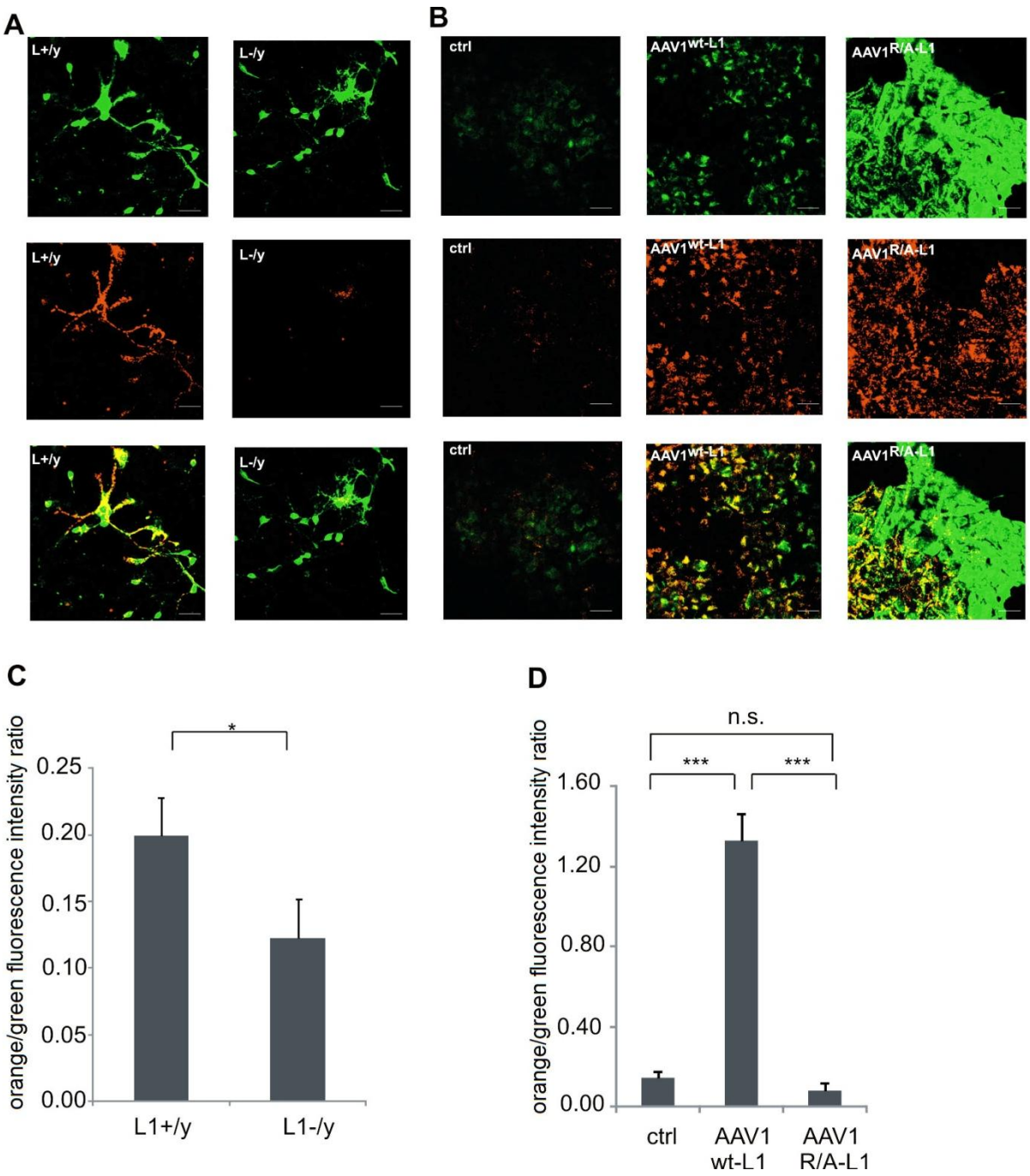

Figure 5.8: Mitochondrial membrane potential is reduced in cells lacking L1 or the L1 fragment, respectively. ***A*** and ***B***, Cerebellar neurons from L1-deficient (L1-/y) and wild-type (L1+/y) mice (***A***) and HEK293 cells that had been transduced with AAV1$^{wt\text{-}L1}$, AAV1$^{R/A\text{-}L1}$ or an empty virus (ctrl) (***B***), were cultured on PLL coated glass coverslips and the cell-based assay was performed to monitor the energetic status of mitochondria. Representative images are shown from two independent experiments after cells were observed for 10 minutes under the confocal microscope. Scale bars, 8 µm. ***C*** and ***D***, The total cell fluorescence intensity was calculated for the green and orange channel separately and the orange to green fluorescence intensity ratio was determined. Mean values + S.E.M. from at least 5 images per group per experiment obtained with HEK293 cells and from at least 17 images per group per experiment obtained with cerebellar neurons are shown (* $p<0.05$; one-tailed Student's t-test, *** $p<0.001$; one-way ANOVA with Holm-Sidak multiple comparison test).

5.1.3 Ablation of L1-70 increases mitophagy

An impaired mitochondrial membrane potential is a characteristic indicator for damaged mitochondria. To ensure sufficient ATP production for all cellular functions these dysfunctional mitochondria are removed by a selective autophagic process called mitophagy (Ashrafi and Schwarz, 2013). Since mitochondria have an impaired membrane potential in the absence of L1-70, the next step was to investigate whether more mitochondria undergo mitophagy in L1-lacking cells than in L1-containing cells. For this aim, L1-deficient HEK293 cells were transduced with AAV1 encoding wild-type L1 or L1R/A, or with an empty virus and transfected with a plasmid encoding for the mitophagy selective marker EGFP-LC3. The Pearson's coefficient was used to compare co-localization of labeled mitochondria with the mitophagy marker protein LC3. The co-localization of labeled mitochondria with EGFP-LC3 was enhanced in cells expressing L1R/A or cells transduced with an empty virus compared to cells expressing wild-type L1 (Figure 5.9). This result suggests that the presence of L1-70 leads to less degradation of mitochondria by mitophagy and therefore to a reduced co-localization of labeled mitochondria and the mitophagy marker protein LC3. Consequentially, the number of damaged mitochondria undergoing mitophagy was increased in L1- and L1-70-lacking cells.

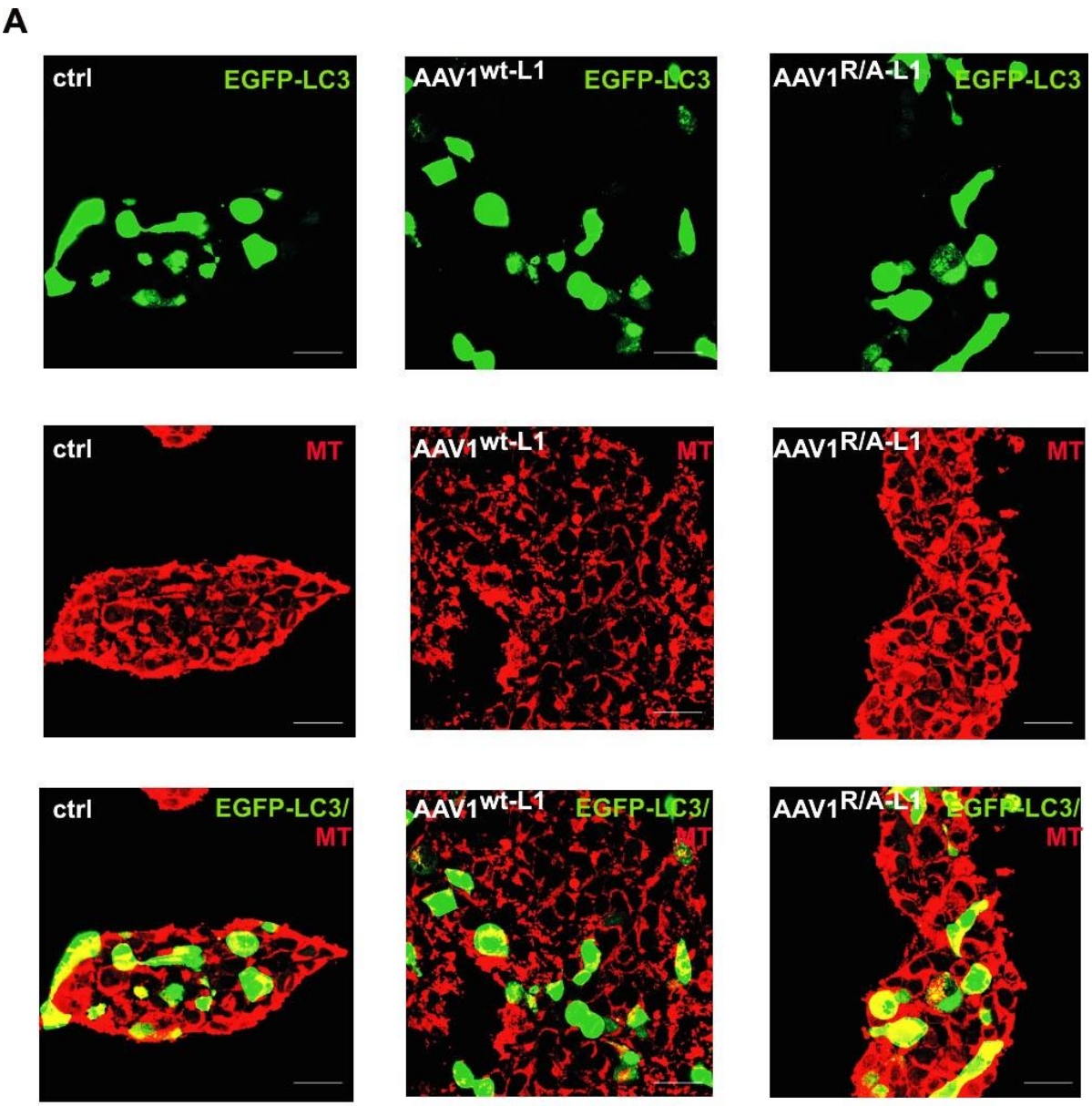
A
ctrl
EGFP-LC3
AAV1wt-L1
EGFP-LC3
AAV1R/A-L1
EGFP-LC3
ctrl
MT
AAV1wt-L1
MT
AAV1R/A-L1
MT
ctrl
EGFP-LC3/
MT
AAV1wt-L1
EGFP-LC3/
MT
AAV1R/A-L1
EGFP-LC3/
MT

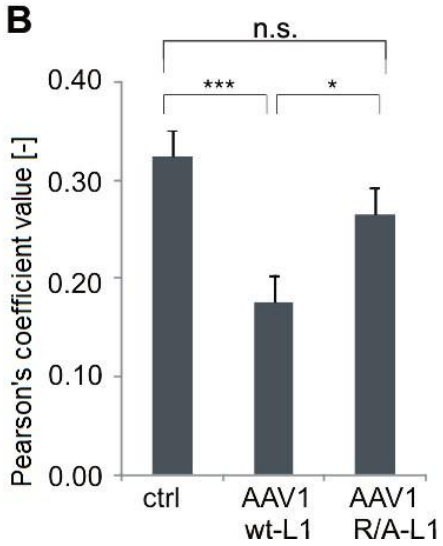
B
n.s.
***
*
0.40
0.30
0.20
0.10
0.00
Pearson's coefficient value [-]
ctrl
AAV1
wt-L1
AAV1
R/A-L1

Figure 5.9: L1-70 reduces mitophagy. ***A***, HEK293 cells that had been transduced with AAV1$^{wt\text{-}L1}$, AAV1$^{R/A\text{-}L1}$ and an empty virus (ctrl) were cultured on PLL coated glass coverslips, transfected with EGFP-LC3 and mitochondria were labeled with MitoTracker® Red CMXRos (MT). After fixation of the cells, fluorescence imaging was performed. Representative images are shown from two independent experiments. Scale bars, 10 µm. ***B***, Pearson's coefficient was calculated as a parameter to describe the degree of co-localization between mitochondria and EGFP-LC3. Mean values + S.E.M. from at least 11 images per group per experiment are shown for the Pearson's coefficient (* $p<0.05$, *** $p<0.001$; one-way ANOVA with Holm-Sidak multiple comparison test).

5.1.4 Ablation of L1-70 decreases mitochondrial fusion

An impaired membrane potential not only induces mitophagy but also affects mitochondrial dynamics such as fusion and fission. When mitochondrial functions are impaired the PINK1/Parkin pathway prevents mitochondrial fusion via modification of Mfn1 and Mfn2, therefore mitochondria are not able to fuse and feature a fragmented morphology. To investigate which impact L1 has on mitochondrial fusion and fission dynamics, mitochondrial fusion was analyzed. To this purpose, HEK293 cells transduced with an empty virus or with AAV1 encoding wild-type L1 or L1R/A were transfected with the photo-convertible fluorescence plasmid mito-dendra2 and time-lapse-video microscopy was performed. Cells expressing mito-dendra2 were identified by green fluorescence (without photoconversion). Upon activation with the 405 nm laser in a defined region of interest, mito-dendra2 converted from green to red fluorescent state. With time-lapse-video microscopy mitochondrial fusion was determined by taking pictures in the green and red channel. Areas of fused mitochondria were similar in cells that had been transduced with an empty virus or with AAV1 expressing L1R/A (Figure 5.10). Areas of fused mitochondria were significant enhanced in cells that had been transduced with AAV1 expressing wild-type L1 relative to areas of fused mitochondria in transduced cells expressing L1R/A. This result indicates an influence of L1 or L1-70 on mitochondrial fusion. Mitochondria showed a higher degree of fusion in the presence of L1-70 than in absence of L1 or L1-70.

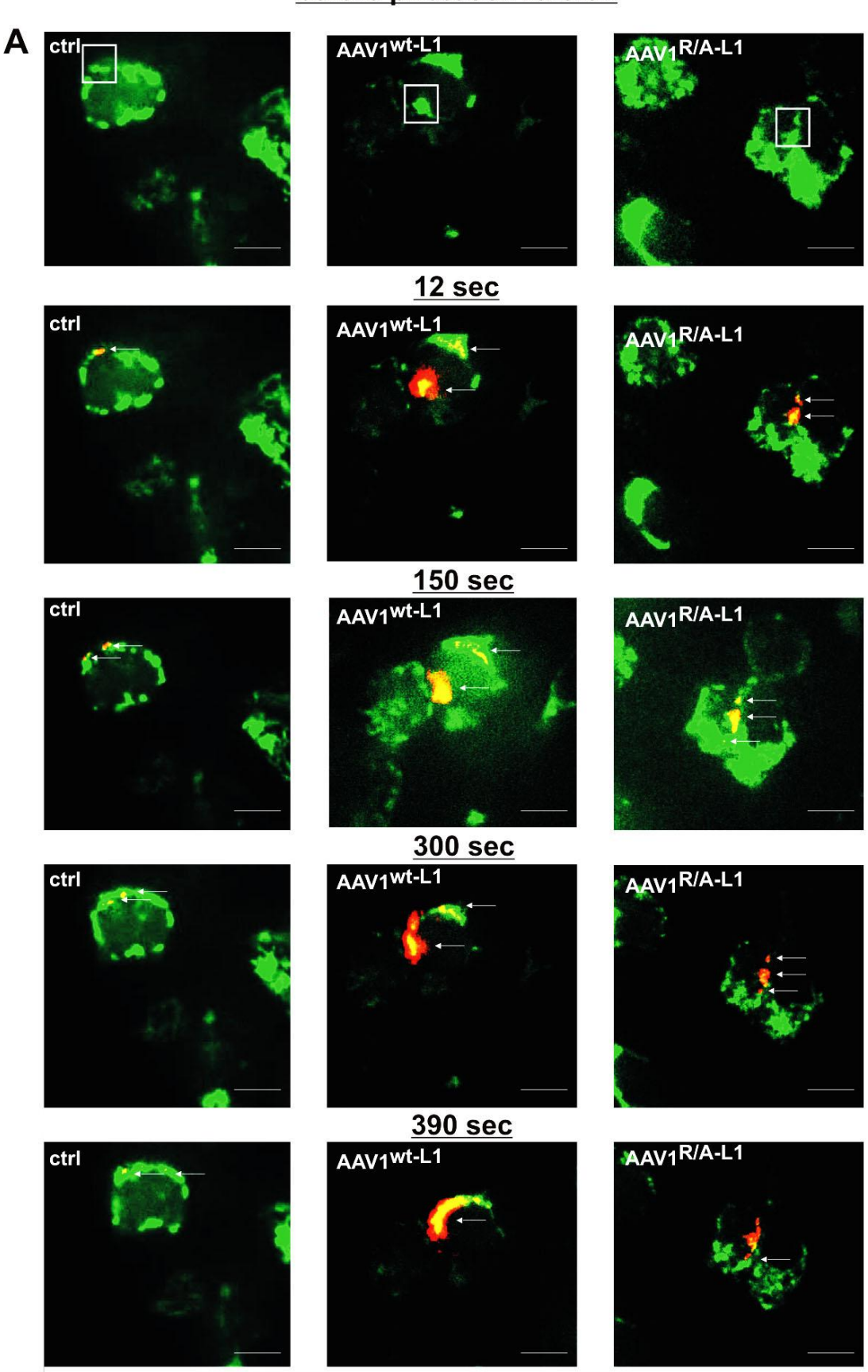
before photoconversion
A
ctrl
AAV1wt-L1
AAV1R/A-L1
12 sec
150 sec
300 sec
390 sec

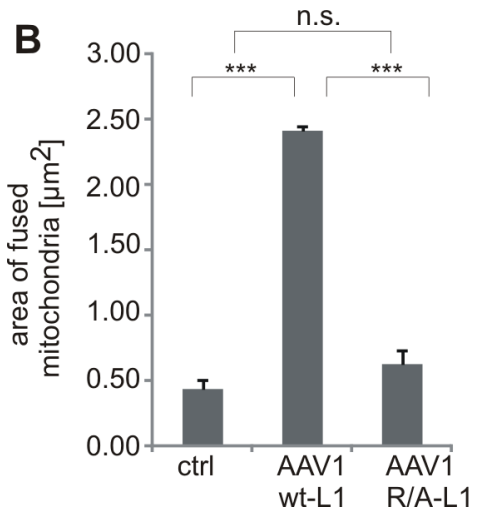

Figure 5.10: L1-70 enhances area of fused mitochondria. ***A***, HEK293 cells were transduced with AAV1 carrying AAV1$^{wt\text{-}L1}$, AAV1$^{R/A\text{-}L1}$ and with an empty virus (ctrl) and were maintained on PLL coated glass coverslips, transfected with the photo-convertible fluorescence plasmid mito-dendra2 and analyzed by time-lapse-video microscopy with FRAP. At time 0, 405 nm light was applied to a defined region of interest (white square box) to allow mito-dendra2 photo-conversion from green to red fluorescent state of mitochondria. Mitochondrial fusion was monitored for a maximum of 10 minutes. Representative images are shown from two independent experiments with mitochondrial fusion from time point 12-390 seconds (sec). Scale bars, 2 µm. ***B***, Area of fused mitochondria after 5 minutes imaging was measured with the ImageJ software. Mean values + S.E.M. from at least three videos per group per experiment are shown (*** $p<0.001$; one-way ANOVA with Holm-Sidak multiple comparison test).

Since mitochondrial fusion is impaired in the absence of L1-70 and loss of mitochondrial fusion is characterized by higher occurrence of fragmented mitochondria (Westrate et al., 2014), the morphology of mitochondria was analyzed. Labeled mitochondria in cultured cerebellar neurons of wild-type and L1-deficient mice were analyzed with confocal microscopy. In cerebellar neurons of L1-deficient mice mitochondria were fragmented, whereas in cerebellar neurons from wild-type mice mitochondria were less fragmented and more elongated (Figure 5.11 A). These results show the altered mitochondrial morphology in the absence of L1. Furthermore, in order to determine whether L1-70 alters mitochondrial morphology, labeled mitochondria in HEK293 cells expressing AAV1-derived L1R/A and AAV1-derived wild-type L1 or in cells transduced with an empty virus were investigated. L1-lacking HEK293 cells showed pronounced fragmentation of mitochondria in comparison to cells expressing AAV-derived wild-type L1, suggesting an influence of L1 on the morphology of mitochondria. Additionally, in the absence of L1-70

mitochondria had a more fragmented shape than in presence of L1-70 (Figure 5.11 B).

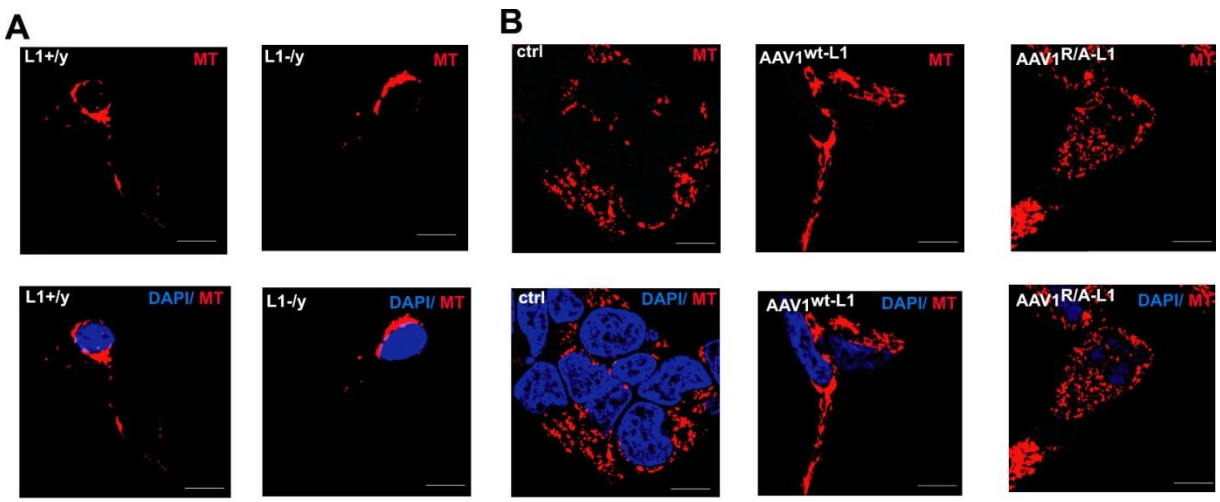

Figure 5.11: L1-70 alters mitochondrial morphology. Cerebellar neurons from L1-deficient (L1-/y) and wild-type (L1+/y) mice (***A***) and HEK293 cells that had been transduced with AAV1 carrying AAV1^{wt-L1}, AAV1$^{R/A-L1}$ and an empty virus (ctrl, ***B***) were cultured on PLL coated glass coverslips and mitochondria were labeled with MitoTracker® Red CMXRos (MT). After fixation of the cells, cell nuclei were stained with DAPI and fluorescence imaging was performed with confocal microscopy. Representative images are shown from two independent experiments. Scale bars, 2 µm.

5.1.5 Ablation of L1-70 decreases mitochondrial motility and mitochondrial anterograde transport

An impaired membrane potential has an impact not only on fusion and fission balances, but also on mitochondrial transport. Mitochondrial depolarization leads to disruption of the binding complex of kinesin/dynein motors and adaptor proteins followed by a hindered mitochondrial transport. To test the influence of L1-70 on mitochondrial trafficking, the motility of mitochondria was determined. Mitochondria were labeled in cultured cerebellar and hippocampal neurons from wild-type and L1-deficient mice and imaging of the mitochondrial transport using time-lapse video microscopy was performed. To compare mitochondrial trafficking in neurons from wild-type and L1-deficient mice, the motility and the mobility were quantified using kymographs. The term motility describes the velocity of dynamic mitochondria in axons and dendrites represented by diagonal lines in the kymographs, whereas the term mobility specifies the number of stationary mitochondria in neurons represented by vertical lines in kymographs. Mitochondria in L1-deficient cerebellar as well hippocampal neurons showed a significant reduced motility in comparison to

mitochondria in wild-type neurons (Figure 5.12 A and C, E and G). Additionally, time-lapse video microscopy of labeled mitochondria was performed after treatment of wild-type neurons without and with monoclonal L1 antibody 557, which is known to trigger L1-dependent cellular responses. Stimulation by the L1 antibody led to increased motility of mitochondria in wild-type cerebellar (Figure 5.12 B and D) and hippocampal neurons (Figure 5.12 F and H). These results show that presence of L1 and stimulation of L1-dependent signaling pathways in neurons has an effect on mitochondrial transport by changing the motility of mitochondria.

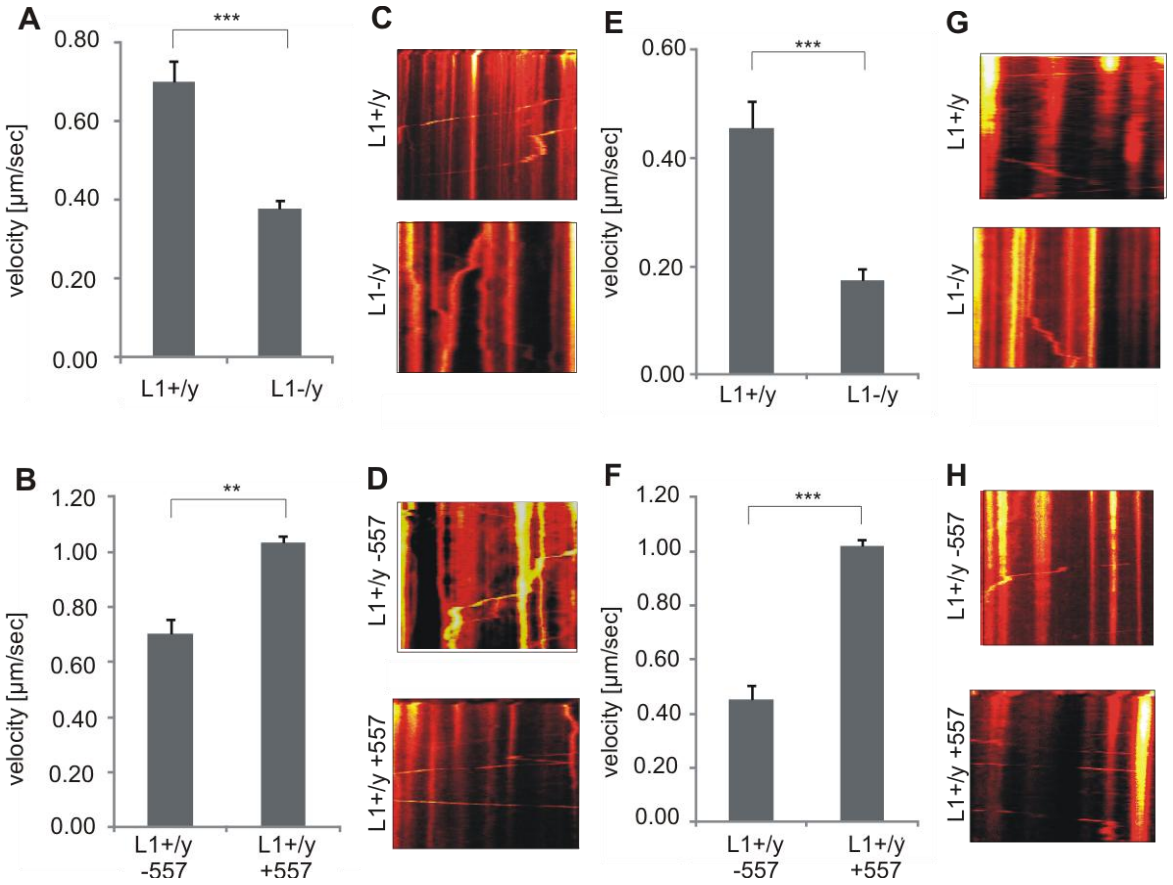

Figure 5.12: Velocity of mitochondria is reduced in neurons from L1-deficient mice. Dissociated cerebellar (***A***-***D***) and hippocampal neurons (***E***-***H***) from L1-deficient mice (L1-/y) and wild-type littermates (L1+/y) were cultured on PLL-coated glass coverslips and time-lapse video microscopy was performed after treatment without (-557) or with a function-triggering L1 antibody (+557) in at least two independent experiments. The velocity was determined in total for 50 mobile mitochondria in cerebellar and hippocampal neurons with the kymograph plugin and the velocity tool from ImageJ. Mean values + S.E.M. are shown (*** $p<0.001$; ** $p<0.01$; two-tailed Student's t-test). Representative images from the kymograph analysis for mitochondrial movement in cerebellar neurons (***C*** and ***D***) and hippocampal neurons (***G*** and ***H***) from L1-deficient mice and wild-type littermates after treatment without (-557) or with a L1 antibody (+557) are shown. Vertical lines represent no movement, while diagonal lines show dynamic mitochondria.

Interestingly, L1 did not influence the mobility of mitochondria in cerebellar neurons (Figure 5.13, A) and hippocampal neurons (Figure 5.13 B). The number of mobile mitochondria in cerebellar and hippocampal neurons from wild-type and L1-deficient mice was similar and the number of mobile mitochondria in non-treated or with 557 antibody-treated neurons, was also similar (Figure 5.13 C and D). Therefore, the number of moving mitochondria in neurons is not influenced by L1, but the velocity of mobile mitochondria.

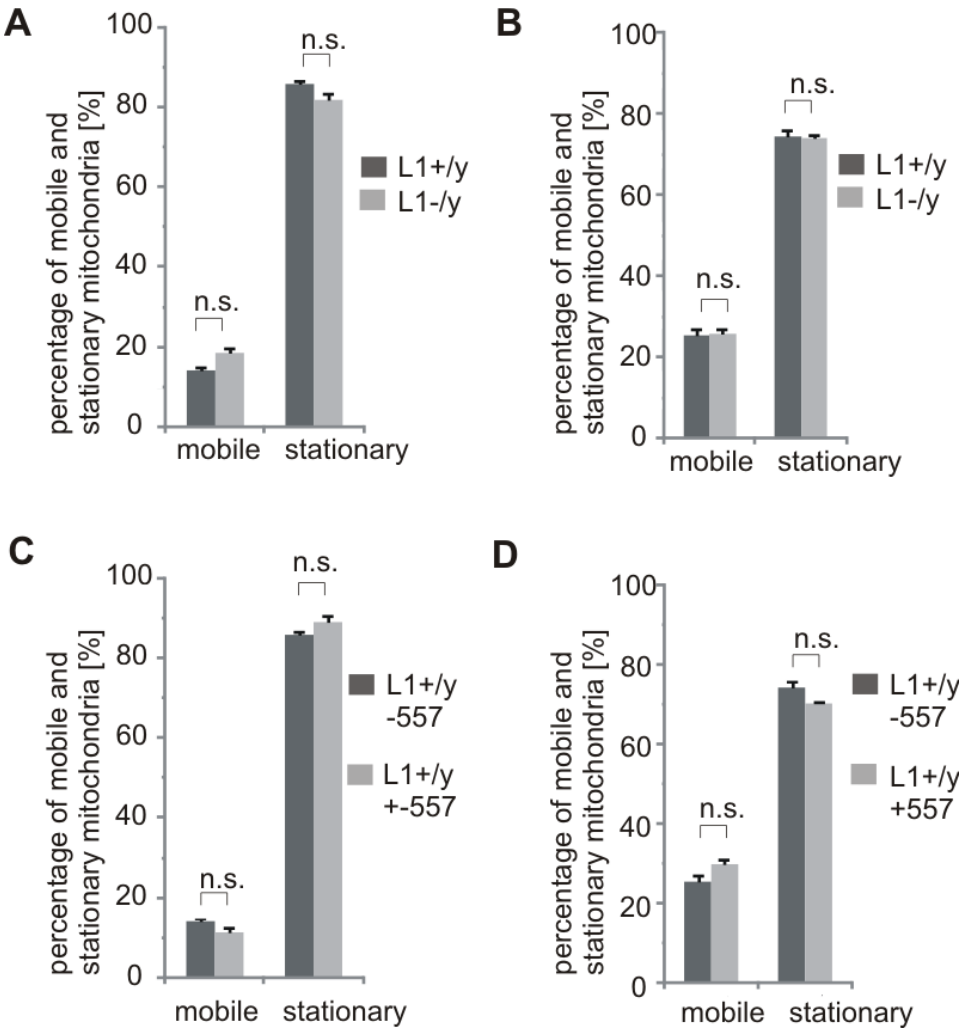

Figure 5.13: L1 does not influence the mobility of mitochondria. Cultured cerebellar (***A*** and ***C***) and hippocampal neurons (***B*** and ***D***) from L1-deficient (L1-/y) and wild-type (L1+/y) mice were seeded on PLL-coated glass coverslips and time-lapse video microscopy was performed after treatment of cells without (-557) or with L1 antibody (+557) in at least two independent experiments. The numbers of mobile and stationary mitochondria of cerebellar and hippocampal neurons were determined from at least 30 kymographs with the kymograph plugin and the velocity tool from ImageJ. Vertical lines were counted as stationary mitochondria and diagonal lines represented mobile mitochondria. Mean values + S.E.M. are shown (n. s.; two-tailed Student's t-test).

To analyze whether full-length L1 or L1 fragments affect mitochondrial motility, cerebellar neurons from L1-deficient mice were transduced with empty AAV1 or with AAV1 expressing either non-mutated wild-type L1 or expressing L1R/A mutant. Labeled mitochondria in neurons from L1-deficient mice that had been transduced with AAV1 encoding L1R/A or empty AAV1 showed decreased motility (Figure 5.14) relative to mitochondria in neurons from L1-deficient mice that had been transduced with AAV1 encoding wild-type L1. This result indicates that absence of L1-70 results in a reduced motility of mitochondria, suggesting that this L1 fragment affects mitochondrial motility.

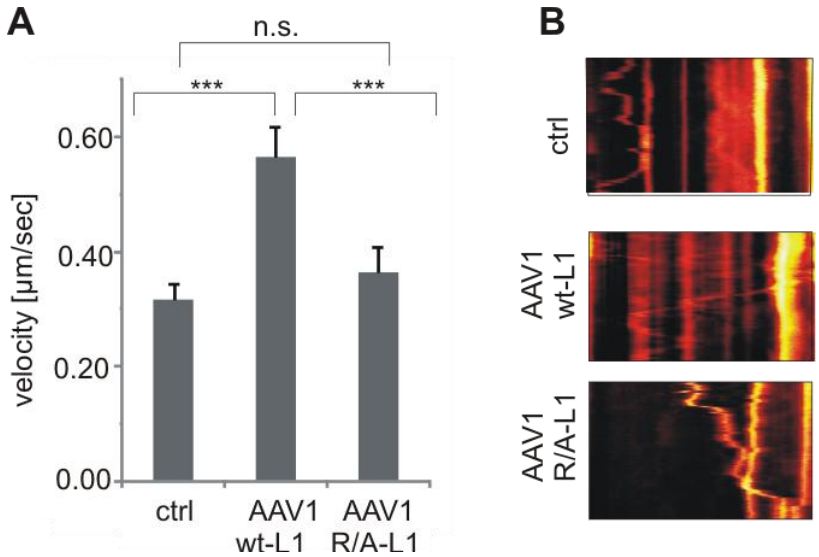

Figure 5.14: L1-70 increases the velocity of mitochondria in cerebellar neurons. Dissociated cerebellar neurons from L1-deficient mice that had been transduced with AAV1 carrying AAV1$^{wt\text{-}L1}$, AAV1$^{R/A\text{-}L1}$ or with an empty virus (-) (***A***) were cultured on PLL-coated glass coverslips and time-lapse video microscopy was performed in at least two independent experiments. The velocity was determined in total for 50 mobile mitochondria with the kymograph plugin and the velocity tool from ImageJ. Mean values + S.E.M. are shown (*** $p<0.001$; one-way ANOVA with Holm-Sidak multiple comparison test). ***B,*** Representative images from the kymograph analysis for mitochondrial movement in cerebellar neurons that had been transduced with AAV1 carrying AAV1$^{wt\text{-}L1}$, AAV1$^{R/A\text{-}L1}$ and with an empty virus are shown.

To support the notion that L1-70 generated by MBP is required for enhanced mitochondrial transport, the mitochondrial motility was investigated in *shiverer* mice. *Shiverer* mice are characterized by loss of MBP due to an autosomal recessive mutation, which leads to a shivering phenotype in affected mice (Mikoshiba et al., 1983). Because MBP is not expressed in *shiverer* mutant mice, L1-70 is not

generated and only full-length L1 and L1 fragments generated by other proteases exist in this mutant (Lutz et al., 2014a). For this aim, mitochondrial motility in cerebellar neurons from MBP-deficient *shiverer* mutant mice and wild-type littermates was determined with time-lapse video microscopy and this analysis showed that mitochondria in cerebellar neurons from *shiverer* mutant mice had a much lower velocity than mitochondria in cerebellar neurons from wild-type littermates (Figure 5.15). This result confirms the assumption that mitochondrial motility is decreased in the absence of L1-70 illustrating the important role of L1-70 for mitochondrial motility.

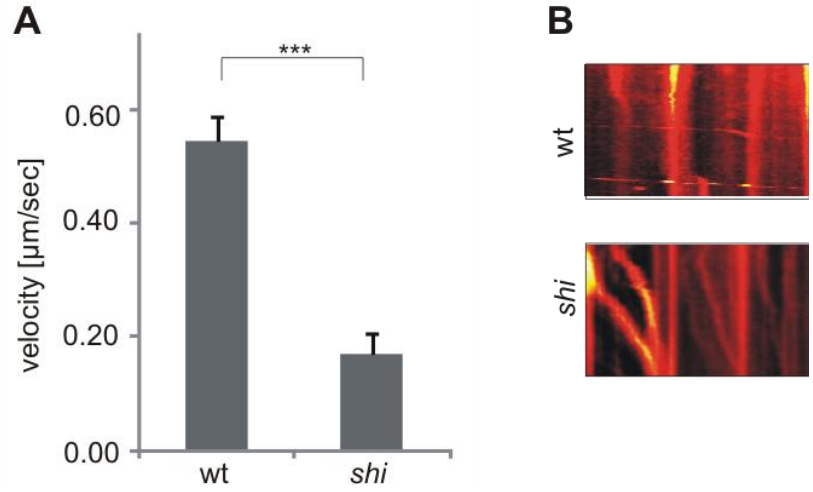

Figure 5.15: Velocity of mitochondria is decreased in cerebellar neurons from MBP-deficient *shiverer* mutant mice. ***A***, Dissociated cerebellar neurons from MBP-deficient *shiverer* mutant (*shi*) and wild-type (wt) mice were cultured on PLL-coated glass coverslips and time-lapse video microscopy was performed in at least two independent experiments. The velocity was determined in total for 50 mobile mitochondria with the kymograph plugin and the velocity tool from ImageJ. Mean values + S.E.M. are shown (*** $p<0.001$; two-tailed Student's t-test). ***B***, Representative images from the kymograph analysis for mitochondrial movement in cerebellar neurons from MBP-deficient *shiverer* mutant and wild-type mice are shown.

Mitochondrial transport can be anterogradely or retrogradely. Anterograde transport of mitochondria from the cell body to synaptic terminals is crucial during periods of high energy demand, whereas retrograde transport of mitochondria from synaptic terminals to the cell soma is required for removal of defective mitochondria that have an impaired membrane potential (Niescier et al., 2016). Since the direction of mitochondrial transport is of functional relevance, this key parameter in mitochondrial trafficking was investigated in cerebellar neurons from wild-type and L1-deficient mice. Direction of mitochondrial transport was indicated by left or right diagonal lines

in the kymographs, depending on the position of the cell soma (Marra et al., 2015). In neurons from wild-type mice ~60% of mobile mitochondria were transported anterogradely and ~40% moved retrogradely (Figure 5.16). In contrast, mitochondria in neurons from L1-deficient mice predominantly moved retrogradely (~80%), demonstrating an influence of L1 on the direction of mitochondrial transport.

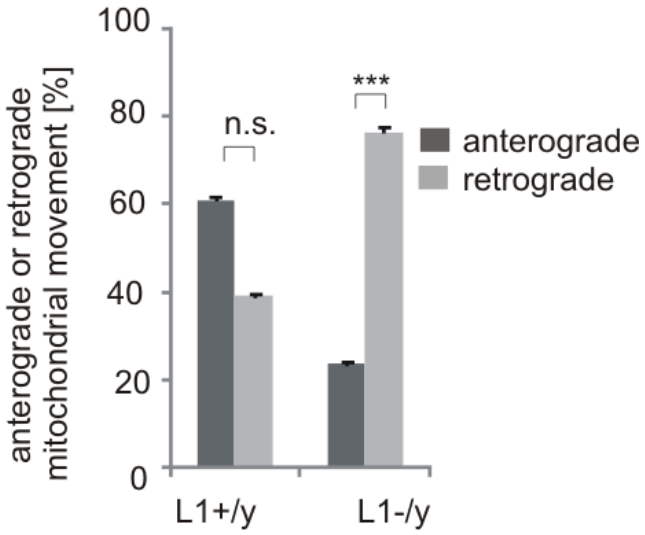

Figure 5.16: Retrograde transport of mitochondria is enhanced in cerebellar neurons from L1-deficient mice. Dissociated cerebellar neurons from L1-deficient mice (L1-/y) and wild-type littermates (L1+/y) were cultured on PLL-coated glass coverslips and time-lapse video microscopy was performed in at least two independent experiments. The transport direction of mitochondria was determined in total for 50 mobile mitochondria with the kymograph plugin from ImageJ. The direction was indicated by left or right diagonal lines in the kymographs, depending on the position of the cell soma (Marra et al., 2015). Mean values +S.E.M. are shown (*** $p<0.001$; two-tailed Student's t-test).

5.1.6 L1-70 interacts with NDUFV2, Drp1 and Miro1

Mass spectrometry analysis of L1 and CHL1 eluates (performed by Peter Lobel and Haiyan Zheng, Rutgers Mass Spectrometry Center for Integrative Neuroscience Research, New Jersey, USA) after performing an affinity chromatography with immobilized recombinant his-tagged intracellular domains of mouse L1 or CHL1 and with a mitochondrial fraction from brains of adult wild-type mice, revealed several potential binding candidates for L1 (Table 5.1).

Table 5.1: Peptide counting. Mass spectrometry analysis was performed by Peter Lobel and Haiyan Zheng (Rutgers Mass Spectrometry Center for Integrative Neuroscience Research, New Jersey, USA) from eluates obtained after affinity chromatography with L1 and CHL1 and mitochondrial fractions. The affinity chromatography was carried out with lysed mitochondria from brains of wild-type mice and with

recombinant his-tagged intracellular L1 or CHL1 domains. Eluates were applied for SDS-PAGE and the gel was stained with Coomassie brilliant blue solution. Regions with stained bands were cut out and send for mass spectrometry analysis. Peptide counting is shown for mitochondrial transport relevant potential binding candidates for the L1 intracellular domain such as NDUFV2, Miro1, Mfn2 and Drp1.

Peptide	Peptide count in L1 eluate	Peptide count in CHL1 eluate
NDUFV2 25-35 kDa band region	62	1
Miro1/RhoT1 75-100 kDa band region	36	0
Mfn2 75-100 kDa band region	36	0
Drp1 75-100 kDa band region	30	0

Tryptic peptides whose masses matched the mass of NDUFV2, a hydrophilic subunit of the N-module of complex I with a molecular mass of ~24kDa, were identified in the L1 eluate (62 peptides counted). Based on this finding and my findings that mitochondria in brains of L1-deficient mice have an impaired membrane potential and a reduced complex I activity as well as the fact that NDUFV2 is a subunit of complex I, it was possible that L1-70 directly interacts with NDUFV2 and that this interaction regulates complex I activity. To verify an interaction between NDUFV2 and L1, co-immunoprecipitation and ELISA were performed. First, potential binding of L1 to NDUFV2 was investigated in ELISA using recombinant NDUFV2 as substrate-coat and the intracellular domains of L1 and CHL1 as ligands. Intracellular domain of L1 was binding to NDUFV2 in a concentration-dependent manner, whereas no binding of the intracellular doman of CHL1 to NDUFV2 was detected (Figure 5.17 A). Additionally, immunoprecipitation using mitochondrial lysates from brains of wild-type and L1-deficient mice and a NDUFV2 antibody was performed and NDUFV2 immunoprecipitates were subjected to Western blot analysis with the L1 antibody L1CAM. Detection with L1-specific antibody revealed a L1 protein band of ~70 kDa in the immunoprecipitate of mitochondrial lysates from brains of wild-type mice but not in the immunoprecipitate of mitochondrial lysates from brains of L1-deficient mice.

Mitochondrial lysates from wild-type mice confirmed the size of the L1 protein band. The immunoprecipitates with non-immune control antibody showed no protein band of ~70 kDa in mitochondrial lysates from brains of wild-type and L1-deficient mice (Figure 5.17 B). These results suggest that L1-70 interacts with NDUFV2 in mitochondria. In summary, the proposed binding of L1-70 to NDUFV2 of complex I was verified by ELISA and immunoprecipitation and indicates a functional relevance of the interaction of L1 and NDUFV2 for complex I activity.

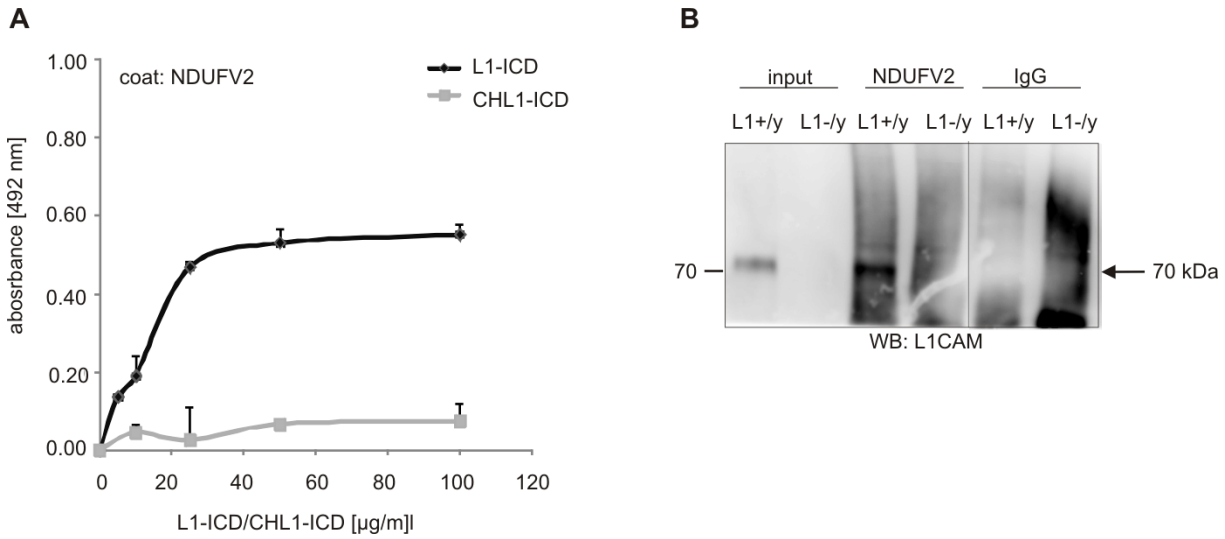

Figure 5.17: L1 binds to NDUFV2. ***A***, ELISA was performed with surface coated NDUFV2 recombinant protein and different concentrations of the intracellular domain of L1 or CHL1 as a control. L1CAM antibody was used to determine the binding of L1 to NDUFV2 and CHL1 antibody to determine binding of CHL1 to NDUFV2. The absorption was measured at 492 nm. Three independent experiments were performed in triplicates and mean values + S.E.M. are shown. ***B***, Immunoprecipitation was performed with mitochondrial lysates from L1-deficient mice (L1-/y) and wildtype (L1+/y) littermates and with an NDUFV2 antibody or a non-immune control antibody. Mitochondrial lysates (input) and NDUFV2 and IgG immunoprecipitates were subjected to WB analysis with L1CAM antibody, which recognizes an epitope (amino acid 1153-1182) within the intracellular L1 domain. Representative blot out of three independent experiments is shown. L1-70 is indicated by an arrow. Lanes not adjacent to each other but derived from the same blot are indicated by a vertical line.

Interestingly, the mass spectrometry analysis also indicated key players in mitochondrial transport such as Miro1 and in mitochondrial fusion and fission such as Drp1 and Mfn2 as additional potential L1 binding partners (Table 5.1). To test whether L1 indeed interacts with Miro1, Mfn2 and Drp1 immunoprecipitation was performed with mitochondrial lysates from brains of wild-type and L1-deficient mice using Miro1, Drp1 and Mfn2 specific antibodies. Immunoprecipitates were subjected

to Western blot analysis with the L1 antibody L1CAM. The detection revealed a L1 protein band of ~70 kDa in immunoprecipitates from mitochondrial lysates from brains of wild-type mice using Miro1 and Drp1 antibodies (Figure 5.18), but not with Mfn2 antibody (data not shown). In immunoprecipitates of mitochondrial lysates from brains of L1-deficient mice no positive L1 band was detected. The protein band of approximately ~70 kDa was also detected in mitochondrial lysates from brains of wild-type mice but not in mitochondrial lysates from brains of L1-deficient mice. Immunoprecipitates with non-immune control antibody showed no protein band of ~70 kDa in mitochondrial lysates from brains of wild-type and L1-deficient mice. These results suggest a specific binding of Miro1 and Drp1 to L1-70 at the outer mitochondrial membrane and this interaction may contribute to the effect of L1-70 on mitochondrial transport and fusion and fission mechanisms.

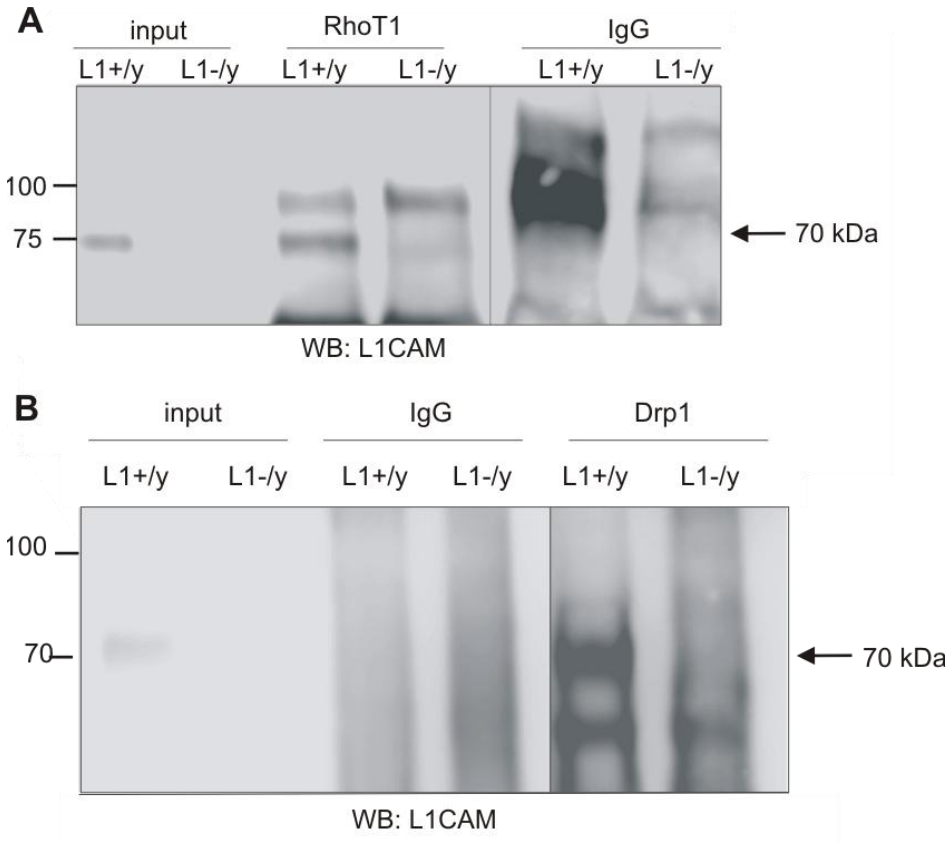

Figure 5.18: L1-70 precipitates with Miro1 (RhoT1) and Drp1. Soluble mitochondrial proteins from brains of L1-deficient (L1-/y) and wild-type (L1+/y) mice were subjected to immunoprecipitation with Miro1 (RhoT1) and Drp1 antibodies or a non-immune control (IgG) antibody. Mitochondrial lysates (input) and Miro1 (RhoT1) and Drp1 immunoprecipitates were subjected to WB analysis with a L1CAM antibody from Abcam. Representative blots out of three independent experiments are shown. L1-70 is indicated by an arrow. Lanes not adjacent to each other but derived from the same blot are indicated by vertical lines.

5.2 L1 interacts with nuclear receptors and this interaction is important for the development of the murine central nervous system

5.2.1 L1-70 interacts with nuclear receptors via its LXXLL and FXXLF motif

L1-70 contains the LXXLL motif (L_{1136}LILL) in the transmembrane domain and a FXXLF motif (F_{1046}HILF) in the fifth fibronectin type III domain. These motifs are present in coregulator proteins and are associated with binding of coactivator proteins to nuclear receptors in order to activate transcription. David Lutz (ZMNH, Universitätsklinikum Hamburg-Eppendorf, Germany) performed immunoprecipitation with nuclear extracts from mouse brains and the L1 antibody 555 followed by Western blot analysis against the nuclear receptors AR, ERβ and PPARɣ and could detect ERβ and PPARɣ, but not AR, in the L1 immunoprecipitate (Figure 5.19 A). Since this result indicates a possible interaction of L1 with the nuclear receptors ERβ and PPARɣ, the question was raised whether L1-70 is imported into the nucleus and interacts with nuclear ERβ and PPARɣ. Furthermore, the LXXLL and FXXLF motifs in L1 were mutated from L_{1136}LILL to A_{1136}LIAA and F_{1046}HILF to Y_{1046}HIAY to analyze if the binding of L1-70 to ERβ and PPARɣ depends on these motifs.

To rule out that mutation of the LXXLL and FXXLF motifs in L1 affects the nuclear import of L1, nuclear extracts from neurons of wild-type and L1-deficient mice and L1-deficient mice that had been transduced with AAV1 carrying wild-type L1 or mutated L1 were subjected to Western blot analysis with the L1 antibody L1CAM. L1-70 was detected in the nuclear extract from wild-type neurons and in the nuclear extract from L1-deficient neurons that had been transduced with AAV1 carrying wild-type L1 and mutated L1, but not in the lysate from L1-deficient neurons (Figure 5.19 B). This result shows that nuclear import of L1-70 is not affected by the disruption of the LXXLL and FXXLF motifs.

To determine if the LXXLL and FXXLF motifs within L1 are necessary for the interaction of L1-70 with ERβ and PPARɣ, nuclear fractions from L1-deficient neurons and from L1-deficient neurons that had been transduced with AAV1 expressing wild-type L1 or mutated L1 were used in ELISA. The interaction was not only tested with coated ERβ and PPARɣ but also with other coated nuclear receptors, namely recombinant RXRβ, ERα, AR, VDR and LXRβ. Recombinant PPARγ, RXRβ and ERα/β proteins bound to L1 present in nuclear extracts isolated

from neurons of L1-deficient mice that had been transduced with AAV1 carrying wild-type L1. In nuclear extracts isolated from L1-deficient neurons that had not been transduced or had been transduced with AAV1 carrying mutated L1 no visible binding was measured (Figure 5.19 C-F). This result suggests that interaction of nuclear L1-70 with nuclear receptors is mediated by the LXXLL and FXXLF motifs. Furthermore, ELISA showed no specific binding of AR, VDR and LXRβ recombinant proteins to L1 in the nuclear fractions from cultured neurons, since similar values were obtained using nuclear fractions from wild-type and L1-deficient mice (Figure 5.19 G-I).

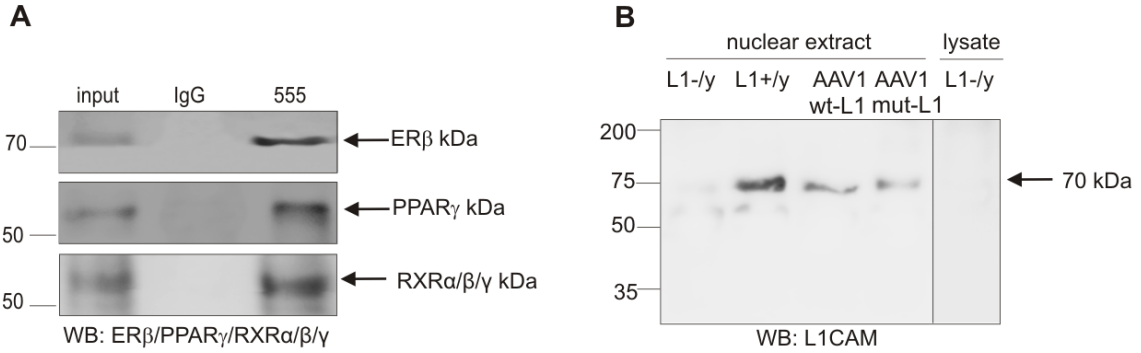
A
input
IgG
555
70
50
50
ERβ kDa
PPARγ kDa
RXRα/β/γ kDa
WB: ERβ/PPARγ/RXRα/β/γ
B
nuclear extract
lysate
L1-/y
L1+/y
AAV1 wt-L1
AAV1 mut-L1
L1-/y
200
75
50
35
70 kDa
WB: L1CAM

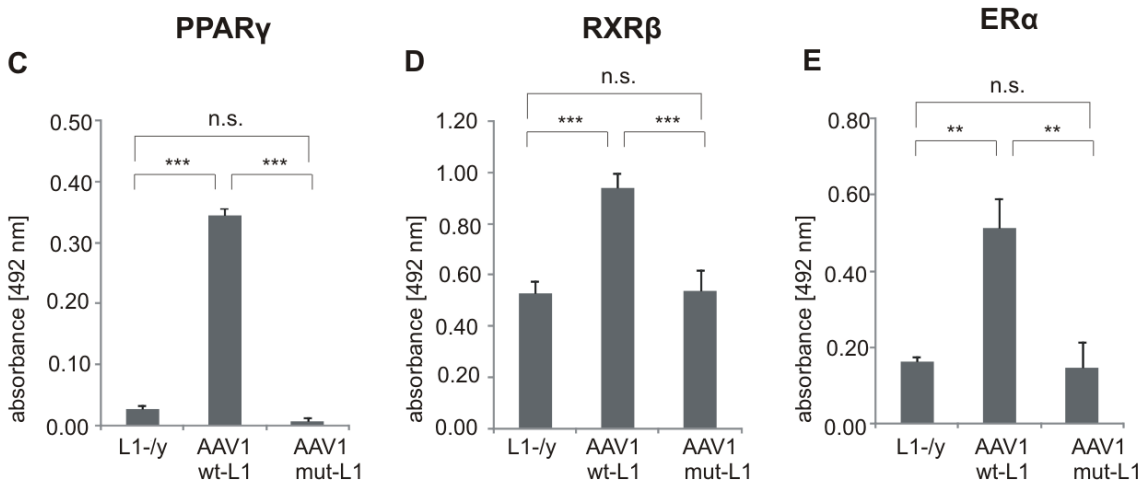
C
PPARγ
D
RXRβ
E
ERα
absorbance [492 nm]
n.s.
***
**
L1-/y
AAV1 wt-L1
AAV1 mut-L1

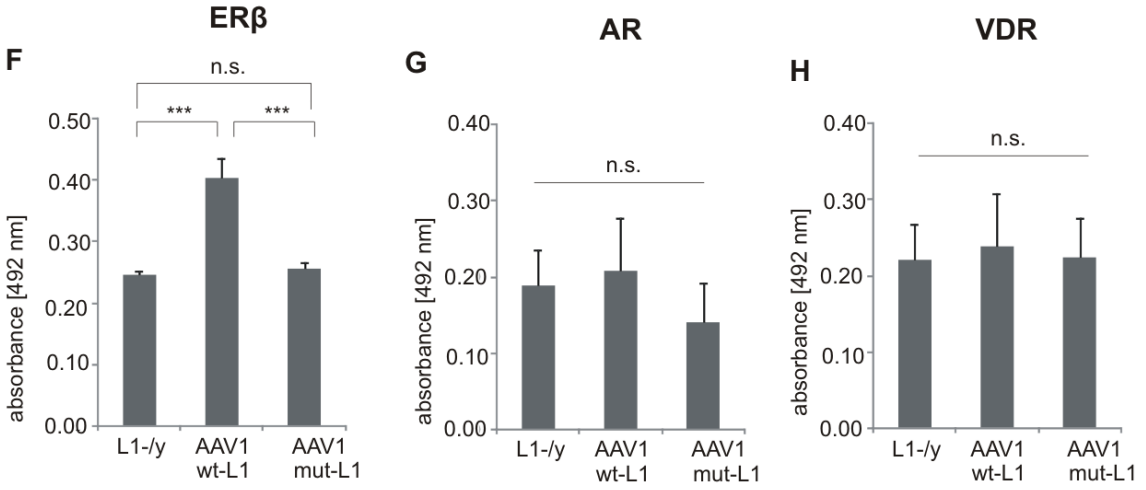
F
ERβ
G
AR
H
VDR
absorbance [492 nm]
n.s.
***
L1-/y
AAV1 wt-L1
AAV1 mut-L1

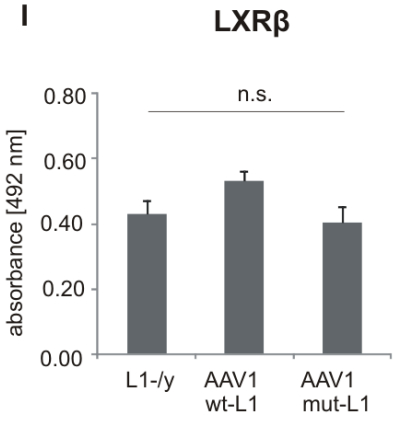
I
LXRβ
absorbance [492 nm]
n.s.
L1-/y
AAV1 wt-L1
AAV1 mut-L1

Figure 5.19: Nuclear L1-70 interacts with nuclear receptors. ***A***, Immunoprecipitation and WB analysis was performed by David Lutz (ZMNH, Universitätsklinikum Hamburg-Eppendorf, Germany) with nuclear extracts isolated from brains of wild-type mice and with L1 antibody 555 or non-immune control antibody (IgG). Samples were subjected to WB analysis with AR, ERβ and PPARɣ antibodies. ***B***, Nuclear fractions from cerebellar neurons of wild-type (L1+/y) and L1-deficient (L1-/y) mice that had been transduced with AAV1 carrying wild-type L1 (wt-L1) or mutated L1 (mut-L1) were analyzed by WB with the L1 antibody L1CAM. Lysates from brains of L1-deficient mice were used as a control. L1-70 is indicated by an arrow. Lanes not adjacent to each other but derived from the same blot are indicated by a vertical line. ***C-I***, ELISA was performed with coated recombinant PPARγ I, RXRβ (***D***), ERα (***E***), ERβ (***F***), AR (***G***), VDR (***H***) and LXRβ (***I***) proteins and nuclear extracts obtained from cerebellar neurons of L1-deficient mice and L1-deficient mice that had been transduced with AAV1 coding for wild-type L1 or mutated L1. L1CAM antibody was used to determine the binding of L1. The absorption was measured at 492 nm. Three independent experiments were performed in triplicates and mean values + S.E.M. are shown (** p<0.01, *** p<0.001; one-way ANOVA with Holm-Sidak multiple comparison test).

5.2.2 Mutation of LXXLL and FXXLF motifs in L1 inhibits neurite outgrowth

Previous data showed a neurite outgrowth and neuronal survival promoting effect of L1-70 (Lutz et al., 2014a). Thus, I tested whether mutation of the LXXLL and FXXLF motifs influence L1-mediated neurite outgrowth. Neurite outgrowth assay was performed with cultured neurons from L1-deficient mice and L1-deficient mice that had been transduced with AAV1 either coding for wild-type L1 or for mutant L1. Reduced total neurite length was observed in L1-deficient neurons and L1-deficient neurons expressing mutated L1 relative to L1-deficient neurons expressing AAV1-derived wild-type L1 (Figure 5.20). Therefore, disruption of the LXXLL and FXXLF motifs in L1 leads to a reduction in neurite outgrowth.

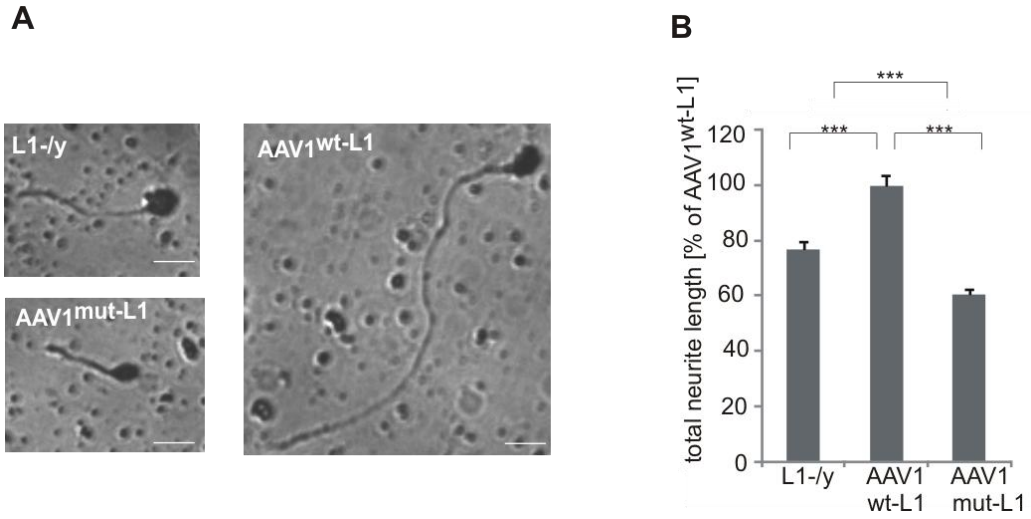

Figure 5.20: Mutation of LXXLL and FXXLF motifs diminishes neurite outgrowth. ***A***, Neurite outgrowth assay was performed in collaboration with Hardeep Kataria (ZMNH, Universitätsklinikum Hamburg-Eppendorf, Germany) in two independent experiments using cerebellar neurons from L1-deficient (L1-/y) mice, which were not transduced or transduced with AAV1 carrying wild-type L1 (wt-L1) or mutated L1 (mut-L1). Neurons were cultured on PLL for 24 h, fixed and stained for imaging with an AxioVert microscope. Scale bars, 10 µm. ***B***, Mean + S.E.M. of total neurite length values from at least 80 neurons per group per experiment are shown (*** p<0.001; one-way ANOVA with Holm-Sidak multiple comparison test).

5.2.3 Mutation of LXXLL and FXXLF motifs in L1 alters structural subelements of hippocampal mossy fiber synapses

Nuclear receptors of the steroid nuclear receptor class like ER have a strong influence on hippocampal functions such as memory formation (Bean et al., 2014). To test whether the interactions of L1 with nuclear receptors via the LXXLL and FXXLF motifs within L1 play a role in regulation of hippocampal structure, parasagital hippocampal sections from six day old wild-type and L1-deficient mice and L1-deficient mice that had been transduced with AAV1 carrying wild-type L1 or mutated L1 were analyzed with transmission electron microscopy. Interestingly, ultrastructural analysis showed a smaller mossy fiber bouton area and total length of the synaptic cleft in hippocampal sections from L1-deficient mice and mice expressing AAV1-derived mutated L1 in comparison to the mossy fiber bouton area and total length of the synaptic cleft in hippocampal sections from wild-type and L1-deficient mice, which expressed AAV1-derived wild-type L1 (Figure 5.21 A and B). Moreover, at the ultrastructural level L1-deficient mice and L1-deficient mice transduced with AAV1 encoding mutated L1 showed an altered synaptic type with ~73% and ~79% symmetric (inhibitory) synaptic clefts and ~28% and ~22% asymmetric (excitatory) synaptic clefts, whereas wild-type mice and mice expressing AAV1-derived wild-type L1 showed no significant differences in the proportion of symmetric (inhibitory, ~59% and ~56%) and asymmetric synaptic clefts (excitatory, ~42% and ~44%) (Figure 5.21 C). Thus, L1-deficient mice and L1-deficient mice transduced with AAV1 encoding mutated L1 have more inhibitory synapses and less excitatory synapses than wild-type mice and mice expressing AAV1-derived wild-type L1. These results indicate that L1 influences structural subelements of the hippocampal mossy fiber synapses and disruption of LXXLL and FXXLF motifs in L1 might affect signal processing and neuronal plasticity in the hippocampus.

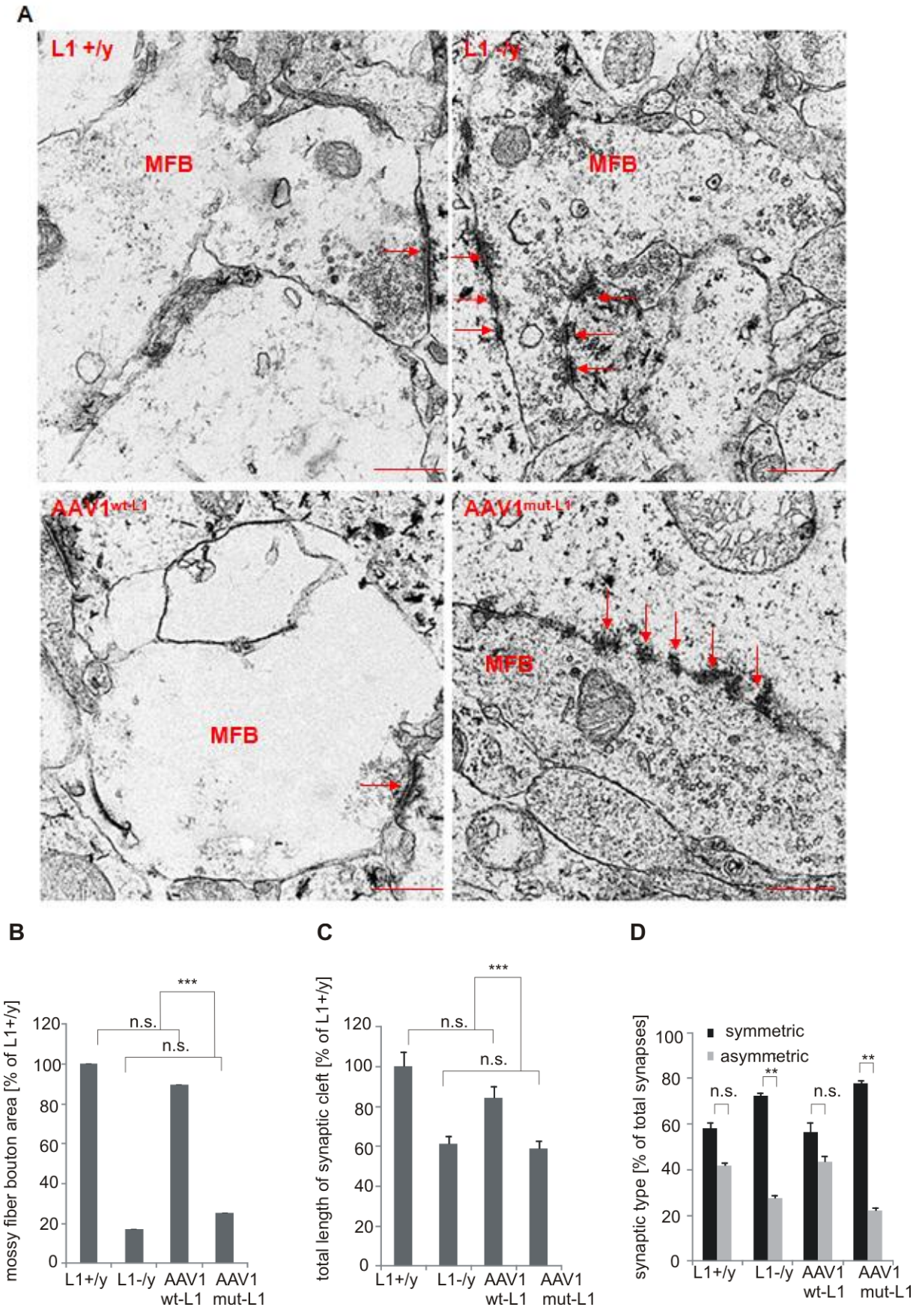
A
L1 +/y
MFB
L1 -/y
MFB
AAV1wt-L1
MFB
AAV1mut-L1
MFB
B
mossy fiber bouton area [% of L1+/y]
120
100
80
60
40
20
0
***
n.s.
n.s.
L1+/y
L1-/y
AAV1 wt-L1
AAV1 mut-L1
C
total length of synaptic cleft [% of L1+/y]
120
100
80
60
40
20
0
***
n.s.
n.s.
L1+/y
L1-/y
AAV1 wt-L1
AAV1 mut-L1
D
synaptic type [% of total synapses]
symmetric
asymmetric
100
80
60
40
20
0
n.s.
**
n.s.
**
L1+/y
L1-/y
AAV1 wt-L1
AAV1 mut-L1

Figure 5.21: Mutation of LXXLL and FXXLF motifs in L1 leads to reduced mossy fiber bouton area, shorter synaptic cleft length and altered synaptic type. ***A***, Transmission electron micrographs of ultrathin hippocampal sections from L1+/y, L1-/y, AAV1$^{wt\text{-}L1}$ and AAV1$^{mut\text{-}L1}$ mice show mossy fiber bouton area (MFB) and synaptic cleft (red arrows). Representative images were taken by David Lutz (ZMNH, Universitätsklinikum Hamburg-Eppendorf, Germany). Scale bars, 500 nm. Parasagital hippocampal sections from six days old L1-deficient mice that had been transduced with AAV1 carrying wild-type L1 or L1 with mutated LXXLL and FXXLF motifs *in utero* at embryonic day 14, were subjected to transmission electron microscopy for assessment of mossy fiber bouton area (***B***), total length of the synaptic cleft (***C***) and synaptic type according to the electron density (***C***) in comparison to six day old wild-type and L1-deficient mice. Mean values + S.E.M. relative to the values of wild-type mice or total synapses are shown and were obtained from at least 24 images per group from three independent experiments (** $p<0.01$; *** $p<0.001$; one-way ANOVA with Holm-Sidak multiple comparison test; one-tailed Student's t-test).

5.2.4 Mutation of LXXLL and FXXLF motifs in L1 leads to impaired motor coordination

L1 is associated with motor learning and synapse formation and the cerebellum regulates motor coordination and learning, and can be regulated by nuclear receptor's function. Therefore, I asked the question whether the interaction of L1 with nuclear receptors via its LXXLL and FXXLF motifs plays a role in cerebellum-dependent motor coordination and learning. Expression of L1 in brains of L1-deficient mice transduced with AAV1 coding for wild-type or mutated L1 was analyzed by Western blot and immunostaining after performing behavioral tests with these mice. Western blot analysis with L1-specific and GAPDH antibody of brain homogenates showed L1 expression in wild-type and transduced mice, but not in L1-deficient mice (Figure 5.22 A). Immunostaining confirmed expression of L1 in the granule cell layer, the Purkinje cell layer and the molecular cell layer in cerebella of L1-deficient mice that had been transduced with AAV1 carrying wild-type or mutated L1, while immunostaining with L1 antibody in cerebella of L1-deficient mice was negative (Figure 5.22 B).

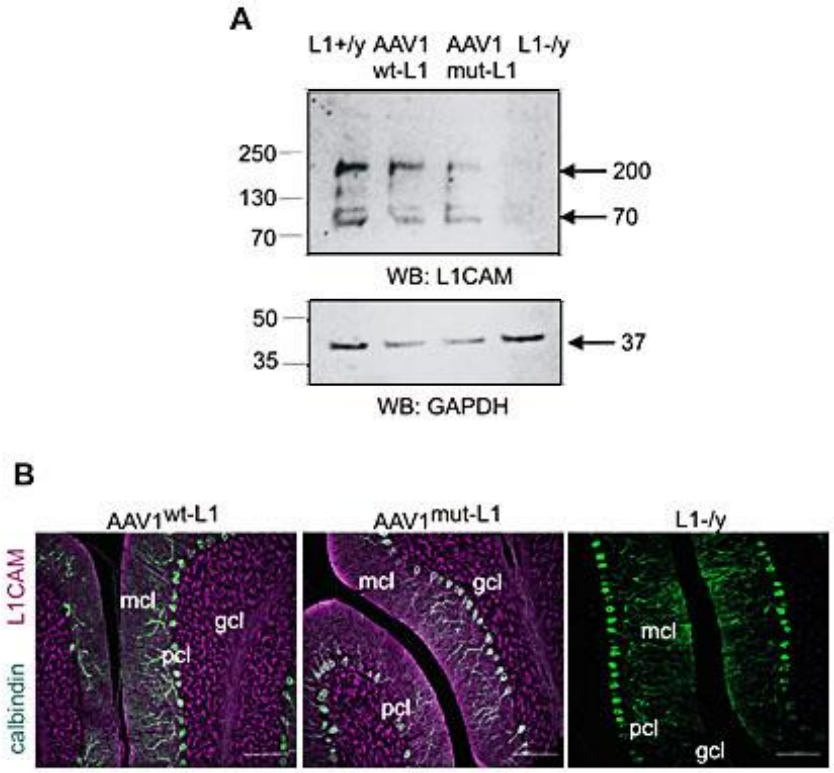

Figure 5.22: L1 is expressed in brains of transduced mice. Brains of 12 weeks old mice that had been transduced with AAV1 carrying wild-type L1 ($AAV1^{wt\text{-}L1}$) or mutant L1 ($AAV1^{mut\text{-}L1}$) *in utero* at embryonic day 16 and of wild-type (L1+/y) and L1-deficient (L1-/y) mice, were subjected to WB analysis with the L1-specific antibody L1CAM and GAPDH antibody (***A***) and to immunostaining with the L1CAM antibody and calbindin antibody showing expression of L1 (shown in purple) in the molecular cell layer (mcl), the Purkinje cell layer (pcl) and the granule cell layer (gcl) (***B***). Representative blot and immunostaining from one experiment is shown and was developed by David Lutz (ZMNH, Universitätsklinikum Hamburg-Eppendorf, Germany). Scale bars, 200 µm.

To investigate the effect of the interaction of L1 with nuclear receptors on motor coordination *in vivo*, behavioral tests were performed. Rotarod and pole test were carried out with L1-deficient mice that had been transduced with AAV1 encoding wild-type L1 or mutated L1. Mice were transduced *in utero* by injection of the virus particles into the area of plexus brachialis of L1-deficient embryos at embryonic day 16. Twelve weeks later mice were tested in motor coordination tests and their performance was compared to the performance of wild-type and L1-deficient mice. To analyze motor coordination, the latency of mice to fall down from the accelerating rod was compared. L1-deficient mice and mice expressing AAV1-derived mutated L1 showed a lower latency to fall in comparison to wild-type mice and mice expressing AAV1-derived wild-type L1 that showed a higher latency to fall. Also, L1-deficient mice and mice expressing AAV1-derived mutated L1 showed no visible improvement

of the performance on the accelerating rod in subsequent trials relative to wild-type mice and mice expressing AAV1-derived wild-type L1 that showed improvement in their performance in subsequent trials (Figure 5.23 A). Furthermore, the pole test showed that L1-deficient and L1-deficient mice transduced with AAV1 encoding mutated L1 performed significantly inferior than wild-type and L1-deficient mice transduced with AAV1 encoding wild-type L1. In the first trial, L1-deficient mice transduced with AAV1 encoding wild-type L1 needed more time to climb down than wild-type mice, but the performance was better than that of L1-deficient mice and the performance was enhanced in subsequent trials (Figure 5.23 B). In the first trial, ~25% of L1-deficient mice and ~33% of L1-deficient mice expressing AAV1-derived mutated L1 felt down the vertical pole, but showed an improvement in subsequent trials not to fall down from the pole (Figure 5.23 C). Wild-type and L1-deficient mice transduced with AAV1 encoding wild-type L1 did not fall down in all consecutive trials (Figure 5.23 C). These results indicate that L1 with its LXXLL and FXXLF motifs influences motor control and mutation of the LXXLL and FXXLF motifs leads to impairment in cerebellum-dependent motor coordination and learning.

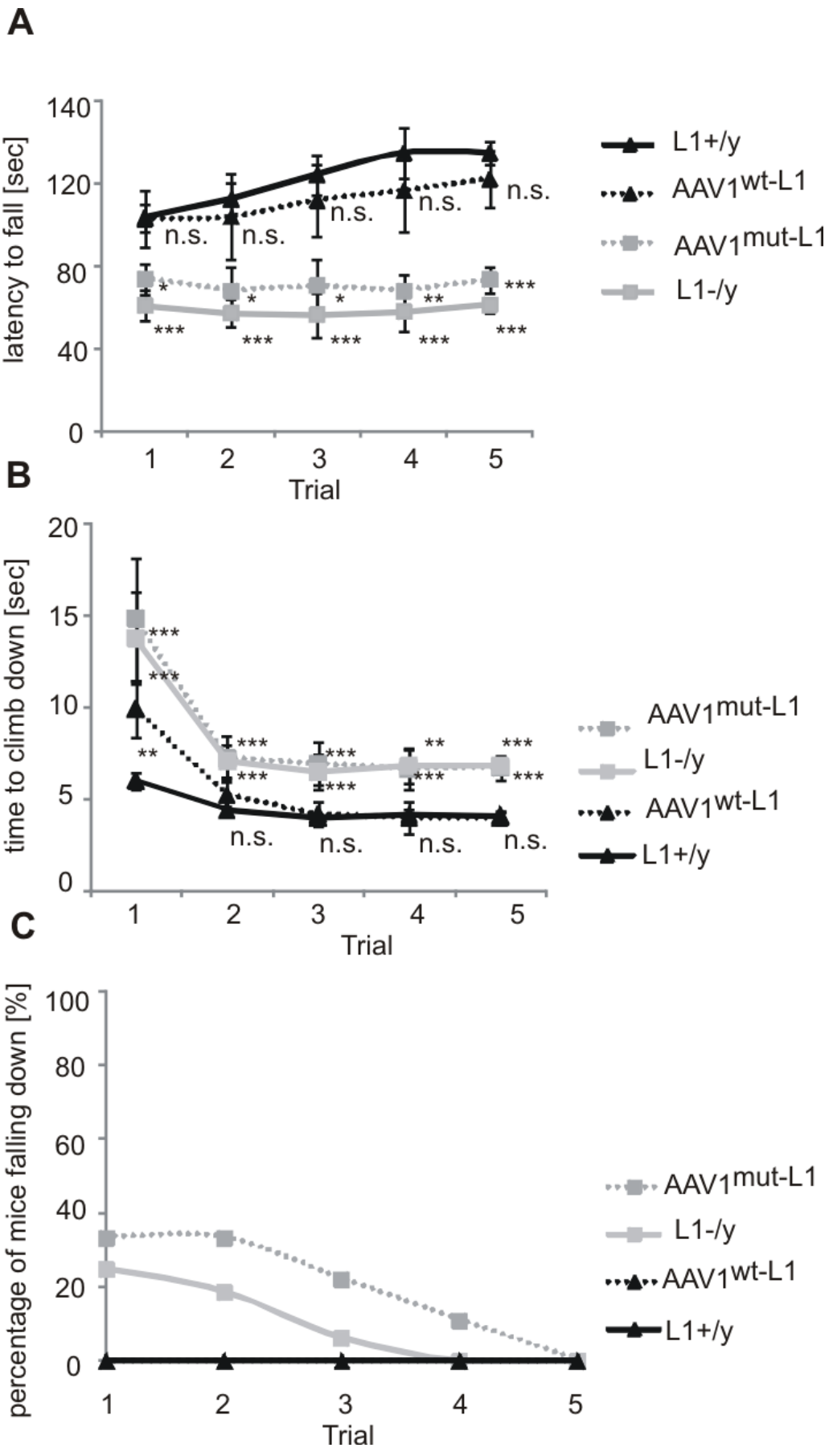
A
latency to fall [sec]
140
120
80
40
0
1
2
3
4
5
Trial
n.s.
*
***
**
L1+/y
AAV1wt-L1
AAV1mut-L1
L1-/y
B
time to climb down [sec]
20
15
10
5
0
1
2
3
4
5
Trial
***
**
n.s.
AAV1mut-L1
L1-/y
AAV1wt-L1
L1+/y
C
percentage of mice falling down [%]
100
80
60
40
20
0
1
2
3
4
5
Trial
AAV1mut-L1
L1-/y
AAV1wt-L1
L1+/y

Figure 5.23: Mutation of the LXXLL and FXXLF motifs in L1 impairs motor coordination. Rotarod and pole test were performed with 12 weeks old L1-deficient (L1-/y, n=16) mice in comparison to wild-type (L1+/y, n=26) littermates and L1-deficient mice that had been transduced with AAV1 carrying wild-type L1 (AAV1$^{wt\text{-}L1}$, n=9) or L1 with mutated LXXLL and FXXLF motifs (AAV1$^{mut\text{-}L1}$, n=9) *in utero* at embryonic day 16. ***A*** and ***B***, Assessment of the latency to fall from a rotating rod accelerated in a range between 4 to 40 rpm on five consecutive days and the time needed to climb down the vertical pole in five trials. Mean values + S.E.M. are shown (* p<0.05; ** p<0.01; *** p<0.001; one-way ANOVA with Holm-Sidak multiple comparison test). ***C***, Total amount of mice falling down the vertical pole from every trial in five trials is shown.

5.2.5 L1-deficient mice have reduced forelimb strength

To rule out that the impaired motor coordination of L1-deficient mice is due to a reduced muscle strength, the muscle strength of wild-type and L1-deficient mice was analyzed. L1-deficient mice showed lower muscle strength than wild-type mice after performing the Rotarod and pole test, but a significant difference in grip strength was not visible before the training was performed. This result indicates an improvement in forelimb strength and motor coordination in wild-type mice which is abolished in L1-deficient mice (Figure 5.24).

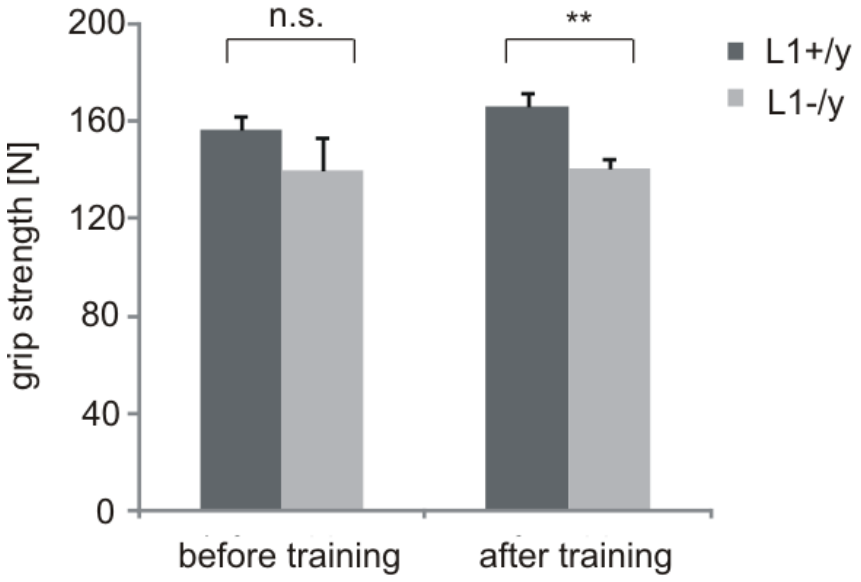

Figure 5.24: L1-deficient mice show reduced forelimb strength after training. Grip strength test was performed with wild-type (L1+/y, n=12) and L1-deficient (L1-/y, n=8) mice before performing and after performing the Rotarod and pole test. Mice were hold by the tail and the maximal force the mice needed to hold on a grip bar attached to a dynamometer before releasing the grip bar was recorded with the Grip Strength Meter system. The Grip strength test was performed twice and mean values + S.E.M. are shown (** p<0.01; two-tailed Student's t-test).

5.2.6 Mice expressing L1 with mutated LXXLL and FXXLF motifs show altered climbing fiber input to Purkinje cells

The behavioral studies revealed that L1-deficient mice and mice expressing AAV1-derived mutated L1 have impairments in motor coordination and learning and since Purkinje cell neuroplasticity is directly associated with reduced motor learning (Nguyen-Vu et al., 2013), excitatory input to Purkinje cells from climbing fibers was investigated. Climbing fiber input to Purkinje cell dendrites was analyzed with cerebellar sections from 12 weeks old wild-type and L1-deficient mice and L1-deficient mice that had been transduced with AAV1 encoding wild-type L1 or mutated L1 with transmission electron microscopy. Ultrastructural analysis, performed by David Lutz (ZMNH, Universitätsklinikum Hamburg-Eppendorf, Germany), showed a smaller climbing fiber bouton area in cerebella of L1-deficient mice and mice expressing AAV1-derived mutated L1 in comparison to the climbing fiber bouton area in cerebella from wild-type mice and mice expressing AAV1-derived wild-type L1 (Figure 5.25 A and B). The density of vesicles was reduced in climbing fiber terminals of cerebella from L1-deficient mice and from mice expressing AAV1-derived mutated L1, whereas vesicle density in climbing fiber terminals of cerebella from wild-type mice and of cerebella from mice expressing AAV1-derived wild-type L1 was enhanced (Figure 5.25 B). These results demonstrate that L1 with its LXXLL and FXXLF motifs is important for climbing fiber input to Purkinje cells.

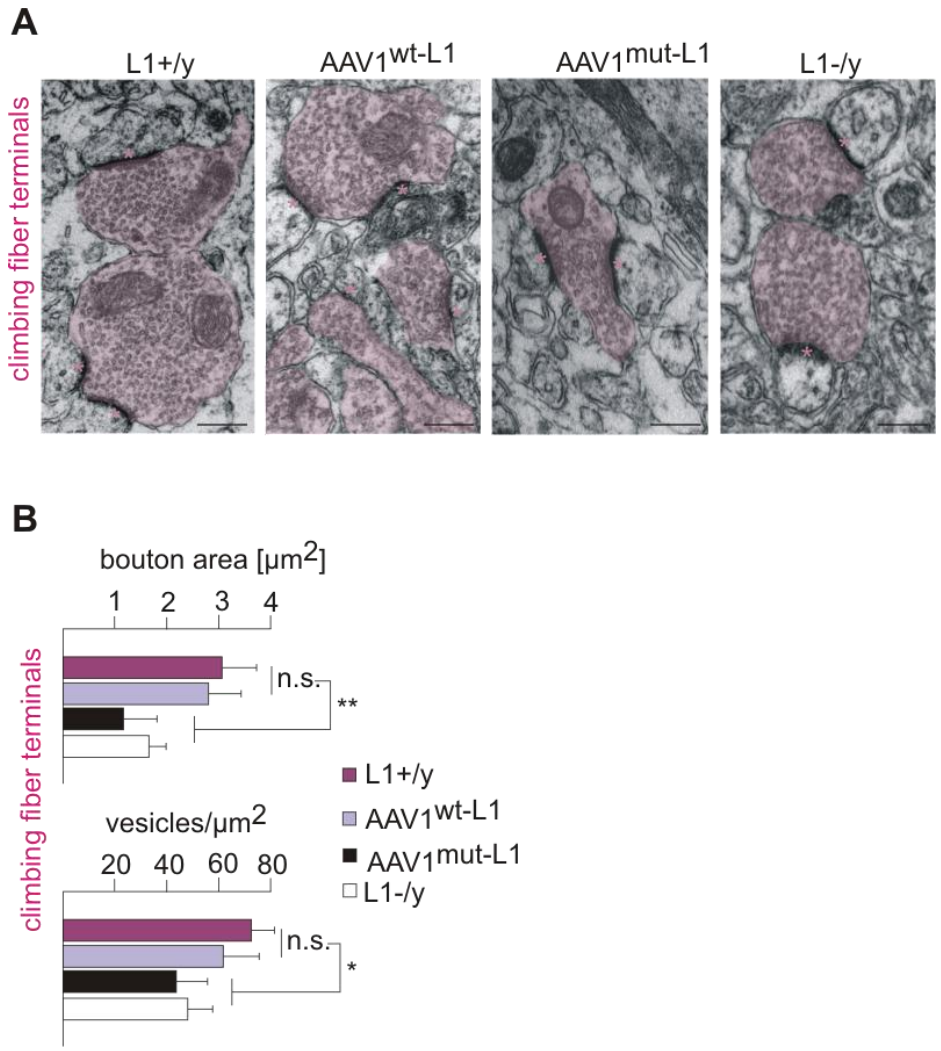

Figure 5.25: Mutation of LXXLL and FXXLF motifs in L1 alters climbing fiber bouton area and vesicle density. Transmission electron microscopy for assessment of climbing fiber terminal areas and amount of synaptic vesicles was performed with brains of L1-deficient mice that had been transduced with AAV1 carrying wild-type L1 ($AAV1^{wt\text{-}L1}$) or mutant L1 ($AAV1^{mut\text{-}L1}$) *in utero* at embryonic day 16 and of wild-type (L1+/y) and L1-deficient (L1-/y) mice. ***A***, Climbing fiber terminals with a characteristic homogenous distribution of vesicles are highlighted in pink. Scale bars, 250 nm. ***B***, Number of boutons and vesicles per area were quantified. Mean values + S.E.M. are shown and were obtained from 50 bouton profiles in randomized ultrathin sections per group from three independent experiments (* $p<0.05$, ** $p<0.01$; one-way ANOVA with Holm-Sidak multiple comparison test). Representative images and quantification were developed by David Lutz (ZMNH, Universitätsklinikum Hamburg-Eppendorf, Germany).

5.2.7 Mice expressing L1 with mutated LXXLL and FXXLF motifs have reduced synaptic contacts of gamma-aminobutyric acidergic and glutamatergic terminals with Purkinje cells

Nuclear receptors are considered to be involved in cerebellar development (Nishihara, 2008). To test whether innervations by gamma-aminobutyric acid

(GABA)ergic and glutamatergic terminals on Purkinje cell dendrites in the cerebellum are influenced in the absence of L1 or by disruption of the LXXLL and FXXLF motifs in L1, immunostaining was performed with cerebella of 12 weeks old wild-type and L1-deficient mice and of mice expressing AAV-derived wild-type L1 or mutant L1. Immunostaining with the GABAergic marker antibody GAD67 showed that the number of GABAergic-positive puncta in the granule cell layer of cerebella from all tested mice did not differ significantly (Figure 5.26 A and C). Interestingly, the numbers of GABA-positive puncta in the Purkinje cell layer and molecular layer of cerebella from L1-deficient mice and mice expressing AAV1-derived mutated L1 were lower relative to the numbers in wild-type mice and mice expressing AAV1-derived wild-type L1. Furthermore, the number of GABA-positive puncta in the molecular layer of mice expressing AAV1-derived wild-type L1 mice was lower compared to that of wild-type mice.

Immunostaining with the glutamatergic marker antibody Vglut1 showed that the innervations by glutamatergic terminals on Purkinje cells was altered in L1-deficient mice and in mice expressing AAV1-derived mutant L1 compared to wild-type mice and mice expressing AAV1-derived wild-type L1 (Figure 5.26 B and D). The number of glutamate-positive puncta in the granule, Purkinje and molecular cell layer of cerebella from L1-deficient mice and mice expressing AAV-derived mutated L1 was decreased compared to the numbers in wild-type mice and mice expressing AAV1-derived wild-type L1. Of note, L1-deficient mice transduced with AAV1 encoding wild-type L1 showed a lower number of glutamate-positive puncta than wild-type mice, but their number was still larger than the number of glutamate-positive puncta in L1-deficient mice and mice expressing AAV1-derived mutated L1. Interestingly, the number of glutamate-positive puncta on Purkinje cell dendrites in the molecular layer in cerebella of L1-deficient mice was larger than that in cerebella of L1-deficient mice after transduction with AAV1 encoding mutated L1. These results demonstrate that the LXXLL and FXXLF motifs in L1 are important for formation of synaptic contacts of GABAergic and glutamatergic terminals with Purkinje cell dendrites and may contribute to cerebellar development and cerebellar-dependent functions.

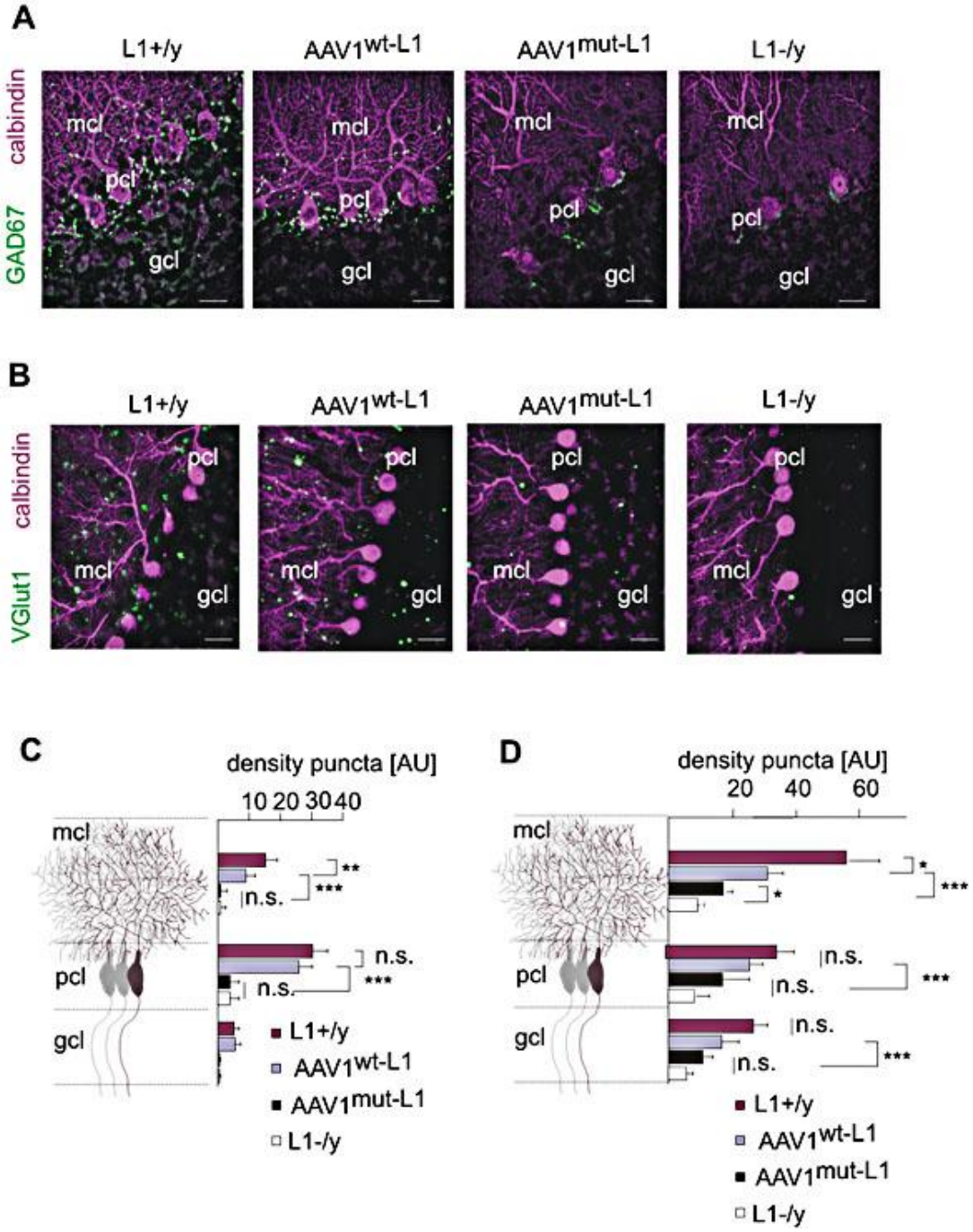

Figure 5.26: Mutation of LXXLL and FXXLF motifs in L1 reduces levels of GABAergic and glutamatergic terminals on Purkinje cells. Paraffin-embedded tissue sections of cerebella of L1-deficient mice that had been transduced with AAV1 carrying wild-type L1 ($AAV1^{wt\text{-}L1}$) or mutant L1 ($AAV1^{mut\text{-}L1}$) *in utero* at embryonic day 16 and of wild-type (L1+/y) and L1-deficient (L1-/y) mice, were subjected to immunostaining with the marker protein calbindin for Purkinje cells and the marker proteins GAD67 and Vglut1 after performance of behavioral studies. Representative immunofluorescence images for calbindin/GAD67 (***A***) and calbindin/Vglut1 (***B***) staining are shown. Scale bars, 50 µm. ***C*** and ***D***, Density of GAD67- and Vglut1-posititve puncta was quantified. Mean values + S.E.M. from at least four images per group from three independent experiments are shown (* p<0.05, ** p<0.01, *** p<0.001; two-tailed Student's t-test). Representative images and quantification was developed by David Lutz (ZMNH, Universitätsklinikum Hamburg-Eppendorf, Germany).

6 DISCUSSION

The present study analyzed two main aspects: i) the import of L1-70 from the cytoplasm into mitochondria and its influence on mitochondrial functions and dynamics and ii) the interaction of L1-70 with nuclear receptors via its LXXLL and FXXLF motifs and the functional consequences of disruption of these interactions by mutation of the motifs on hippocampal structure and cerebellar-related functions.

6.1 Mitochondrial functions are affected by L1-70

6.1.1 L1-70 is imported into mitochondria, interacts with GAPDH, the complex I subunit NDUFV2 and regulates complex I activity and the mitochondrial membrane potential

In the present work L1-70 was detected in mitochondrial lysates from brains of wild-type mice. Full-length L1 or other L1 fragments could not be detected in mitochondrial lysates. Control antibodies directed against nuclear, endoplasmic reticulum or cytoplasmic proteins showed that the mitochondrial fraction was not contaminated with other fractions, indicating that L1-70 is indeed located in mitochondria. *In vitro* import assays showed transport of L1-70 from L1-70-containing cytoplasm of wild-type mice into L1-lacking mitochondria from L1-deficient mice. Treatment of cytoplasmic fractions with a L1 antibody blocked the *in vitro* import of L1-70 into mitochondria. The *in vitro* transport of L1-70 was also blocked by a TOM70 antibody, but not by an antibody against TOM40. Therefore, it is very likely that L1-70 is recognized by TOM70, the receptor of the outer mitochondrial membrane for nuclear encoded mitochondrial precursor proteins without cleavable mitochondrial translocation signal sequence, and that L1-70 binds directly to TOM70. TOM40, the channel-forming protein of the TOM complex, either does not bind directly to L1-70 and the translocation of L1-70 does not require direct interaction with TOM40 or binding of the TOM40-specific antibody to TOM40 does not interfere with binding of L1-70 to TOM40 or with the translocation of L1-70 via TOM40. Previous studies show that precursor proteins can be inserted into the outer mitochondrial membrane without involvement of TOM40 (Otera et al., 2007, Becker et al., 2011, Papic et al., 2011). Thirty percent of mitochondrial proteins lack N-terminal targeting signals and for many mitochondrial proteins the internal targeting signals are not known (Diekert et al., 1999). L1-70 does not contain an N-terminal import signal or one of the

following internal targeting signals: a targeting signal within the last β-strand, multiple α-helical transmembrane segments or multiple cysteine residues which are present in intermembrane space proteins. Precursor proteins with an N-terminal signal use the presequence pathway for import into mitochondria. Precursor proteins which contain a targeting signal within the last β-strand are imported into mitochondria through the β-barrel pathway, whereas precursor proteins with multiple α-helical transmembrane segments or multiple cysteine residues are imported through the Mim1 pathway or the MIA pathway, respectively (Kutik et al., 2008, Schmidt et al., 2011, Becker et al., 2012). Hence, it is very likely that L1-70 is not imported into mitochondria through the presequence pathway, the β-barrel pathway, the MIA pathway or the Mim1 pathway. Therefore, the only known pathway which might be responsible for import of L1-70 into mitochondria is the pathway for precursor proteins with an internal targeting signal through recognition by TOM70 and translocation via TOM40 to the TIM22 complex. Precursor proteins which take this pathway are transported to the inner mitochondrial membrane; therefore it is very likely that L1-70 is localized at the inner mitochondrial membrane.

First hints about the function of L1-70 in mitrochondria come from the observation that mitochondria of L1-deficient mice showed reduced complex I activity compared to mitochondria from wild-type mice. Thus, L1-70 appears to be imported from the outer mitochondrial membrane by TOM70 through the intermembrane space to the inner mitochondrial membrane by the TIM22 complex or an unknown import pathway to regulate the activity of complex I. Complex I is located in the inner mitochondrial membrane and protrudes into the mitochondrial matrix to create an L-shaped structure with a hydrophobic membrane and a hydrophilic peripheral arm with two independent functions (Hofhaus et al., 1991, Guénebaut et al., 1997, Friedrich and Bottcher, 2004). The peripheral arm consists of the electron input module with a NADH oxidation site and the NADH-oxidizing dehydrogenase module (N-module) which contains the subunit NDUFV2. The N-module is responsible for electron transfer via a flavinmononucleotide molecule and a series of iron-sulfur clusters. The electron output module, the Q-module, which transfers electrons to the ubiquinone reduction site, is the second part of the peripheral arm (Mathiesen and Hägerhäll, 2002, Sazanov, 2015). The membrane arm contains the proton-translocating P-module that catalyzes protein transport through the membrane (Brandt, 2006,

Sazanov, 2015). By mass spectrometry analysis of probes from affinity chromatography using the intracellular domain of L1 as bait, NDUFV2, a complex I subunit, was identified as a potential binding candidate for the intracellular domain of L1. ELISA and co-immunoprecipitation verified that NDUFV2 directly interacts with L1-70. Therefore, L1-70 might influence complex I activity by binding to the core subunit of the hydrophilic part of complex I. Complex I activity was enhanced after *in vitro* import of L1-70 from L1-70-containing cytoplasm into L1-lacking mitochondria, showing that L1-70 is involved in the regulation of complex I activity. Literature data describe that inhibition of the electron transport chain at the site of complex I induces depolarization of the mitochondrial membrane potential (Pravdic et al., 2012). In the present study I could detect that L1-lacking cells, e.g. cerebellar neurons from L1-deficient mice and HEK293 cells, or transduced HEK293 cells lacking L1-70 exhibit an impaired membrane potential compared to cells containing L1 or L1-70. Since L1 influences complex I activity, it is likely that the mitochondrial membrane potential is disturbed by dysfunctional complex I activity in the absence of L1 or L1-70. In contrast to complex I, the activity of complex II, III, IV or V was not altered in mitochondria of L1-deficient mice. The fact that the complex I activity in mitochondria of CHL1- and NCAM-deficient mice and their wild-type littermates did not differ indicates that the influence on complex I activity is L1-specific.

The interaction of L1-70 with mitochondrial GAPDH was shown by co-immunoprecipitation. GADPH produces NADH via oxidative phosphorylation and it was shown that L1 binds to GAPDH via the Ig-like domains I-VI and the fibronectin type III homologous repeats 4-5 at the cell surface of neurons (Makhina et al., 2009). Here, binding of mitochondrial L1-70 that lacks the Ig-like domains with GAPDH was shown. Since L1-70 lacks all Ig-like domains and fibronectin type III homologous repeats 1-3 are not needed for binding of GAPDH, the binding of L1-70 with GAPDH can only be mediated by the fibronectin type III homologous repeats 4-5. Whether L1-70 binds GAPDH to promote NADH production that is used by complex I for oxidation of NADH and generation of a proton gradient at the intermembrane space, and whether NDUFV2 and binding of L1-70 to this complex I subunit affects this process is not known and needs to be further studied. Another interesting aspect is the finding that GAPDH binds to cytochrome *c* oxidase of complex IV and that complex IV maintains the assembly and stability of complex I (Diaz et al., 2006, Li et al., 2007,

Ramzan et al., 2013). Disrupted interaction between L1 and GAPDH in mitochondria could induce changes in complex IV that in turn alters the structure and function of complex I. However, an argument against this idea is that no impact of L1 on complex IV activity in mitochondria of L1-deficient mice could be observed.

6.1.2 Impaired mitochondrial membrane potential induces mitophagy in the absence of L1-70

The present study showed that the co-localization of mitochondria and the mitophagy marker protein LC3 was enhanced in HEK293 cells not expressing L1 or L1-70. Consequentially, more mitochondria were degraded in L1- and L1-70-lacking cells. Literature data describe that mitochondria with impaired membrane potential are degraded preferentially compared to mitochondria with intact membrane potential (Twig et al., 2008). The most studied mechanism for mitophagy in mammalian cells is the PINK1/Parkin-mediated mitophagy pathway (Youle and Narendra, 2011, Ding and Yin, 2012). Intact membrane potential leads to import of cytosolic PINK1 via the outer mitochondrial membrane and transfer of PINK1 to the inner mitochondrial membrane for proteolytic processing. Interestingly, TOM70 is essential for import of PINK1 into mitochondria, whereas TOM40 seems not to be involved in the import of PINK1 (Kato et al., 2013). Impaired membrane potential induces accumulation of PINK1 at the outer membrane of dysfunctional mitochondria and inhibits PINK1 cleavage which leads to recruitment of Parkin and to Parkin-induced mitophagy (Narendra et al., 2010a). Since absence of L1 leads to reduced complex I activity and impaired mitochondrial membrane potential, it is reasonable that the mitophagy process is more pronounced in L1- and L1-70-lacking cells. Whether impaired mitochondria resulting from the absence of L1 and L1-70 are degraded by the PINK1/Parkin-mediated mitophagy pathway remains not known and needs to be further studied. However, the levels of Parkin determined by Western blot analysis did not differ in mitochondria from wild-type and L1-deficient mice (data not shown), suggesting that PINK1-mediated translocation of cytosoplasmic Parkin to mitochondria is not altered in L1-deficient mitochondria.

6.1.3 Impaired mitochondrial membrane potential induces mitochondrial fission in the absence of L1-70

Mitochondrial fusion in untransduced L1-lacking HEK293 cells was enhanced after transduction with AAV1 coding for wild-type L1. Additionally, mitochondria in

cerebellar neurons of L1-deficient mice showed mostly a fragmented morphology, whereas mitochondria in cerebellar neurons from wild-type mice appeared less fragmented and more elongated. In HEK293 cells lacking L1 or lacking the transmembrane fragment of L1, mitochondria seemed to be strongly fragmented relative to mitochondria in HEK293 cells expressing L1. For degradation of mitochondria, fusion of mitochondria exhibiting an impaired membrane potential with the functional mitochondrial network is prevented. To achieve this effect, mitochondrial proteins required for mitochondrial fusion, such as Mfn1 and Mfn2 are ubiquitinated by Parkin (Gegg et al., 2010, Ashrafi and Schwarz, 2013). Therefore, it is likely that absence of L1-70 induces defects in complex I activity resulting in an impaired membrane potential and dysfunction of fusion that leads to mitophagy.

6.1.4 Impaired mitochondrial membrane potential induces reduced motility and retrograde transport of mitochondria in the absence of L1-70

An impaired mitochondrial membrane potential that induces mitophagy is also accredited to disturbed mitochondrial trafficking. Mitochondrial trafficking on microtubules over long distances and on actin microfilaments for short-range movements is impaired by disruption of the binding of kinesin/dynein motors and adapter proteins with mitochondria which have an impaired membrane potential. The present work demonstrated that mitochondrial motility was reduced in cerebellar and hippocampal neurons from L1-deficient mice relative to mitochondrial motility in neurons from wild-type mice. After stimulation with an antibody that triggers L1-dependent cellular responses, the mitochondrial motility was enhanced in cerebellar and hippocampal neurons from wild-type mice relative to the mitochondrial motility before stimulation. In contrast, mitochondrial mobility was not different in cerebellar neurons and hippocampal neurons from wild-type and L1-deficient mice as well as in cerebellar and hippocampal neurons from wild-type mice before and after stimulation with an antibody that triggers L1-dependent functions. Mitochondria from cerebellar neurons of *shiverer* mutant mice that do not express MBP and in which generation of L1-70 is prevented show reduced mitochondrial motility compared to motility of mitochondria in cerebellar neurons from wild-type mice. This result demonstrates that L1-70, but not full-length L1, is responsible for higher mitochondrial motility.

Literature data show that neurons exhibit a complex mitochondrial motility pattern along axons and dendrites with 20-30% (Kang et al., 2008, Chen and Sheng, 2013)

or 10-40% (Schwarz, 2013) motile mitochondria, respectively, and 60-90% stationary mitochondria (Morris and Hollenbeck, 1993, Ligon and Steward, 2000, Misgeld et al., 2007, Russo et al., 2009, Wang and Schwarz, 2009). The results from my thesis were comparable to these values showing ~11-30% motile mitochondria and ~70-89% of stationary mitochondria in the analyzed neurons. Motile mitochondria move along microtubules and actin microfilaments with an average velocity of 0.3-2.0 µm/sec (Morris and Hollenbeck, 1995, Chada and Hollenbeck, 2003, Hirokawa and Takemura, 2005, Milone and Benarroch, 2012, Sheng and Cai, 2012). In L1- and L1-70-lacking neurons mitochondria were transported with a velocity of ~0.2-0.4 µm/sec, while in L1-expressing neurons mitochondria moved with a velocity of ~0.5-0.7 µm/sec and after stimulation with a L1-specific antibody with a velocity of ~1.02-1.04 µm/sec. This strengthens the notion that L1-70 has an impact on mitochondrial motility, but not on mitochondrial mobility.

In general, motile mitochondria with intact membrane potential move anterogradely to synaptic regions with high metabolic demand, while motile mitochondria with impaired membrane potential move retrogradely for degradation and repair (Milone and Benarroch, 2012). The analysis showed that the bidirectional transport of mitochondria in L1-lacking neurons is disturbed. Twenty four percent of mitochondria in L1-lacking neurons moved anterogradely, while 76% of mitochondria in L1-lacking neurons were transported retrogradely. The pronounced mitochondrial retrograde transport in L1-lacking neurons might be due to the impaired membrane potential of mitochondria caused by dysfunctional complex I in the absence of L1 or L1-70. Absence of L1 or L1-70 induces mitophagy to degrade damaged mitochondria with a dysfunctional membrane potential.

6.1.5 Mitochondrial dynamic proteins Miro1 and Drp1 are interaction partners of L1-70 at the outer mitochondrial membrane

Co-immunoprecipitation using mitochondrial lysates of wild-type mice indicated binding of L1-70 to Miro1. Miro1 and Miro2 are anchored to the outer mitochondrial surface and function as calcium-dependent regulators in control of mitochondrial motility. In absence of Ca^{2+} the C-terminal end of kinesin is anchored to the mitochondrium by interacting with Miro1 and Miro2 and the TRAK/milton complex. The N-terminal end of kinesin is free to associate with microtubules for transport. Elevated Ca^{2+} levels in activated synapses lead to binding of Ca^{2+} to the calcium-

binding EF-hand motif at the N- and C-terminal end of Miro1 and Miro2 followed by dissociation of Miro1 and Miro2 from kinesin due to conformational change (Fransson et al., 2003 and 2006, Cai and Sheng, 2009, MacAskill et al., 2009, Reis et al., 2009). Therefore, Ca^{2+}-dependent control of mitochondrial motility is important for determining the localization of stationary mitochondria at active synapses (Saotome et al., 2008, MacAskill et al., 2009, Wang and Schwarz, 2009). Interaction of L1-70 with Miro1 might influence motility of mitochondria, but the mechanism underlying this interaction and the role of Ca^{2+} for this interaction remains to be determined. Since mitochondrial motility in neurons of L1-deficient mice is reduced and motility is dependent on the mitochondrial Ca^{2+} level, it is possible that the Ca^{2+} level is reduced in mitochondria of L1-deficient mice compared to the Ca^{2+} level in mitochondria of wild-type mice. But an argument against this aspect is that the stationary pool of mitochondria does not differ in L1-deficient and wild-type mice and only the motility is influenced by L1 or L1-70 in an unidentified way.

Co-immunoprecipitation using mitochondrial lysates of wild-type mice revealed binding of L1-70 to Drp1. Post-translational modifications including phosphorylation, ubiquitylation, and sumoylation of Drp1 induce its recruitment to the outer mitochondrial membrane for fission. Mitochondrial fission factor recruits Drp1 to the mitochondrion and fission protein 1 is responsible for the assembly of the fission apparatus. Drp1 oligomerizes to form spirals for fission of the outer mitochondrial membrane (Ingerman et al., 2005, Wasiak et al., 2007, Otera et al., 2010). The role of L1-70 in fission might be to control Drp1 to provide a regulated balance of fusion and fission. Literature data describe a novel Drp1 regulator, the peptide inhibitor 110, which is neuroprotective by inhibition of mitochondrial fragmentation and improvement of mitochondrial membrane potential and mitochondrial integrity. Peptide inhibitor 110 interacts with Drp1 and inhibits Drp1's GTPase activity and association with mitochondria. In this case, Drp1-induced mitochondrial fission and cell death is blocked (Qi et al., 2013, Filichia et al., 2016). It is possible that L1-70 has a similar role as peptide inhibitor 110 and this possibility remains to be examined in future studies. Literature data show that L1 is responsible for neuroprotection against oxidative stress (Lutz et al., 2014a) and enhances the survival of neurons by prevention of cell death (Chen et al., 1999). Hence, mitochondrial L1-70 might have a similar function and might reduce cell death through interaction with Drp1 and by

regulating mitochondrial fission and mitochondrial degradation. The mechanisms behind regulation of complex I activity and membrane potential of mitochondria, and regulation of mitochondrial trafficking and fusion and fission remain elusive. Whether the interaction of L1-70 with major mitochondrial dynamic proteins such as Miro1 and Drp1 is required to stabilize mitochondrial complex I activity and the PINK1/Parkin-mediated mitophagy pathway or if L1-70 has an additional role for mitochondrial dynamics needs to be further studied.

6.2 Central nervous system functions are affected by the LXXLL and FXXLF motifs in L1

6.2.1 LXXLL and FXXLF motifs in L1-70 mediate the interaction of L1-70 with the nuclear receptors PPARɣ, RXRβ and ERα/β

Western blot analysis showed that L1-70, which is generated by cleavage of MBP and transported into the nucleus, was present in the nuclear extract from wild-type neurons as well as in the nuclear extract from L1-deficient neurons transduced to express wild-type L1 or mutated L1. In ELISA experiments performed with nuclear fractions from L1-deficient neurons and from AAV1-transduced L1-deficient neurons expressing wild-type L1 or mutated L1, binding of nuclear wild-type L1-70 with PPARɣ, RXRβ and ERα/β recombinant proteins was demonstrated. Binding of nuclear wild-type L1-70 to AR, VDR and LXRβ recombinant proteins could not be shown. Whether L1 interacts with these receptors *in vivo* or if L1 interacts with other nuclear receptors, was not investigated. Furthermore, ELISA experiments showed that mutation of the LXXLL and FXXLF motifs in L1 led to disruption of the binding between L1-70 and PPARɣ, RXRβ and ERα/β, suggesting that binding between L1-70 and PPARɣ, RXRβ and ERα/β is mediated by these motifs in L1. Thus, it is likely that L1-70 might act as a coactivator for nuclear receptor-mediated gene expression. In the literature, over 350 different coregulators comprising coactivators and corepressors are described, but proteomic analyses of coregulators showed that the total number of coregulators is by far much higher (Lonard and O'Malley, 2012). Binding of coactivators to either ligand-bound or unliganded nuclear receptors is associated with interaction between the AF-2 region within the LBD of nuclear receptors and single or multiple LXXLL or FXXLF motifs in order to regulate transcriptional activation. However, approximately half of the currently known coactivators do not contain LXXLL or FXXLF motifs, but they are still able to

associate with nuclear receptors. Coactivators have enzymatic activities and mediate posttranslational protein modifications such as methylation, acetylation, phosphorylation, sumoylation, and ubiquitination (Bulynko and O'Malley, 2011). In which biochemical process L1-70 takes part as a coactivator and affects transcriptional activity of the nuclear receptors PPARɣ, RXRβ and ERα/β needs to be determined in further experiments. Also, whether L1-70 binds to liganded or unliganded PPARɣ, RXRβ and ERα/β needs to be further analyzed.

6.2.2 LXXLL and FXXLF motifs in L1-70 are essential for L1-mediated promotion of neurite outgrowth

L1 is essential for neuron to neuron interaction during early development of the central nervous system and influences neurite outgrowth and neuronal survival (Lutz et al., 2014a). Neurite outgrowth assay which tested the impact of the LXXLL and FXXLF motifs on neurites showed enhanced total neurite length in L1-deficient neurons transduced to express wild-type L1 in comparison to the total neurite length of L1-lacking neurons and neurons expressing mutated L1 lacking the motifs LXXLL and FXXLF. Hence, the motifs LXXLL and FXXLF in nuclear L1-70 seem to be necessary for L1-induced neurite outgrowth.

6.2.3 LXXLL and FXXLF motifs in L1-70 are required for hippocampal mossy fiber synapse formation

Nuclear receptors have regulatory functions in the development of the central nervous system and nuclear receptors, which can be regulated by coactivators that contain the LXXLL and FXXLF motifs, influence hippocampal-dependent synaptic plasticity (Chiang et al., 1998, Fugger et al., 2000, Isgor et al., 2003, Bodo and Rissman, 2006). Ultrastructural analysis revealed a smaller mossy fiber bouton area and a reduced total length of the synaptic cleft in hippocampal sections from L1-deficient mice or mice expressing mutated L1 relative to the mossy fiber bouton area and total length of the synaptic cleft in hippocampal sections from wild-type mice and L1-deficient mice transduced to express wild-type L1. In addition, in hippocampal sections from L1-lacking mice and mice expressing mutated L1 more symmetric inhibitory synapses and less asymmetric excitatory synapses were identified than in hippocampal sections from L1-expressing mice. These findings indicate that disruption of the interaction of L1-70 with the nuclear receptors PPARɣ, RXRβ and ERα/β via the LXXLL and FXXLF motifs affect the hippocampal circuit due to

impairments in the connectivity of mossy fiber synapses. Mossy fiber synapses are non-myelinated axons of the granule cells of the dentate gyrus that provide inhibitory and excitatory input in the dentate gyrus hilus and the proximal apical and basal dendrites of CA3 pyramidal cells. Mossy fiber synapses are crucial in processing, storage and recall of spatial information in the hippocampal trisynaptic circuit (Lisman, 1999, Nicoll and Schmitz, 2005, Bischofberger et al., 2006). Literature data show that large mossy fiber bouton terminals project to CA3 pyramidal cells and hilar mossy cells, whereas small mossy fiber bouton terminals and filopodial extensions target GABA-containing interneurons in the dentate hilus and stratum lucidum of area CA3 (Acsády et al., 1998). The smaller mossy fiber bouton area in hippocampal sections from L1-deficient mice or mice expressing mutated L1 relative to the mossy fiber bouton area in hippocampal sections from L1-expressing mice might hint at an impact of L1 on the CA3 pyramidal cell network and excitatory synaptic input of the dentate gyrus in the hippocampus. Excitatory synaptic input at mossy fiber synapses depends on release of glutamate and stimulation of postsynaptic glutamate receptors (Nicoll and Schmitz, 2005). Less asymmetric excitatory synapses in the L1-lacking hippocampus might indicate a reduced release of glutamate and reduced glutamate uptake by glutamate receptors at the postsynaptic site leading to a disturbed function of the hippocampal trisynaptic circuit.

Interestingly, a large body of evidence suggests an influence of nuclear receptors in maintenance of hippocampal structure and synaptic plasticity. ERα/β of the steroid nuclear receptor family were found throughout the dentate gyrus (Weiland et al., 1997, Herrick et al., 2006, McEwen and Milner, 2007) and their ligand estradiol enhances the synaptic excitability and glutamatergic synaptic transmission in the hippocampus of male rats (Teyler et al., 1980). Decrease of estradiol concentration modifies the density and morphology of spines in CA1-CA3 neurons (Hasegawa et al., 2015). Furthermore, testosterone, a ligand for AR, increases the survival of new dentate gyrus neurons via an AR-dependent mechanism and testosterone supplementation has a positive effect upon spatial memory in men (Cherrier et al., 2001, Sherwin, 2003, Janowsky, 2006, Driscoll and Resnick, 2007, Hamson et al., 2013, Atwi et al., 2016). Another nuclear receptor, PPARα and its ligands hydroxydimethylbutyrate, hexadecanamide and octadecenamide may have an influence on synaptic activity and hippocampal synaptic plasticity (Burris, 2016). To

test whether the interaction of L1-70 with the nuclear receptors PPARɣ, RXRβ and ERα/β via the LXXLL and FXXLF motifs has functional *in vivo* importance, the spatial learning abilities of wild-type and L1-deficient mice or mice expressing mutant L1 lacking the LXXLL and FXXLF motifs need to be analyzed in suitable behavioral tests such as the Morris-type water maze test. To determine the influence on the CA3 pyramidal cell network in the hippocampus, hippocampal tissue sections of wild-type mice, L1-deficient mice and mice expressing wild-type L1 or mutated L1 could be stained with the glutamatergic marker Vglut that labels glutamatergic CA3 pyramidal neurons. This might provide information about an impact of L1 on the CA3 pyramidal cell network and elucidate whether L1 influences the hippocampal trisynaptic circuit via the LXXLL and FXXLF motifs. Currently, hippocampal pyramidal cells and their synaptic function are studied with electrophysiological techniques such as paired whole cell recordings. This method works with organotypic hippocampal slices and enables direct characterization of the synaptic connections between single neurons. It involves concurrent whole cell patch clamp recordings from two synaptically connected neurons. Paired whole cell recordings provide highly accurate details on the properties of synaptic transmission and plasticity and were already successful in CA3-CA1 pairs (Fourie et al., 2014). Therefore, this technique might be of interest to analyze the influence of L1 with its LXXLL and FXXLF motifs on the hippocampal transmission in the CA3 pyramidal cell network.

6.2.4 LXXLL and FXXLF motifs in L1-70 affect motor coordination and learning and synaptic connectivity in the cerebellum

Nuclear receptors can be regulated by coactivators which contain the LXXLL and FXXLF motifs and influence cerebellar-dependent functions. Therefore, the influence of the interaction of L1 and nuclear receptors via the LXXLL and FXXLF motifs in L1 in cerebellar regulated motor coordination and learning were investigated. Rotarod and pole test showed that L1-deficient mice and mice expressing mutated L1 had a lower latency to fall without showing motor learning in subsequent trials, while wild-type mice and mice expressing wild-type L1 had a higher latency to fall and showed motor learning in subsequent trials. The pole test confirmed that L1-deficient mice and mice expressing mutated L1 had impairments in motor coordination and evidenced that L1-deficient mice and mice expressing mutated L1 performed significantly worse than wild-type mice and mice transduced to express wild-type L1. Against expectation, L1-deficient mice and mice expressing mutated L1 showed an

improvement not to fall down the vertical pole in subsequent trials. As expected, wild-type and mice transduced to express wild-type L1 did not fall down from the vertical pole in all consecutive trials. It is likely that the Rotarod test has a higher level of difficulty and requires additional motor balance skills on the accelerating rod than the pole test. An explanation for the impairments in motor coordination and learning in L1-deficient mice and mice expressing mutated L1 might be the disturbed synaptic connectivity in the L1-lacking cerebellum. Immunostaining showed expression of L1 on Purkinje cells in the granule layer, the Purkinje cell layer and the molecular layer of wild-type mice and mice expressing mutated L1. Ultrastructural analysis revealed a smaller climbing fiber bouton area with a decreased density of vesicles in cerebella of L1-deficient mice and mice expressing mutated L1 relative to the climbing fiber bouton area and vesicle density in cerebella of wild-type mice and of mice expressing wild-type L1. Moreover, the analysis showed that innervations by GABAergic and glutamatergic terminals on Purkinje cell dendrites were influenced by L1. Disruption of the LXXLL and FXXLF motifs in L1 led to a reduction of the number of GABA-positive puncta in the Purkinje cell layer and molecular layer. The same reduction was observed in L1-deficient brains. Besides, a reduction of the number of glutamate-positive puncta in the granule, Purkinje and molecular cell layer of cerebella from L1-deficient mice and mice expressing mutated L1 was shown. In the cerebellar circuitry, GABAergic Purkinje cells modulate the inhibitory cerebellar output and are likely to be responsible for motor coordination and learning. Glutamatergic excitatory input is provided by climbing fibers that directly form synaptic contacts with Purkinje cells and mossy fibers. Mossy fiber synapses contact indirectly Purkinje cells through paralles fibers that are the axons of the glutamatergic granule cells. GABAergic inhibitory input to Purkinje cells is provided by basket and stellate cells (Purves et al., 2001). Lack of L1 as well as disruption of the interaction of L1-70 via its LXXLL and FXXLF motifs with the nuclear receptors PPARɣ, RXRβ and ERα/β might cause a disturbed cerebellar circuitry within the glutamategic input from climbing fibers and mossy fibers in the granule cell layer. This leads to impaired synapse formation in the Purkinje cell layer of climbing fibers with Purkinje cells and of mossy fibers with glutamatergic granule cells. These alterations might result in reduced inhibitory synapse innervations of Purkinje cell dendrites in the molecular layer by basket, stellate and parallel fibers and might explain the reduction of GAD67 that labels inhibitory GABAergic synapses in L1-deficient mice and mice expressing

mutated L1. These findings indicate dysfunctional Purkinje cell output that might lead to deficits in motor coordination and learning *in vivo*. Dysfunctional Purkinje cell output might result from lack of L1 or disruption of the interaction of nuclear L1-70 with the nuclear receptors PPARɣ, RXRβ and ERα/β. Nuclear receptors and their coregulators are known to play essential roles in cerebellar development. Upon estrogen treatment the level of GABAergic receptors in the cerebellum decreases and estrogens and anti-estrogens change the regulation of glutamate signaling by Purkinje cells (Smith et al., 1988 and 1989). Furthermore, for members of the p160 steroid receptor coactivator family it was shown that they interact with the nuclear receptors progesterone receptor, glucocorticoid receptor, ER, thyroid receptor, RXR and PPARγ (Xu and O'Malley, 2002). Steroid receptor coactivator 1 was detected in the Purkinje cell layer and weakly in the molecular layer and the granule layer of the cerebellum at neonatal stage (Yousefi et al., 2005). Adult steroid receptor coactivator 1-lacking mice show impaired motor function in behavioral tests and abnormal development of Purkinje cells (Nishihara et al., 2003 and 2008). Another coactivator with LXXLL motifs is the ubiquitin-protein ligase E6-associated protein, which interacts with the liganded nuclear receptors progesterone receptor, ER, AR, glucocorticoid receptor, retinoic acid receptor and thyroid receptor (Nawaz et al., 1999). Loss of the functional maternal E6-associated protein allele leads to a disease called Angelman syndrome with tremor, ataxia, deficits in motor control and impaired motor learning, a reduced cerebellar volume and apoptosis of Purkinje cells and internal granule neurons (Jiang et al., 1998, Nishihara, 2008). Therefore, it is very likely that L1-70 - via its LXXLL and FXXLF motifs - acts also as a coactivator of the nuclear receptors PPARɣ, RXRβ and ERα/β and regulates their function in generation and maintenance of cerebellar innervations and in coordination of cerebellar controlled movements.

6.2.5 L1 influences forelimb strength in mice after training

The grip strength test showed that the muscle strength of L1-deficient mice was significantly lower relative to the muscle strength of wild-type mice after performance of the Rotarod and pole test, but no significant difference was measured before performance of the behavioral tests. This suggests that L1 ablation causes impaired improvement of muscle strength of the forelimbs in L1-deficient mice, whereas wild-type mice are able to improve their muscle strength. Literature data describe muscle weakness and loss of strength in the lower limbs together with spasticity as a

characteristic factor of hereditary spastic paraplegia due to a mutation in the gene of L1 (Muñoz et al., 2016). Also, it was shown for L1-deficient mice which have weak hind limbs, to exhibit a reduced size of corticospinal tracts and hypoplastic cerebellar vermis (Dahme et al., 1997, Fransen et al., 1998). The behavior of L1-deficient mice was described as reminiscent of that of rodents with cerebellar lesions (Fransen et al., 1998). The result that L1-deficient mice have lower muscle strength than wild-type mice and are not able to improve their muscle strength after performance of behavioral tests is a matter of interest. It is likely that defects in the connectivity of the cerebellar circuitry impair the efficiency of motor control tasks and result in reduced development of muscle strength. But the exact mechanism for motor control and motor learning in relation to development of muscle strength could not be clarified.

6.3 Ablation of mitochondrial and nuclear L1-70 might be associated with neurodegenerative diseases

Common neurodegenerative diseases include Alzheimer's disease, Parkinson's disease and Huntington's disease. Previous studies describe significant impact of L1 on Alzheimer's disease. L1 binds to β-amyloid, reduces its aggregation and diminishes Alzheimer's disease pathology in a mouse model (Djogo et al., 2013). Also, increased amounts of soluble L1 fragments in the cerebrospinal fluid are associated with Alzheimer's disease and dementia syndromes (Strekalova et al., 2006). Furthermore, alterations of L1-70 levels after spinal cord injury or in a mouse model of Alzheimer's disease show that L1-70 has functions in development, regeneration, neurodegeneration and tumorigenesis (Lutz et al., 2012). Beyond that, neurodegenerative diseases are associated with impaired mitochondrial function (Oettinghaus et al., 2012, Itoh et al., 2013, Burté et al., 2015). The present study contributes to these aspects and indicates that L1 and its influence on mitochondria might be associated with neurodegenerative diseases. In the first part of my study I showed that L1 ablation impacts mitochondrial characteristics. L1 ablation leads to alterations in complex I activity and mitochondrial membrane potential. Defects in complex I activity were identified first in the substantia nigra and blood platelets of patients with Parkinson's disease and also in lymphocytes and in muscle tissue from these patients (Beal, 2007). In addition, complex I activity is reduced in mitochondria, platelets, and lymphocytes from patients with Alzheimer's disease and their postmortem brain tissue (Johri and Beal, 2012). It has been shown that in sporadic Alzheimer's disease mitochondrial dysfunction causes β-amyloid peptide

accumulation, synaptic degeneration, and formation of neurofibrillary tangles (Swerdlow et al., 2010, Johri and Beal, 2012). The present study gives further hints for the impact of L1 on neurodegenerative diseases and shows that L1 ablation alters mitochondrial dynamics like fusion and motility. Several studies describe alterations in mitochondrial dynamics, morphology, motility and activity that are linked to Alzheimer's disease (Nunomura et al., 2001, Moreira et al., 2010, Cai and Tammineni, 2016). In Huntington's disease abnormal ultrastructure of mitochondria in cortical biopsies obtained from patients with both juvenile and adult-onset Huntington's disease is described. Also, reductions in numbers of mitochondria in Huntington's disease postmortem brain tissue and in striatal cells were shown (Johri and Beal, 2012). Additionally, mutant huntingtin abnormally recruits Drp1 on the outer mitochondrial membrane and leads to pronounced fission and neuronal sensitivity to apoptosis in rat neurons and in fibroblasts from patients with Huntington's disease (Song et al., 2011, Archer, 2013) and influences calcium handling and mitochondrial trafficking in axons (Chang et al., 2006, Petrasch-Parwez et al., 2007, Orr et al., 2008). Hence, L1 ablation in mitochondria might contribute to defects in neurodegenerative diseases.

The second part of my thesis shows that L1-70 acts as a coactivator of nuclear recptors such as PPARɣ, RXRβ and ERα/β via its LXXLL and FXXLF motifs. Lack of L1 and disruption of this interaction by mutation of the LXXLL and FXXLF motifs induces defects in neurite outgrowth, hippocampal and cerebellar circuitry as well as in cerebellar regulated functions *in vivo*. Nuclear receptors are known to have crucial functions in neurodegenerative disorders. PPARɣ is required for regulation of insulin sensitivity, glucose homeostasis, fatty acid oxidation, immune responses, redox balance, cardiovascular integrity and cell fates (Chen et al., 2012). Literature data show that elevated PPARɣ levels were found in brains of patients with Alzheimer's disease and that the PPARɣ agonist rosiglitazone was associated with improved cognition and memory in patients with Alzheimer's disease (Jiang et al., 2008). In addition, PPARγ activation is described to improve mitochondrial metabolism and biogenesis (Alaynick, 2008). The functions of the nuclear receptor RXRβ are not yet fully understood. Literature data suggest a role for retinoid receptors such as RXRβ in chronic degeneration of the spinal cord in a rat model of amyotrophic lateral sclerosis (Jokic et al., 2007). It has been shown that the use of RXR-specific ligands

in combination with PPARγ agonists reduced spinal cord inflammatory reaction in a model of experimental allergic encephalomyelitis (Diab et al., 2004). It was also reported that ERα/β have neuroprotective effects in stroke, Parkinson's disease and Alzheimer's disease (Deroo and Korach, 2006). Therefore, a dysregulation of the interaction of L1-70 with the nuclear receptors PPARɣ, RXRβ and ERα/β might influence neurodegenerative diseases.

7 ABBREVIATIONS

A	alanine
AAV1	adeno-associated virus 1
ADP	adenosine diphosphate
AF	activation function
ANT	adenine nucleotide translocator
APS	ammonium persulfate
AR	androgen receptor
Arg	arginine
ATP	adenosine triphosphate
BCA	bicinchoninic acid
BSA	bovine serum albumine
BS3	bis(sulfosuccinimidyl)-suberate
Ca^{2+}	calcium
CAM	cell adhesion molecule
CHL1	close homolog of L1
CHL1-/-	CHL1-deficient mice
CHL1+/+	CHL1 wild-type mice
CNBr	cyanogen bromide
CoRNR	corepressor nuclear-receptor
CTCF	corrected total cell fluorescence
DAPI	2-(4-amidinophenyl)-1H-indole-6-carboxamidine
DBD	DNA-binding domain
DMEM	Dulbecco's modified Eagle medium
DMSO	dimethyl sulfoxide
DNA	deoxyribonucleic acid
Drp1	dynamin-related protein 1
DTT	dithiothreitol
EDTA	ethylenediaminetetraacetic acid
EGTA	ethylene ethylene glycol-bis(β-aminoethyl ether)-N,N,N',N'-tetraacetic acid

ELISA	enzyme-linked immunosorbent assay
ERα/β	estrogen receptor α/β
ESR1	estrogen receptor 1
ESR2	estrogen receptor 2
F	phenylalanine
$FADH_2$	flavin adenine dinucleotide
FGF	fibroblast growth factor
Fis1	mitochondrial fission protein 1
FRAP	fluorescence recovery after photobleaching
GABA	gamma-aminobutyric acid
GAD67	glutamic acid decarboxylase 67
GAPDH	glyceraldehyde 3-phosphate dehydrogenase
gcl	granule cell layer
GED	GTPase effector domain
GTPase	guanosine triphosphatase
H	hinge or histidine
H^+	proton
HBSS	Hank’s balanced salt solution
HCl	hydrogen chloride
HEK293	human embryonic kidney 293
HEPES	4-(2-hydroxyethyl)-1-piperazineethanesulfonic acid
HR1/2	heptad repeat regions 1 and 2
HRP	horse radish peroxidase
I	isoleucine
Ig	immunoglobulin
IP	immunoprecipitation
JACoP	Just Another Colocalization Plugin
KCl	potassium chloride
kDa	kilo dalton
L	leucine
L1-/y	L1-deficient mice
L1+/y	L1 wild-type mice
LB	lysogeny broth
LBD	ligand-binding domain

LXR	liver X receptor
MAPLC3	microtubule-associated protein light chain 3
MBP	myelin basic protein
mcl	molecular cell layer
Mfn	mitofusin
Mg^{2+}	magnesium
$MgCl_2$	magnesium chloride
$MgSO_4$	magnesium sulfate
MIA	mitochondrial intermembrane space assembly
MIB	mitochondrial isolation buffer
Mim1	mitochondrial import protein 1
Miro	mitochondrial rho guanosine triphosphatase
MOI	multiplicity of infection
MPP	mitochondrial processing peptidase
mRNA	messenger ribonucleic acid
mut-L1	L1 mutation of L_{1136}LILL to A_{1136}LIAA and F_{1046}HILF to Y_{1046}HIAY
MTS	mitochondrial targeting sequence
NaCl	sodium chloride
NAD^+	oxidized nicotinamide adenine dinucleotide
NADH	nicotinamide adenine dinucleotide
Na_2EDTA	disodium ethylenediaminetetraacetate dihydrate
$NaHCO_3$	sodium bicarbonate
Na_2HPO4	disodium hydrogen phosphate
NaN_3	sodium azide
Na_3PO_4	trisodium phosphate
NCAM-/-	NCAM-deficient mice
NCAM+/+	NCAM wild-type mice
NDUFV2	NADH:ubiquinone oxidoreductase core subunit V2
NP-40	nonyl phenoxypolyethoxylethanol
NR box	nuclear-receptor box
NR1H2	nuclear receptor subfamily 1 group H member 2
OPA1	optic atrophy protein 1
OPD	o-phenylenediamine dihydrochloride

OXA	oxidase assembly
p62	pore glycoprotein 62
PAM	presequence translocase-associated motor
PBS	phosphate buffered saline
PBS-T	phosphate buffered saline-Tween-20
PC	Pearson’s coefficient
PFA	paraformaldehyde
Pi	phosphate
PINK1	putative protein kinase 1
PLL	poly-L-lysine
PPARγ	peroxisome proliferator activated receptor γ
pcl	Purkinje cell layer
R/A-L1	L1 mutated in the MBP cleavage site
rho	ras homolog family member
RIPA	radioimmunoprecipitation assay
RXRβ	retinoid X receptor β
SAM	sorting and assembly machinery
SDS	sodium dodecyl sulfate
shi	*shiverer*
TBS	Tris-buffered saline
TBS-T	Tris-buffered saline-Tween-20
TEMED	tetramethylethylenediamine
TIM	translocase of inner mitochondrial membrane
TM	transmembrane
TOM	translocase of outer mitochondrial membrane
TPRs	tandem tetratricopeptide repeats
TRAK	trafficking protein kinesin-binding
Tris-HCl	Tris-hydrogen chloride
VDR	vitamin D receptor
Vglut1	vesicular glutamate transporter 1
WB	Western blot
wt-L1	L1 wild-type
X	any amino acid
Y	tyrosine

8 REFERENCES

Acsády L, Kamondi A, Sík A, Freund T, Buzsáki G (1998) GABAergic cells are the major postsynaptic targets of mossy fibers in the rat hippocampus. J Neurosci 18(9):3386-403.

Alaynick WA (2008) Nuclear receptors, mitochondria and lipid metabolism. Mitochondrion 8(4):329-37.

Amaral DG (1979) Synaptic extensions from the mossy fibers of the fascia dentate. Anat Embryol (Berl) 155(3):241-51.

Andreescu CE, Milojkovic BA, Haasdijk ED, Kramer P, De Jong FH, Krust A, De Zeeuw CI, De Jeu MT (2007) Estradiol improves cerebellar memory formation by activating estrogen receptor beta. J Neurosci 27(40):10832-9.

Appel F, Holm J, Conscience JF, Schachner M (1993) Several extracellular domains of the neural cell adhesion molecule L1 are involved in neurite outgrowth and cell body adhesion. J Neurosci 13(11):4764-75.

Archer SL (2013) Mitochondrial dynamics-mitochondrial fission and fusion in human diseases. N Engl J Med 369(23):2236-51.

Ashrafi G, Schwarz TL (2013) The pathways of mitophagy for quality control and clearance of mitochondria. Cell Death Differ 20(1):31-42.

Askew EB, Minges JT, Hnat AT, Wilson EM (2012) Structural features discriminate androgen receptor N/C terminal and coactivator interactions. Mol Cell Endocrinol 348(2):403-10.

Atwi S, McMahon D, Scharfman H, MacLusky NJ (2016) Androgen Modulation of Hippocampal Structure and Function. Neuroscientist 22(1):46-60.

Bain DL, Heneghan AF, Connaghan-Jones KD, Miura MT (2007) Nuclear Receptor Structure: Implications for Function. Annu Rev Physiol 69:201-20.

Banci L, Bertini I, Calderone V, Cefaro C, Ciofi-Baffoni S, Gallo A, Kallergi E, Lionaki E, Pozidis C, Tokatlidis K (2011) Molecular recognition and substrate mimicry drive the electron-transfer process between MIA40 and ALR. Proc Natl Acad Sci U S A 108(12):4811-6.

Baradaran R, Berrisford JM, Minhas GS, Sazanov LA (2013) Crystal structure of the entire respiratory complex I. Nature 494(7438):443-8.

Basel-Vanagaite L, Straussberg R, Friez MJ, Inbar D, Korenreich L, Shohat M, Schwartz CE (2006) Expanding the phenotypic spectrum of L1CAM-associated disease. Clin Genet 69(5):14-419.

Beal MF (2007) Mitochondria and neurodegeneration. Novartis Found Symp 287:183-92.

Bean LA, Ianov L, Foster TC (2014) Estrogen receptors, the hippocampus, and memory. Neuroscientist 20(5):534-45.

Becker T, Wenz LS, Krüger V, Lehmann W, Müller JM, Goroncy L, Zufall N, Lithgow T, Guiard B, Chacinska A, Wagner R, Meisinger C, Pfanner N (2011) The mitochondrial import protein Mim1 promotes biogenesis of multispanning outer membrane proteins. J Cell Biol 194(3):387-95.

Becker T, Böttinger L, Pfanner N (2012) Mitochondrial protein import: from transport pathways to an integrated network. Trends Biochem Sci 37(3):85-91.

Berg JS, Powell BC, Cheney RE (2001) A millennial myosin census. Mol Biol Cell 12(4):780-94.

Bihlmaier K, Mesecke N, Terziyska N, Bien M, Hell K, Herrmann JM (2007) The disulfide relay system of mitochondria is connected to the respiratory chain. J Cell Biol 179(3):389-95.

Bischofberger J, Engel D, Frotscher M, Jonas P (2006) Timing and efficacy of transmitter release at mossy fiber synapses in the hippocampal network. Pflugers Arch 453(3):361-72.

Blaabjerg M, Zimmer J (2007) The dentate mossy fibers: structural organization, development and plasticity. Prog Brain Res 163:85-107.

Bodo C, Rissman EF (2006) New roles for estrogen receptor beta in behavior and neuroendocrinology. Front Neuroendocrinol 27:217-232.

Bolte S, Cordelieres FP (2006) A guided tour into subcellular colocalization analysis in light microscopy. J Microsc 224(Pt 3):213-32.

Brandt U (2006) Energy converting NADH:quinone oxidoreductase (complex I). Annu Rev Biochem 75:69-92.

Bridgman PC (2004) Myosin-dependent transport in neurons. J Neurobiol 58(2):164-74.

Bulynko YA, O'Malley BW (2011) Nuclear receptor coactivators: structural and functional biochemistry. Biochemistry 50(3):313-28.

Burris TP (2016) Nuclear receptors: PPARα ligands make memories. Nat Chem Biol 12(12):993-994.

Burté F, Carelli V, Chinnery PF, Yu-Wai-Man P (2015) Disturbed mitochondrial dynamics and neurodegenerative disorders. Nat Rev Neurol 11(1):11-24.

Cai Q, Gerwin C, Sheng ZH (2005) Syntabulin-mediated anterograde transport of mitochondria along neuronal processes. J Cell Biol 170(6):959-69.

Cai Q, Sheng ZH (2009) Moving or Stopping Mitochondria: Miro as a Traffic Cop by Sensing Calcium. Neuron 61(4):493-6.

Cai Q, Tammineni P (2016) Alterations in mitochondrial quality control in Alzheimer's disease. Front Cell Neurosci 9;10:24.

Cerminara NL, Lang EJ, Sillitoe RV, Apps R (2015) Redefining the cerebellar cortex as an assembly of non-uniform Purkinje cell microcircuits. Nat Rev Neurosci 16(2):79-93.

Chaban Y, Boekema EJ, Dudkina NV (2014) Biochim Biophys Acta 1837(4):418-26.

Chacinska A, Pfannschmidt S, Wiedemann N, Kozjak V, Sanjuan Szklarz LK, Schulze-Specking A, Truscott KN, Guiard B, Meisinger C, Pfanner N (2004) Essential role of Mia40 in import and assembly of mitochondrial intermembrane space proteins. EMBO J 23(19):3735-46.

Chacinska A, Koehler CM, Milenkovic D, Lithgow T, Pfanner N (2009) Importing Mitochondrial Proteins:Machineries and Mechanisms. Cell 138(4):628-44.

Chada SR, Hollenbeck PJ (2003) Mitochondrial movement and positioning in axons: the role of growth factor signaling. J Exp Biol 206(Pt 12):1985-92.

Chambers WW, Sprague J M (1955) Functional localization in the cerebellum II: somatotopic organization in cortex and nuclei. AMA Arch Neurol Psychiatry 74(6):653-80.

Chan DC (2006) Mitochondria: dynamic organelles in disease, aging, and development. Cell 125(7):1241-52.

Chan NC, Salazar AM, Pham AH, Sweredoski MJ, Kolawa NJ, Graham RL, Hess S, Chan DC (2011) Broad activation of the ubiquitin-proteasome system by Parkin is critical for mitophagy. Hum Mol Genet 20(9):1726-37.

Chang DT, Rintoul GL, Pandipati S, Reynolds IJ (2006) Mutant huntingtin aggregates impair mitochondrial movement and trafficking in cortical neurons. Neurobiol Dis 22(2):388-400.

Chen S, Mantei N, Dong L, Schachner M (1999) Prevention of neuronal cell death by neural adhesion molecules L1 and CHL1. J Neurobiol 38(3):428-39.

Chen H, Chomyn A, Chan DC (2005) Disruption of fusion results in mitochondrial heterogeneity and dysfunction, J Biol Chem 280(28):26185-92.

Chen YC, Wu JS, Tsai HD, Huang CY, Chen JJ, Sun GY, Lin TN (2012) Peroxisome Proliferator-Activated Receptor Gamma (PPAR-γ) and Neurodegenerative Disorders. Mol Neurobiol 46(1):114-24

Chen Y, Sheng ZH (2013) Kinesin-1-syntaphilin coupling mediates activity-dependent regulation of axonal mitochondrial transport. J Cell Biol 202(2):351-64.

Cherrier MM, Asthana S, Plymate S, Baker L, Matsumoto AM, Peskind E (2001) Testosterone supplementation improves spatial and verbal memory in healthy older men. Neurology 57(1):80-8.

Chiang MY, Misner D, Kempermann G, Schikorski T, Giguère V, Sucov HM, Gage FH, Stevens CF, Evans RM (1998) An essential role for retinoid receptors RARbeta and RXRgamma in long-term potentiation and depression. Neuron (6):1353-61.

Cho KI, Cai Y, Yi H, Yeh A, Aslanukov A, Ferreira PA (2007) Association of the kinesin-binding domain of RanBP2 to KIF5B and KIF5C determines mitochondria localization and function. Traffic 8(12):1722-35.

Cipolat S, Martins de Brito O, Dal Zilio B, Scorrano L (2004) OPA1 requires mitofusin 1 to promote mitochondrial fusion. Proc Natl Acad Sci U S A 101(45):15927-32.

Claiborne BJ, Amaral DG, Cowan WM (1986) A light and electron microscopic analysis of the mossy fibers of the rat dentate gyrus. J Comp Neurol 246(4):435-458.

Colombo F, Meldolesi J (2015) L1-CAM and N-CAM: From Adhesion Proteins to Pharmacological Targets. Trends in Pharmacol Sci 36(11):769-81.

Dabir DV, Leverich EP, Kim SK, Tsai FD, Hirasawa M, Knaff DB, Koehler CM (2007) A role for cytochrome c and cytochrome c peroxidase in electron shuttling from Erv1. EMBO J 26(23):4801-11.

Dahme M, Bartsch U, Martini R, Anliker B, Schachner M, Mantei N (1997) Disruption of the mouse L1 gene leads to malformations of the nervous system. Nat Genet 17(3):346-9.

Deas E, Plun-Favreau H, Gandhi S, Desmond H, Kjaer S, Loh SH, Renton AE, Harvey RJ, Whitworth AJ, Martins LM, Abramov AY, Wood NW (2011) PINK1 cleavage at position A103 by the mitochondrial protease PARL. Hum Mol Genet 20(5):867-79.

Deroo BJ, Korach KS (2006) Estrogen receptors and human disease. J Clin Invest 116(3):561-70.

Diab A, Hussain RZ, Lovett-Racke AE, Chavis JA, Drew PD, Racke MK (2004) Ligands for the peroxisome proliferator-activated receptor-gamma and the retinoid X receptor exert additive anti-inflammatory effects on experimental autoimmune encephalomyelitis. J Neuroimmunol 148(1-2):116-26.

Diaz F, Fukui H, Garcia S, Moraes CT (2006) Cytochrome c Oxidase Is Required for the Assembly/Stability of Respiratory Complex I in Mouse Fibroblasts. Mol Cell Biol 26(13):4872-81.

Diekert K, Kispal G, Guiard B, Lill R (1999) An internal targeting signal directing proteins into the mitochondrial intermembrane space. Proc Natl Acad Sci USA 96(21):11752-11757.

Ding WX, Yin XM (2012) Mitophagy: mechanisms, pathophysiological roles, and analysis. Biol Chem 393(7):547-64.

Djogo N, Jakovcevski I, Müller C, Lee HJ, Xu JC, Jakovcevski M, Kügler S, Loers G, Schachner M (2013) Adhesion molecule L1 binds to amyloid beta and reduces Alzheimer's disease pathology in mice. Neurobiol Dis 56:104-15.

Dow R S, Moruzzi G (1958) The Physiology and Pathology of the Cerebellum. Minneapolis: The University of Minnesota Press.

Driscoll I, Resnick SM (2007) Testosterone and cognition in normal aging and Alzheimer’s disease: an update. Curr Alzheimer Res 4(1):33-45.

Dubbink HJ, Hersmus R, Pike AC, Molier M, Brinkmann AO, Jenster G, Trapman J (2006) Androgen receptor ligand-binding domain interaction and nuclear receptor specificity of FXXLF and LXXLL motifs as determined by L/F swapping. Mol Endocrinol 20(8):1742-55.

Dudek J, Peter Rehling P, Van der Laan M (2013) Mitochondrial protein import: Common principles and physiological networks. Biochim Biophys Acta 1833(2):274-85

Eccles J C, Ito M, Szentágothai J (1967) The Cerebellum as a Neuronal Machine. Springer-Verlag, New York.

Efremov RG, Baradaran R, Sazanov LA (2010) The architecture of respiratory complex I. Nature 465(7297):441-5.

Ferramosca A, Zara V (2013) Biogenesis of mitochondrial carrier proteins: Molecular mechanisms of import into mitochondria. Biochim Biophys Acta 1833(3):494-502.

Fields RD, Itoh K (1996) Neural cell adhesion molecules in activity-dependent development and synaptic plasticity. Trends Neurosci 19(11):473-80.

Filichia E, Hoffer B, Qi X, Luo Y (2016) Inhibition of Drp1 mitochondrial translocation provides neural protection in dopaminergic system in a Parkinson’s disease model induced by MPTP. Scientific Reports 6, Article number: 32656.

Fischer G, Kunemund V, Schachner M (1986) Neurite outgrowth patterns in cerebellar microexplant cultures are affected by antibodies to the cell surface glycoprotein L1. J Neurosci 6(2):605-12.

Fourie C, Kiraly M, Madison DV, Montgomery JM (2014) Paired whole cell recordings in organotypic hippocampal slices. J Vis Exp (91):51958.

Fransen E, D'Hooge R, Van Camp G, Verhoye M, Sijbers J, Reyniers E, Soriano P, Kamiguchi H, Willemsen R, Koekkoek SK, De Zeeuw CI, De Deyn PP, Van der Linden A, Lemmon V, Kooy RF, Willems PJ (1998) L1 knockout mice show dilated ventricles, vermis hypoplasia and impaired exploration patterns. Hum Mol Genet 7(6):999-1009.

Fransson A, Ruusala A, Aspenstrom P (2003) Atypical Rho GTPases have roles in mitochondrial homeostasis and apoptosis. J Biol Chem 278(8):6495-502.

Fransson S, Ruusala A, Aspenstrom P (2006) The atypical Rho GTPases Miro-1 and Miro-2 have essential roles in mitochondrial trafficking. Biochem Biophys Res Commun 344(2):500-10.

Friedman JR, Nunnari J (2014) Mitochondrial form and function. Nature 505(7483):335-43.

Friedrich T, Bottcher B (2004) The gross structure of the respiratory complex I: a Lego System. Biochim Biophys Acta 1608(1):1-9.

Frotscher M, Seress L, Schwerdtfeger WK, Buhl E (1991) The mossy cells of the fascia dentata: a comparative study of their fine structure and synaptic connections in rodents and primates. J Comp Neurol 312(1):145-63.

Fugger HN, Foster TC, Gustafsson J, Rissman EF (2000) Novel effects of estradiol and estrogen receptor alpha and beta on cognitive function. Brain Res 883(2):258-264.

Galván EJ, Cosgrove KE, Barrionuevo G (2011) Multiple forms of long-term synaptic plasticity at hippocampal mossy fiber synapses on interneurons. Neuropharmacology 60(5):740-747.

Gegg ME, Cooper JM, Chau KY, Rojo M, Schapira AH, Taanman JW (2010) Mitofusin 1 and mitofusin 2 are ubiquitinated in a PINK1/parkin-dependent manner upon induction of mitophagy. Hum Mol Genet 19(24):4861-70.

Gentle I, Gabriel K, Beech P, Waller R, Lithgow T (2004) The Omp85 family of proteins is essential for outer membrane biogenesis in mitochondria and bacteria. J Cell Biol 164(1):19-24.

Ghezzi D, Zeviani M (2012) Assembly Factors of Human Mitochondrial Respiratory Chain Complexes: Physiology and Pathophysiology. Adv Exp Med Biol 748:65-106.

Giles RE, Blanc H, Cann HM, Wallace DC (1980) Maternal inheritance of human mitochondrial DNA. Proc Natl Acad Sci U S A 77(11):6715-9.

Glauser L, Sonnay S, Stafa K, Moore DJ (2011) Parkin promotes the ubiquitination and degradation of the mitochondrial fusion factor mitofusin 1. J Neurochem 118(4):636-45.

Gornicka A, Bragoszewski P, Chroscicki P, Wenz LS, Schulz C, Rehling P, Chacinska A (2014) A discrete pathway for the transfer of intermembrane space proteins across the outer membrane of mitochondria. Mol Biol Cell 25(25):3999-4009.

Greene AW, Grenier K, Aguileta MA, Muise S, Farazifard R, Haque ME, McBride HM, Park DS, Fon EA (2012) Mitochondrial processing peptidase regulates PINK1 processing, import and Parkin recruitment. EMBO Rep 13(4):378-85.

Gronemeyer H, Gustafsson JA, Laudet V (2004) Principles for modulation of the nuclear receptror superfamily. Nat Rev Drug Discov 3(11):950-64.

Grumbt B, Stroobant V, Terziyska N, Israel L, Hell K (2007) Functional characterization of Mia40p, the central component of the disulfide relay system of the mitochondrial intermembrane space. J Biol Chem 282(52):37461-70.

Guénebaut V, Vincentelli R, Mills D, Weiss H, Leonard KR (1997) Three-dimensional structure of NADH–dehydrogenase from Neurospora crassa by electron microscopy and conical tilt reconstruction. J Mol Biol 265(4):409-18.

Hamson DK, Wainwright SR, Taylor JR, Jones BA, Watson NV, Galea LA (2013) Androgens increase survival of adult-born neurons in the dentate gyrus by an androgen receptor-dependent mechanism in male rats. Endocrinology 154(9):3294-304.

Hasegawa Y, Hojoa Y, Kojimaa H, Ikedaa M, Hottaa K, Satoa R, Ooishia Y, Yoshiyaa M, Chungc BC, Yamazakie T, Kawato S (2015) Estradiol rapidly modulates synaptic plasticity of hippocampal neurons: Involvement of kinase networks. Brain Res 1621:147-61.

Hayashi JI, Yonekawa H, Gotoh O, Watanabe J, Tagashira Y (1978) Strictly maternal inheritance of rat mitochondrial DNA. Biochem Biophys Res Commun 83(3):1032-8.

He B, Kemppainen JA, Wilson EM (2000) FXXLF and WXXLF sequences mediate the NH2-terminal interaction with the ligand binding domain of the androgen receptor. J Biol Chem 275(30):22986-94.

He B, Bowen NT, Minges JT, Wilson EM (2001) Androgen-induced NH2- and COOH-terminal Interaction Inhibits p160 coactivator recruitment by activation function 2. J Biol Chem 276(45):42293-301.

He B, Minges JT, Lee LW, Wilson EM (2002) The FXXLF motif mediates androgen receptor-specific interactions with coregulators. J Biol Chem 277(12):10226-35.

Hedges VL, Ebner TJ, Meisel RL, Mermelstein PG (2012) The cerebellum as a target for estrogen action. Front Neuroendocrinol 33(4):403-11.

Herrick SP, Waters EM, Drake CT, McEwen BS, Milner TA (2006) Extranuclear estrogen receptor beta immunoreactivity is on doublecortin-containing cells in the adult and neonatal rat dentate gyrus. Brain Res 1121:46-58.

Herron LR, Hill M, Davey F, Gunn-Moore FJ (2009) The intracellular interactions of the L1 family of cell adhesion molecules. Biochem J 419(3):519-31.

Hirokawa N, Takemura R (2005) Molecular motors and mechanisms of directional transport in neurons. Nat Rev Neurosci 6(3):201-14.

Hofhaus G, Weiss H, Leonard K (1991) Electron microscopic analysis of the peripheral and membrane parts of mitochondrial NADH dehydrogenase (complex I). J Mol Biol 221(3):1027-43.

Hollenbeck PJ, Saxton WM (2005) The axonal transport of mitochondria. J Cell Sci 118(Pt 23):5411-9.

Hoppins S, Nunnari J (2012) Cell Biology. Mitochondrial dynamics and apoptosis-the ER connection. Science 337(6098):1052-4.

Hortsch M (1996) The L1 Family of Neural Review Cell Adhesion Molecules: Old Proteins Performing New Tricks. Neuron 17(4):587-93.

Hüttemann M, Lee I, Samavati L, Yu H, Doan JW (2007) Regulation of mitochondrial oxidative phosphorylation through cell signaling. Biochim Biophys Acta 1773(12):1701-20.

Hutchison CA, Newbold JE, Potter SS, Edgell MH (1974) Maternal inheritance of mammalian mitochondrial DNA. Nature 251(5475):536-8.

Hwang S, Disatnik MH, Mochly-Rosen D (2015) Impaired GAPDH-induced mitophagy contributes to the pathology of Huntington's disease. EMBO Mol Med 7(10):1307-26.

Ingerman E, Perkins EM, Marino M, Mears JA, McCaffery JM, Hinshaw JE, Nunnari J. (2005) Dnm1 forms spirals that are structurally tailored to fit mitochondria. J Cell Biol 170(7):1021-7.

Isgor C, Cecchi M, Kabbaj M, Akil H, Watson SJ (2003) Estrogen receptor beta in the paraventricular nucleus of hypothalamus regulates the neuroendocrine response to stress and is regulated by corticosterone. Neuroscience 121(4):837-845.

Ishihara N, Eura Y, Mihara K (2004) Mitofusin 1 and 2 play distinct roles in mitochondrial fusion reactions via GTPase activity. J Cell Sci 117(Pt 26):6535-46.

Ishihara N, Otera H, Oka T, Mihara K (2013) Regulation and physiologic functions of GTPases in mitochondrial fusion and fission in mammals. Antioxid Redox Signal 19(4):389-99.

Ito M (2000) Mechanisms of motor learning in the cerebellum. Brain Research 886:237-245.

Itoh K, Nakamura K, Iijima M, Sesaki H (2013) Mitochondrial dynamics in neurodegeneration. Trends Cell Biol 23(2):64-71.

Janowsky JS (2006) The role of androgens in cognition and brain aging in men. Neuroscience 138(3):1015-20.

Jiang YH, Armstrong D, Albrecht U, Atkins CM, Noebels JL, Eichele G, Sweatt JD, Beaudet AL, Davidson LA, Aymond CM, Turner ND, Lupton JR, Chapkin RS (1998) Mutation of the Angelman ubiquitin ligase in mice causes increased cytoplasmic p53 and deficits of contextual learning and long-term potentiation. Neuron 21(4):799-811.

Jiang Q, Heneka M, Landreth GE (2008) The role of peroxisome proliferator-activated receptor-gamma (PPARgamma) in Alzheimer's disease: therapeutic implications. CNS Drugs 22(1):1-14.

Johri A, Beal MF (2012) Mitochondrial dysfunction in neurodegenerative diseases. J Pharmacol Exp Ther 342(3):619-30.

Jokic N, Ling YY, Ward RE, Michael-Titus AT, Priestley JV, Malaspina A (2007) Retinoid receptors in chronic degeneration of the spinal cord: observations in a rat model of amyotrophic lateral sclerosis. J Neurochem 103(5):1821-33.

Kadenbach B (2012) Introduction to mitochondrial oxidative phosphorylation. Adv Exp Med Biol 748:1-11.

Kalus I, Schnegelsberg B, Seidah NG, Kleene R, Schachner M (2003) The proprotein convertase PC5A and a metalloprotease are involved in the proteolytic processing of the neural adhesion molecule L1. J Biol Chem 278(12):10381-8.

Kamiguchi H, Lemmon V (1998) A neuronal form of the cell adhesion molecule L1 contains a tyrosine-based signal required for sorting to the axonal growth cone. J Neurosci 18(17):3749-3756.

Kang JS, Tian JH, Pan PY, Zald P, Li C, Deng C, Sheng ZH (2008) Docking of axonal mitochondria by syntaphilin controls their mobility and affects short-term facilitation. Cell (1):137-48.

Kato H, Lu Q, Rapaport D, Kozjak-Pavlovic V (2013) Tom70 is essential for PINK1 import into mitochondria. PLoS One 8(3):e58435.

Kenwrick S, Watkins A, De Angelis E (2000) Neural cell recognition molecule L1: relating biological complexity to human disease mutations. Hum Mol Genet 9(6):879-86.

Kitazawa S, Wolpert DM (2005) Rhythmicity, randomness and synchrony in climbing fiber signals. Trends Neurosci 28(11):611-9.

Knott AB, Perkins G, Schwarzenbacher R, Bossy-Wetzel E (2008) Mitochondrial fragmentation in neurodegeneration. Nat Rev Neurosci 9(7):505-18.

Kowitz A, Kadmon G, Eckert M, Schirrmacher V, Schachner M, Altevogt P (1992) Expression and function of the neural cell adhesion molecule L1 in mouse leukocytes. Eur J Immunol 22(5):1199-205.

Kroon AM, Vos WM, Bakker H (1978) The heterogeneity of rat-liver mitochondrial DNA. Biochim Biophys Acta 519(1):269-73.

Kruse J, Mailhammer R, Wernecke H, Faissner A, Sommer I, Goridis C, Schachner M (1984) Neural cell adhesion molecules and myelin-associated glycoprotein share a common carbohydrate moiety recognized by monoclonal antibodies L2 and HNK-1. Nature 311(5982):153-5.

Kucharczyk R, Zick M, Bietenhader M, Rak M, Couplan E, Blondel M, Caubet SD, di Rago JP (2009) Biochim Biophys Acta 1793(1):186-99.

Kujat R, Miragall F, Krause D, Dermietzel R, Wrobel KH (1995) Immunolocalization of the neural cell adhesion molecule L1 in non-proliferating epithelial cells of the male urogenital tract. Histochem Cell Biol 103(4):311-21.

Kurumaji A, Nomoto H, Okano T, Toru M (2001) An association study between polymorphism of L1CAM gene and schizophrenia in a Japanese sample. Am J Med Genet 105(1):99-104.

Kutik S, Stojanovski D, Becker L, Becker T, Meinecke M, Krüger V, Prinz C, Meisinger C, Guiard B, Wagner R, Pfanner N, Wiedemann N (2008) Dissecting membrane insertion of mitochondrial β-barrel proteins. Cell 132(6):1011-24.

Lazarou M, Jin SM, Kane LA, Youle RJ (2012) Role of PINK1 binding to the TOM complex and alternate intracellular membranes in recruitment and activation of the E3 ligase Parkin. Dev Cell 22(2):320-33.

Lee YJ, Jeong SY, Karbowski M, Smith CL, Youle RJ (2004) Roles of the mammalian mitochondrial fission and fusion mediators Fis1, Drp1, and Opa1 in apoptosis. Mol Biol Cell 15(11):5001-11.

Levy M, Faas GC, Saggau P, Craigen WJ, Sweatt JD (2003) Mitochondrial regulation of synaptic plasticity in the hippocampus. J Biol Chem 278(20):17727-34.

Li Y, D'Aurelio M, Deng JH, Park JS, Manfredi G, Hu P, Lu J, Bai Y (2007) An assembled complex IV maintains the stability and activity of complex I in mammalian mitochondria. J Biol Chem 282(24):17557-62.

Liesa M, Palacín M, Zorzano A (2009) Mitochondrial dynamics in mammalian health and disease. Physiol Rev 89(3):799-845.

Ligon LA, Steward O (2000) Movement of mitochondria in the axons and dendrites of cultured hippocampal neurons. J Comp Neurol 427(3):340-50.

Lin MY, Sheng ZH (2005) Regulation of mitochondrial transport in neurons. Exp Cell Res 334(1):35-44.

Lindner J, Rathjen FG, Schachner M (1983) L1 mono- and polyclonal antibodies modify cell migration in early postnatal mouse cerebellum. Nature 305:427-430.

Lisman JE (1999) Relating hippocampal circuitry to function: recall of memory sequences by reciprocal dentate-CA3 interactions. Neuron 22(2):233-42.

Loers G, Makhina T, Bork U, Dörner A, Schachner M, Kleene R (2012) The interaction between cell adhesion molecule L1, matrix metalloproteinase 14, and adenine nucleotide translocator at the plasma membrane regulates L1-mediated neurite outgrowth of murine cerebellar neurons. The Journal of Neuroscience 32(11):3917-3930.

Lonard DM, O'Malley BW (2012) Nuclear receptor coregulators: modulators of pathology and therapeutic targets. Nat Rev Endocrinol 8(10):598-604.

Lüthl A, Laurent JP, Figurov A, Muller D, Schachner M (1994) Hippocampal long-term potentiation and neural cell adhesion molecules L1 and NCAM. Nature 372(6508):777-9.

Lutz D, Wolters-Eisfeld G, Joshi G, Djogo N, Jakovcevski I, Schachner M, Kleene R (2012) Generation and nuclear translocation of sumoylated transmembrane fragment of cell adhesion molecule L1. J Biol Chem 287(21):17161-75.

Lutz D, Loers G, Kleene R, Oezen I, Kataria H, Katagihallimath N, Braren I, Harauz G, Schachner M (2014a) Myelin basic protein cleaves cell adhesion molecule L1 and promotes neuritogenesis and cell survival. J Biol Chem 289(19):13503-18.

Lutz D, Wolters-Eisfeld G, Schachner M , Kleene R (2014b) Cathepsin E generates a sumoylated intracellular fragment of the cell adhesion molecule L1 to promote neuronal and Schwann cell migration as well as myelination. J Neurochem 128(5):713-24.

MacAskill AF, Rinholm JE, Twelvetrees AE, Arancibia-Carcamo IL, Muir J, Fransson A, Aspenstrom P, Attwell D, Kittler JT (2009) Miro1 Is a calcium sensor for glutamate receptor-dependent localization of mitochondria at synapses. Neuron 61(4):541-555.

MacAskill AF, Kittler JT (2010) Control of mitochondrial transport and localization in neurons. Trends Cell Biol 20(2):102-12.

Makhina M, Loers G, Schulze C, Ueberle B, Schachner M, Kleene R (2009) Extracellular GAPDH binds to L1 and enhances neurite outgrowth. Mol Cell Neurosci 41(2):206-18.

Maness PF, Schachner M (2007) Neural recognition molecules of the immunoglobulin superfamily: signaling transducers of axon guidance and neuronal migration. Nat Neurosci 10(1):19-26.

Mangelsdorf DJ, Thummel C, Beato M, Herrlich P, Schütz G, Umesono K, Blumberg B, Kastner P, Mark M, Chambon P, Evans RM (1995) The nuclear receptor superfamily: the second decade. Cell 83(6):835-9.

Maretzky T, Schulte M, Ludwig A, Rose-John S, Blobel C, Hartmann D, Altevogt P, Saftig P, Reiss K (2005) L1 is sequentially processed by two differently activated

metalloproteases and presenilin/gamma-secretase and regulates neural cell adhesion, cell migration, and neurite outgrowth. Mol Cell Biol 25(20):9040-53.

Marra MH, Tobias ZJ, Cohen HR, Glover G, Weissman TA (2015) *In Vivo* Time-Lapse Imaging in the Zebrafish Lateral Line: A Flexible, Open-Ended Research Project for an Undergraduate Neurobiology Laboratory Course. J Undergrad Neurosci Educ 13(3):A215-A224.

Martini R, Schachner M (1986) Immunoelectron microscopic localization of neural cell adhesion molecules (L1, N-CAM, and MAG) and their shared carbohydrate epitope and myelin basic protein in developing sciatic nerve. J Cell Biol 103(6 Pt 1):2439-48.

Mathiesen C, Hägerhäll C (2002) Transmembrane topology of the NuoL, Mand N subunits of NADH:quinone oxidoreductase and their homologues among membrane-bound hydrogenases and bona fide antiporters. Biochim Biophys Acta 1556(2-3):121-32.

Matsumoto-Miyai K, Ninomiya A, Yamasaki H, Tamura H, Nakamura Y, Shiosaka S (2003) NMDA-dependent proteolysis of presynaptic adhesion molecule L1 in the hippocampus by neuropsin. J Neurosci 23(21):7727-36.

McCloy RA, Rogers S, Caldon CE, Lorca T, Castro A, Burgess A (2014) Partial inhibition of Cdk1 in G 2 phase overrides the SAC and decouples mitotic events. Cell Cycle 13(9):1400-12.

McEwen BS, Milner TA (2007) Hippocampal formation: shedding light on the influence of sex and stress on the brain. Brain Res Rev 55:343-355.

Mechtersheimer S, Gutwein P, Agmon-Levin N, Stoeck A, Oleszewski M, Riedle S, Postina R, Fahrenholz F, Fogel M, Lemmon V, Altevogt P (2001) Ectodomain shedding of L1 adhesion molecule promotes cell migration by autocrine binding to integrins. J Cell Biol 155(4):661-73.

Meissner C, Lorenz H, Weihofen A, Selkoe DJ, Lemberg MK (2011) The mitochondrial intramembrane protease PARL cleaves human Pink1 to regulate Pink1 trafficking. J Neurochem 117(5):856-67.

Mesecke N, Terziyska N, Kozany C, Baumann F, Neupert W, Hel K, Herrmann JM (2005) A disulfide relay system in the intermembrane space of mitochondria that mediates protein import. J Cell Biol 176(5):559-63.

Mikoshiba K, Takamatsu K, Tsukada Y (1983) Peripheral nervous system of shiverer mutant mice: developmental change of myelin components and immunohistochemical demonstration of the absence of MBP and presence of P2 protein. Brain Res 283:71-79.

Milenkovic D, Gabriel K, Guiard B, Schulze-Specking A, Pfanner N, Chacinska A (2007) Biogenesis of the essential Tim9–Tim10 chaperone complex of mitochondria: site-specific recognition of cysteine residues by the intermembrane space receptor Mia40. J Biol Chem 282(31):22472-80.

Milone M, Benarroch EE (2012) Mitochondrial dynamics: general concepts and clinical implications. Neurology 78(20):1612-9.

Misgeld T, Kerschensteiner M, Bareyre FM, Burgess RW, Lichtman JW (2007) Imaging axonal transport of mitochondria in vivo. Nat Methods 4(7):559-61.

Moos M, Tacke R, Scherer H, Teplow D, Früh K, Schachner M (1988) Neural adhesion molecule L1 as a member of the immunoglobulin superfamily with binding domains similar to fibronectin. Nature 334(6184):701-3.

Moreira PI, Carvalho C, Zhu X, Smith MA, Perry G (2010) Mitochondrial dysfunction is a trigger of Alzheimer's disease pathophysiology. Biochim Biophys Acta 1802(1):2-10.

Morris RL, Hollenbeck PJ (1993) The regulation of bidirectional mitochondrial transport is coordinated with axonal outgrowth. J Cell Sci 104(Pt 3):917-27.

Morris RL, Hollenbeck PJ (1995) Axonal transport of mitochondria along microtubules and F-actin in living vertebrate neurons. J Cell Biol 131(5):1315-26.

Muñoz A, Cabrera-López JC, Santana-Rodríguez A, Toledo-Bravo de Laguna L, Santana-Artiles A, Sebastián-García I (2016) X-linked hereditary spastic paraplegia due to mutation in the L1CAM gene: three cases reports of CRASH syndrome. Rev Neurol 62(5):218-22.

Müller JM, Milenkovic D, Guiard B, Pfanner N, Chacinska A (2008) Precursor oxidation by Mia40 and Erv1 promotes vectorial transport of proteins into the mitochondrial intermembrane space. Mol Biol Cell 19(1):226-36.

Nakajima H, Itakura M, Kubo T, Kaneshige A, Harada N, Izawa T, Azuma YT, Kuwamura M, Yamaji R, Takeuchi T (2017) Glyceraldehyde-3-phosphate Dehydrogenase (GAPDH) Aggregation Causes Mitochondrial Dysfunction during Oxidative Stress-induced Cell Death. J Biol Chem 292(11):4727-4742.

Narendra DP, Jin SM, Tanaka A, Suen DF, Gautier CA, Shen J, Cookson MR, Youle RJ (2010a) PINK1 is selectively stabilized on impaired mitochondria to activate Parkin. PLoS Biol 8(1):e1000298.

Narendra DP, Kane LA, Hauser DN, Fearnley IM, Youle RJ (2010b) p62/SQSTM1 is required for Parkin-induced mitochondrial clustering but not mitophagy; VDAC1 is dispensable for both. Autophagy 6(8):1090-106.

Nawaz Z, Lonard DM, Smith CL, Lev-Lehman E, Tsai SY, Tsai MJ, O'Malley BW (1999) The Angelman syndrome-associated protein, E6-AP, is a coactivator for the nuclear hormone receptor superfamily. Mol Cell Biol 19(2):1182-9.

Nayeem N, Silletti S, Yang X, Lemmon VP, Reisfeld RA, Stallcup WB, Montgomery AM (1999) A potential role for the plasmin(ogen) system in the posttranslational cleavage of the neural cell adhesion molecule L1. J Cell Sci 112 (Pt 24):4739-49.

Neves G, Cooke SF, Bliss TVP (2008) Synaptic plasticity, memory and the hippocampus: a neural network approach to causality. Nat Rev Neurosci 9(1):65-75.

Nguyen-Vu TD, Kimpo RR, Rinaldi JM, Kohli A, Zeng H, Deisseroth K, Raymond JL (2013) Cerebellar Purkinje cell activity drives motor learning. Nat Neurosci 16(12):1734-6.

Nicoll RA, Schmitz D (2005) Synaptic plasticity at hippocampal mossy fibre synapses. Nat Rev Neurosci 6(11):863-76.

Niescier RF, Kwak SK, Joo SH, Chang KT, Min KT (2016) Dynamics of Mitochondrial Transport in Axons. Front Cell Neurosci 10:123.

Nishihara E, Yoshida-Komiya H, Chan CS, Liao L, Davis RL, O'Malley BW, Xu J (2003) SRC-1 null mice exhibit moderate motor dysfunction and delayed development of cerebellar Purkinje cells. J Neurosci 23(1):213-22.

Nishihara E (2008) An overview of nuclear receptor coregulators involved in cerebellar development. The Cerebellum 7(1):48-59.

Nunomura A, Perry G, Aliev G, Hirai K, Takeda A, Balraj EK, Jones PK, Ghanbari H, Wataya T, Shimohama S, Chiba S, Atwood CS, Petersen RB, Smith MA (2001) Oxidative damage is the earliest event in Alzheimer disease. J Neuropathol Exp Neurol 60(8):759-67.

Oettinghaus B, Licci M, Scorrano L, Frank S (2012) Less than perfect divorces: dysregulated mitochondrial fission and neurodegeneration. Acta Neuropathol 123(2):189-203.

Orr AL, Li S, Wang CE, Li H, Wang J, Rong J, Xu X, Mastroberardino PG, Greenamyre JT, Li XJ (2008) N-terminal mutant huntingtin associates with mitochondria and impairs mitochondrial trafficking. J Neurosci (11):2783-92.

Otera H, Taira Y, Horie C, Suzuki Y, Suzuki H, Suzuki H, Setoguchi K, Kato H, Oka T, Mihara K (2007) A novel insertion pathway of mitochondrial outer membrane proteins with multiple transmembrane segments. J Cell Biol 179(7):1355-1363.

Otera H, Wang C, Cleland MM, Setoguchi K, Yokota S, Youle RJ, Mihara K (2010) Mff is an essential factor for mitochondrial recruitment of Drp1 during mitochondrial fission in mammalian cells. J Cell Biol 191(6):1141-58.

Papic D, Krumpe K, Dukanovic J, Dimmer KS, Rapaport D (2011) Multispan mitochondrial outer membrane protein Ugo1 follows a unique Mim1-dependent import pathway. J Cell Biol 194(3):397-405.

Paschen SA, Waizenegger T, Stan T, Preuss M, Cyrklaff M, Hell K, Rapaport D, Neupert W (2003) Evolutionary conservation of biogenesis of β-barrel membrane proteins: Nature 426(6968):862-6.

Perissi V, Rosenfeld MG (2005) Controlling nuclear receptors: the circular logic of cofactor cycles. Nat Rev Mol Cell Biol 6(7):542-54.

Petrasch-Parwez E, Nguyen HP, Löbbecke-Schumacher M, Habbes HW, Wieczorek S, Riess O, Andres KH, Dermietzel R, Von Hörsten S (2007) Cellular and subcellular localization of Huntingtin [corrected] aggregates in the brain of a rat transgenic for Huntington disease. J Comp Neurol 501(5):716-30.

Poole AC, Thomas RE, Yu S, Vincow ES, Pallanck L (2010) The mitochondrial fusion-promoting factor mitofusin is a substrate of the PINK1/parkin pathway. PLoS One 5(4):e10054.

Popko B (1999) Mouse Models in the Study of Genetic Neurological Disorders. New York: Advances in Neurochemistry, Springer.

Pravdic D, Hirata N, Barber L, Sedlic F, Bosnjak ZJ, Bienengraeber M (2012) Complex I and ATP synthase mediate membrane depolarization and matrix acidification by isoflurane in mitochondria. Eur J Pharmacol 690(1-3):149-57.

Probstmeier R, Martini R, Tacke R, Schachner M (1990) Expression of the adhesion molecules L1, N-CAM and J1/ tenascin during development of the murine small intestine. Differentiation 44:42-55.

Purves D, Augustine GJ, Fitzpatrick D, et al., editors (2001) Circuits within the Cerebellum. Sunderland (MA): Sinauer Associates.

Qi X, Qvit N, Su YC, Mochly-Rosen D (2013) A novel Drp1 inhibitor diminishes aberrant mitochondrial fission and neurotoxicity. J Cell Sci 126(Pt 3):789-802.

Rambold AS, Lippincott-Schwartz J (2011) Mechanisms of mitochondria and autophagy crosstalk. Cell Cycle 10(23):4032-8.

Ramnani N (2006) The primate cortico-cerebellar system: anatomy and function. Nature Rev. Nat Rev Neurosci 7(7):511-22.

Ramzan R, Weber P, Linne U, Vogt S (2013) GAPDH: the missing link between glycolysis and mitochondrial oxidative phosphorylation? Biochem Soc Trans41(5):1294-7.

Rapaport D, Neupert W (1999) Biogenesis of Tom40, core component of the TOM complex of mitochondria. J Cell Biol 146(2):321-31.

Raveh S, Gavert N, Ben-Ze'ev A (2009) L1 cell adhesion molecule (L1CAM) in invasive tumors. Cancer Lett 282(2):137-145.

Reis K, Fransson A, Aspenström P (2009) The Miro GTPases: At the heart of the mitochondrial transport machinery. FEBS Lett 583(9):1391-8.

Rich PR, Maréchal A (2010) The mitochondrial respiratory chain. Essays Biochem 47:1-23.

Riedle S, Kiefel H, Gast D, Bondong S, Wolterink S, Gutwein P, Altevogt P (2009) Nuclear translocation and signalling of L1-CAM in human carcinoma cells requires ADAM10 and presenilin/gamma-secretase activity. Biochem J 420(3):391-402.

Rietdorf J, Seitz A (2008) Kymograph analysis handout. (https://www.embl.de/eamnet/html/body_kymograph.html). Heidelberg: Homepage of European Advanced Light Microscopy Network.

Rojo M, Legros F, Chateau D, Lombès A (2002) Membrane topology and mitochondrial targeting of mitofusins, ubiquitous mammalian homologs of the transmembrane GTPase Fzo. J Cell Sci 115(Pt 8):1663-74.

Rusakov DA (2006) Ca^{2+}-dependent mechanisms of presynaptic control at central synapses. Neuroscientist 12(4):317-26.

Russo GJ, Louie K, Wellington A, Macleod GT, Hu F, Panchumarthi S, Zinsmaier KE (2009) Drosophila Miro is required for both anterograde and retrograde axonal mitochondrial transport. J Neurosci 29(17):5443-55.

Sadoul K, Sadoul R, Faissner A, Schachner M (1988) Biochemical characterization of different molecular forms of the neural cell adhesion molecule L1. J Neurochem 50(2):510-21.

Saotome M, Safiulina D, Szabadkai G, Das S, Fransson A, Aspenstrom P, Rizzuto R, Hajnóczky G (2008) Bidirectional Ca^{2+}-dependent control of mitochondrial dynamics by the Miro GTPase. Proc Natl Acad Sci U S A 105(52):20728-33.

Sanes JR, Yamagata M (1999) Formation of lamina-specific synaptic connections. Curr Opin Neurobiol 9(1):79-87.

Savkur RS, Burris TP (2004) The coactivator LXXLL nuclear receptor recognition motif. J Pept Res 63(3):207-12.

Sazanov LA (2015) A giant molecular proton pump: structure and mechanism of respiratory complex I. Nat Rev Mol Cell Biol 16(6):375-88.

Schiavo G, Greensmith L, Hafezparast M, Fisher EM (2013) Cytoplasmic dynein heavy chain: the servant of many masters. Trends Neurosci 36(11):641-51.

Schleiff E, Silvius JR, Shore GC (1999) Direct membrane insertion of voltage-dependent anion-selective channel protein catalyzed by mitochondrial Tom20. J Cell Biol 145(5):973-978.

Schmahmann J D (1997) The Cerebellum and Cognition. Boston: Academic Press.

Schmidt O, Pfanner N, Meisinger C (2010) Mitochondrial protein import: from proteomics to functional mechanisms. Nat Rev Mol Cell Biol. 2010 Sep;11(9):655-67.

Schmidt O, Harbauer AB, Rao S, Eyrich B, Zahedi RP, Stojanovski D, Schönfisch B, Guiard B, Sickmann A, Pfanner N, Meisinger C (2011) Regulation of mitochondrial protein import by cytosolic kinases. Cell 144(2):227-39.

Schwarz TL (2013) Mitochondrial Trafficking in Neurons. Cold Spring Harb Perspect Biol 1;5(6). pii: a011304.

Sheng ZH, Cai Q (2012) Mitochondrial transport in neurons: impact on synaptic homeostasis and neurodegeneration. Nat Rev Neurosci 13(2):77-93.

Sherwin BB (2003) Steroid hormones and cognitive functioning in aging men: a mini-review. J Mol Neurosci 20(3):385-93.

Seilheimer B, Persohn E, Schachner M (1989) Neural cell adhesion molecule expression is regulated by Schwann cell-neuron interactions in culture. J Cell Biol 108(5):1909-15.

Sever R, Glass CK (2013) Signaling by Nuclear Receptors. Cold Spring Harb Perspect Biol. 5(3):a016709.

Silletti S, Mei F, Sheppard D, Montgomery AM (2000) Plasmin-sensitive dibasic sequences in the third fibronectin-like domain of L1-cell adhesion molecule (CAM) facilitate homomultimerization and concomitant integrin recruitment. J Cell Biol. 2000 Jun 26;149(7):1485-502.

Smirnova E, Griparic L, Shurland DL, van der Bliek AM (2001) Dynamin-related protein Drp1 is required for mitochondrial division in mammalian cells. Mol Biol Cell 12(8):2245-56.

Smith SS, Waterhouse BD, Woodward DJ (1988) Locally applied estrogens potentiate glutamate-evoked excitation of cerebellar Purkinje cells. Brain Res 475(2):272-82.

Smith SS (1989) Estrogen administration increases neuronal responses to excitatory amino acids as a long-term effect. Brain Res 503(2):354-7.

Song Z, Chen H, Fiket M, Alexander C, Chan DC (2007) OPA1 processing controls mitochondrial fusion and is regulated by mRNA splicing, membrane potential, and Yme1L. J Cell Biol 178(5):749-55.

Song W, Chen J, Petrilli A, Liot G, Klinglmayr E, Zhou Y, Poquiz P, Tjong J, Pouladi MA, Hayden MR, Masliah E, Ellisman M, Rouiller I, Schwarzenbacher R, Bossy B, Perkins G, Bossy-Wetzel E (2011) Mutant huntingtin binds the mitochondrial fission GTPase dynamin-related protein-1 and increases its enzymatic activity. Nat Med 17(3):377-82.

Stojanovski D, Milenkovic D, Müller JM, Gabriel K, Schulze-Specking A, Baker MJ, Ryan MT, Guiard B, Pfanner N, Chacinska A (2008) Mitochondrial protein import: precursor oxidation in a ternary complex with disulfide carrier and sulfhydryl oxidase. J Cell Biol 183(2):195-202.

Strekalova H, Buhmann C, Kleene R, Eggers C, Saffell J, Hemperly J, Weiller C, Müller-Thomsen T, Schachner M (2006) Elevated levels of neural recognition

molecule L1 in the cerebrospinal fluid of patients with Alzheimer disease and other dementia syndromes. Neurobiol Aging 27(1):1-9.

Susalka SJ, Pfister KK (2000) Cytoplasmic dynein subunit heterogeneity: implications for axonal transport. J Neurocytol 29(11-12):819-29.

Swerdlow RH, Burns JM, Khan SM (2010) The Alzheimer's disease mitochondrial cascade hypothesis. J Alzheimers Dis 20 Suppl 2:S265-79.

Taanman JW (1999) The mitochondrial genome: structure, transcription, translation and replication. Biochim Biophys Acta 1410(2):103-23.

Tanaka A, Cleland MM, Xu S, Narendra DP, Suen DF, Karbowski M, Youle RJ (2010) Proteasome and p97 mediate mitophagy and degradation of mitofusins induced by Parkin. J Cell Biol 191(7):1367-80.

Tang Y, Zucker RS (1997) Mitochondrial involvement in post-tetanic potentiation of synaptic transmission. Neuron 18(3):483-91.

Tang BL (2015) MIRO GTPases in Mitochondrial Transport, Homeostasis and Pathology. Cells 5(1).

Tanida I (2011) Autophagy basics. Microbiol Immunol 55(1):1-11.

Tarze A, Deniaud A, Le Bras M, Maillier E, Molle D, Larochette N, Zamzami N, Jan G, Kroemer G, Brenner C (2007) GAPDH, a novel regulator of the pro-apoptotic mitochondrial membrane permeabilization. Oncogene 26(18):2606-20.

Teyler TJ, Vardaris RM, Lewis D, Rawitch AB (1980) Gonadal steroids: effects on excitability of hippocampal pyramidal cells. Science 209(4460):1017-8.

Thach WT (1996) On the specific role of the cerebellum in motor learning and cognition: clues from PET activation and lesion studies in man. Behav Brain Sci 19:411-431.

Togashi H, Sakisaka T, Takai Y (2009) Cell adhesion molecules in the central nervous system. Cell Adh Migr 3(1):29-35.

Tsai MJ, O'Malley BW (1994) Molecular mechanisms of action of steroid/thyroid receptor superfamily members. Annu Rev Biochem 63:451-86.

Twig G, Elorza A, Molina AJ, Mohamed H, Wikstrom JD, Walzer G, Stiles L, Haigh SE, Katz S, Las G, Alroy J, Wu M, Py BF, Yuan J, Deeney JT, Corkey BE, Shirihai OS (2008) Fission and selective fusion govern mitochondrial segregation and elimination by autophagy. EMBO J 27(2):433-46.

Wang X, Schwarz TL (2009) The mechanism of Ca^{2+}-dependent regulation of kinesin-mediated mitochondrial motility. Cell 136(1):163-74.

Wang Y, Loers G, Pan H-C, Gouveia R, Zhao W-J, et al. (2012) Antibody Fragments Directed against Different Portions of the Human Neural Cell Adhesion Molecule L1 Act as Inhibitors or Activators of L1 Function. PLoS One 7(12):e52404.

Washbourne P, Dityatev A, Scheiffele P, Biederer T, Weiner JA, Christopherson KS, El-Husseini A (2004) Cell adhesion molecules in synapse formation. J Neurosci 24(42):9244-9.

Wasiak S, Zunino R, McBride HM (2007) Bax/Bak promote sumoylation of DRP1 and its stable association with mitochondria during apoptotic cell death. J Cell Biol 177(3):439-50.

Wei CH, Ryu SE (2012) Homophilic interaction of the L1 family of cell adhesion molecules. Exp Mol Med 44(7):413-23.

Weiland NG, Orikasa C, Hayashi S, McEwen BS (1997) Distribution and hormone regulation of estrogen receptor immunoreactive cells in the hippocampus of male and female rats. J Comp Neurol 388(4):603-12.

Wessel D, Flügge UI (1984) A method for the quantitative recovery of protein in dilute solution in the presence of detergents and lipids. Anal Biochem 138(1):141-3.

Westrate LM, Drocco JA, Martin KR, Hlavacek WS, MacKeigan JP (2014) Mitochondrial morphological features are associated with fission and fusion events. PLoS One 9(4):e95265.

Wiedemann N, Kozjak V, Chacinska A, Schönfisch B, Rospert S, M.T. Ryan MT, Pfanner N, Meisinger C (2003) Machinery for protein sorting and assembly in the mitochondrial outer membrane. Nature 424(6948):565-71.

Wood PM, Schachner M, Bunge RP (1990) Inhibition of Schwann cell myelination in vitro by antibody to the L1 adhesion molecule. J Neurosci 10(11):3635-45.

Xu J, O'Malley BW (2002) Molecular mechanisms and cellular biology of the steroid receptor coactivator (SRC) family in steroid receptor function. Rev Endocr Metab Disord 3(3):185-92.

Yamagata M, Sanes JR, Weiner JA (2003) Synaptic adhesion molecules. Curr Opin Cell Biol 15(5):621-32.

Youle RJ, Narendra DP (2011) Mechanisms of mitophagy. Nat Rev Mol Cell Biol (1):9-14.

Youle RJ, van der Bliek AM (2012) Mitochondrial fission, fusion, and stress. Science 337(6098):1062-5.

Yousefi B, Jingu H, Ohta M, Umezu M, Koibuchi N (2005) Postnatal changes of steroid receptor coactivator-1 immunoreactivity in rat cerebellar cortex. Thyroid 15(4):314-9.

Yu L, Iwasaki T, Xu M, Lesmana R, Xiong Y, Shimokawa N, Chin WW, Koibuchi N (2015) Aberrant cerebellar development of transgenic mice expressing dominant-

negative thyroid hormone receptor in cerebellar Purkinje cells. Endocrinology 156(4):1565-76

Ziviani E, Tao RN, Whitworth AJ (2010) Drosophila Parkin requires PINK1 for mitochondrial translocation and ubiquitinates Mitofusin. Proc Natl Acad Sci U S A 107(11):5018-23.

Zhan M, Brooks C, Liu F, Sun L, Dong Z (2013) Mitochondrial dynamics: regulatory mechanisms and emerging role in renal pathophysiology. Kidney Int (4):568-81.

Zhao J, Liu T, Jin S, Wang X, Qu M, Uhlén P, Tomilin N, Shupliakov O, Lendahl U, Nistér M (2011) Human MIEF1 recruits Drp1 to mitochondrial outer membranes and promotes mitochondrial fusion rather than fission. EMBO J 30(14):2762-78.

Zhu PP, Patterson A, Stadler J, Seeburg DP, Sheng M, Blackstone C (2004) Intra- and intermolecular domain interactions of the C-terminal GTPase effector domain of the multimeric dynamin-like GTPase Drp1. J Biol Chem 279(34):35967-74.

Zorzano A, Liesa M, Sebastián D, Segalés J, Palacín M (2010) Mitochondrial fusion proteins: dual regulators of morphology and metabolism. Semin Cell Dev Biol 21(6):566-74.

Züchner S, Mersiyanova IV, Muglia M, Bissar-Tadmouri N, Rochelle J, Dadali EL, Zappia M, Nelis E, Patitucci A, Senderek J, Parman Y, Evgrafov O, Jonghe PD, Takahashi Y, Tsuji S, Pericak-Vance MA, Quattrone A, Battaloglu E, Polyakov AV, Timmerman V, Schröder JM, Vance JM (2004) Mutations in the mitochondrial GTPase mitofusin 2 cause Charcot-Marie-Tooth neuropathy type 2A. Nat Genet 36(5):449-51.

9 SUMMARY

In the present study I show that the MBP-generated L1 fragment L1-70 is present in mitochondria from murine brain and is imported from L1-70-containing cytoplasm into L1-lacking mitochondria. The import depends on TOM70 which recognizes proteins with an internal mitochondrial targeting signal. In mitochondria, L1-70 influences complex I activity: mitochondria from brains of L1-deficient mice show a reduced complex I activity compared to mitochondria from brains of wild-type mice. Complex I activity is enhanced after *in vitro* import of L1-70 into isolated L1-lacking mitochondria. The activities of complex II, III, IV and V are not dysregulated in L1-deficient mitochondria. L1-lacking HEK293 cells or HEK293 cells transduced to express mutated L1 which is not cleaved by MBP showed a lower membrane potential compared to HEK293 cells transduced to express wild-type L1. Also, in mitochondria of cerebellar neurons from L1-deficient mice, the mitochondrial membrane potential is lower than that of wild-type neurons. By ELISA, I could show that the intracellular domain of L1 binds to NDUFV2, a subunit of complex I. Co-immunoprecipitation showed that L1-70 binds to the mitochondrial proteins GAPDH, Drp1 and Miro1. Furthermore, absence of L1 or L1-70 enhances the co-localization of labeled mitochondria with the specific mitophagy marker LC3, whereas the co-localization of mitochondria with the specific mitophagy marker LC3 is reduced in HEK293 cells transduced to express wild-type L1. Moreover, absence of L1 or L1-70 in HEK293 cells reduces the fusion rate of mitochondria and these cells exhibit more fragmented mitochondria relative to HEK293 cells transduced to express wild-type L1. In addition, absence of L1 or L1-70 leads to a decreased motility of mitochondria and enhanced retrograde trafficking of mitochondria in neurons of L1-deficient mice. In contrast, the presence of L1 or L1-70 and stimulation of L1 enhances the mitochondrial motility and leads to a balanced bidirectional mitochondrial transport. Thus, the mitochondrial motility, but not the mitochondrial mobility, is influenced by L1-70.

Since L1-70 is also present in the nucleus and carries LXXLL and FXXLF motifs which mediate the binding of coactivators with nuclear receptors, I examined if L1-70 interacts with distinct nuclear receptors. I could show that L1 interacts with the nuclear receptors PPARγ, RXRβ and ERα/β, but not with AR, VDR and LXRβ. The

interaction of L1 with nuclear receptors is mediated by the LXXLL and FXXLF motifs that are present in the transmembrane and the fifth fibronectin type III domain of L1. Disruption of the interaction of L1 with nuclear receptors leads to reduced neurite outgrowth *in vitro*. *In vivo,* mutation of the LXXLL and FXXLF motifs in L1 leads to altered structure of mossy fiber synapses of the dentate gyrus in the hippocampus. In hippocampal sections from brains of L1-deficient mice and mice transduced to express mutated L1, the mossy fiber bouton area, the length of the synaptic cleft and the synaptic type are altered compared to the structural elements of the mossy fiber synapses in hippocampal sections of wild-type mice and mice expressing wild-type L1. In addition, L1-deficient mice and mice expressing L1 mutated in the LXXLL and FXXLF motifs showed disturbed synaptic contacts of GABAergic and glutamatergic terminals with Purkinje cells in the cerebellum compared to wild-type mice. Behavioral studies performed with wild-type mice, L1-deficient mice, mice expressing wild-type L1 and mice expressing L1 mutated in the LXXLL and FXXLF motifs, demonstrated defects in motor coordination and learning in L1-deficient mice and mice expressing mutated L1.

Altogether, the present study reveals novel important aspects about the role of L1-70 in the murine central nervous system. L1-70, which is generated by cleavage of full-length membrane-bound L1 by MBP, influences not only mitochondrial metabolism, but also mitochondrial dynamics. Moreover, it affects the hippocampal structure, the cerebellar circuitry and cerebellar functions such as motor coordination and learning. These findings can be relevant in further understanding of neurodegenerative diseases.

10 ZUSAMMENFASSUNG

Die vorliegende Arbeit zeigt, dass das durch MBP generierte L1-Fragment L1-70 in Mitochondrien lokalisiert ist und aus dem mit L1-70 angereicherten Zytoplasma in L1-defiziente Mitochondrien aus murinem Gehirngewebe importiert wird. Der Import von L1-70 ist dabei abhängig von TOM70, das mit Vorläuferproteinen, die ein internes Signal zur Translokation in die Mitochondrien beinhalten, interagiert. Mitochondriales L1-70 beeinflusst die Aktivität von Komplex I. In L1-defizienten Mitochondrien ist die Komplex I-Aktivität deutlich verringert im Vergleich zur Komplex I-Aktivität in Mitochondrien, die aus Gehirnen von Wildtypmäusen isoliert wurden. Die Komplex I-Aktivität ist nach *in vitro* Import von L1-70 in L1-defiziente Mitochondrien erhöht. Die Aktivität von Komplex II, III, IV und V ist in L1-defizienten Mitochondrien nicht beeinträchtigt. L1-defiziente HEK293 Zellen oder HEK293 Zellen, die transduziert wurden, um mutiertes L1 zu exprimieren, das nicht von MBP proteolysiert wird, zeigen ein geringeres mitochondriales Membranpotential als HEK293 Zellen, die transduziert wurden, um Wildtyp-L1 zu exprimieren. In L1-defizienten Kleinhirnneuronen ist das mitochondriale Membranpotential ebenfalls geringer als in Kleinhirnneuronen isoliert aus Wildtypmäusen. Im ELISA konnte die Bindung der intrazellulären Domäne von L1 an NDUFV2, das eine Untereinheit von Komplex I ist, gezeigt werden. Ko-immunpräzipitationsexperimente zeigten, dass L1-70 an die mitochondrialen Proteine GAPDH, Drp1 and Miro1 bindet. Darüber hinaus ist die Ko-Lokalisation von Mitochondrien mit dem für die Mitophagie spezifischen Marker LC3 in L1- oder L1-70-defizienten HEK293 erhöht. Im Vergleich dazu ist die Ko-Lokalisation von Mitochondrien mit LC3 in HEK293 Zellen, die transduziert wurden, um Wildtyp L1 zu exprimieren, verringert. Weiterhin ist die Fusionsrate in Mitochondrien von L1- oder L1-70-defizienten HEK293 Zellen verringert und die Mitochondrien zeigen überwiegend eine fragmentierte Struktur. Relativ dazu ist die Fusionsrate in L1- oder L1-70-exprimierenden HEK293 Zellen erhöht und weniger fragmentierte und mehr elongierte Mitochondrien liegen vor. Während die mitochondriale Motilität verringert ist, ist der mitochondriale retrograde Transport in L1- oder L1-70-defizienten Kleinhirnneuronen erhöht. Anwesenheit von L1 oder L1-70 und Stimulation von L1 erhöht die mitochondriale Motilität und es liegt ein Gleichgewicht zwischen anterograden und retrograden mitochondrialem Transport in

L1-exprimierenden Kleinhirnneuronen vor. Damit beeinflusst L1-70 lediglich die mitochondriale Motilität, aber nicht die mitochondriale Mobilität.

Zudem ist L1-70 im Zellkern präsent ist und besitzt die LXXLL- und FXXLF-Motive, die die Bindung von Ko-Aktivatoren mit nukleären Rezeptoren vermitteln. Aufgrund dessen untersuchte ich, ob L1-70 im Zellkern an nukleäre Rezeptoren bindet. Mithilfe von Bindungsassays zeigte ich, dass L1 an die nukleären Rezeptoren PPARγ, RXRβ und ERα/β bindet, während keine Interaktion mit AR, VDR und LXRβ gezeigt werden konnte. Die Interaktion von L1 mit PPARγ, RXRβ und ERα/β wird durch die LXXLL- und FXXLF-Motive in der Transmembrandomäne und der fünften Fibronektindomäne vermittelt. Die Aufhebung der Interaktion von L1 mit den nukleären Rezeptoren führt zu einer Verringerung des Neuritenwachstums *in vitro*. *In vivo* führt die Mutation der LXXLL- und FXXLF-Motive in L1 zu Modifikationen der Struktur der *mossy fiber* Synapsen des Gyrus dentatus des Hippocampus. Ultrastrukturelle Analyse zeigte, dass die Fläche der *mossy fiber boutons*, die Länge des synaptischen Spalts und der synaptische Typ im Hippocampus von L1-defizienten Mäusen und Mäusen, die mutiertes L1 exprimieren, im Vergleich zu Wild-typ Mäusen verändert sind. Auch entstehen durch Mutation der LXXLL- und FXXLF-Motive Beeinträchtigungen in der Motorik und dem motorischen Lernen einhergehend mit einer gestörten Konnektivität des Kleinhirns. Ultrastrukturelle Analyse von Kleinhirnschnitten aus Gehirnen von L1-exprimierenden und L1-defizienten Mäusen und Mäusen, die mutiertes L1 exprimieren zeigte Veränderungen in den inhibitorischen und exzitatorischen synaptischen Endigungen mit Purkinje Zellen in Abwesenheit von L1 bzw. bei Vorliegen der Mutation der LXXLL- und FXXLF-Motive.

Zusammenfassend zeigt die hier vorliegende Arbeit neue wichtige Aspekte hinsichtlich der Funktion von L1-70 im murinen zentralen Nervensystem. L1-70, das durch MBP-Spaltung von L1 generiert wird, beeinflusst nicht nur den mitochondialen Metabolismus, sondern auch die mitochondriale Dynamik. Zudem spielt L1-70 eine wichtige Rolle bei der Entwicklung der hippocampalen Struktur und in zerebellären Funktionen wie Motorkoordination und motorischem Lernen im murinen Nervensystem.

11 ACKNOWLEDGEMENTS

This study has been performed in the Institute for Biosynthesis of Neuronal Structures of the Centre for Molecular Neurobiology Hamburg (ZMNH). I would like to thank Prof. Dr. Dr. h. c. Melitta Schachner for providing me with the very interesting research projects and giving me the opportunity to write this thesis in her laboratory. I am grateful for making it possible for me to learn during helpful discussions and support during these years, so I could expand my knowledge in the field of molecular neuroscience and finish my work. Moreover I am grateful to Prof. Dr. Dr. h. c. Melitta Schachner and Prof. Dr. Christian Lohr for the reviewing and co-supervision of my thesis.

I am grateful to Dr. Ralf Kleene and Dr. Gabriele Loers. I thank especially Ralf for his supervision during my entire work, for being supportive and patient. And I would like to thank Ralf for planning the experiments with me, discussing the results and for guidance during the years of my PhD. I thank Gaby who helped me with advices to overcome some experimental problems in the everyday work and for helpful suggestions during the writing of my thesis.

I am grateful to Dr. David Lutz for great support during the years of my PhD and for being creative and competent while helping with my experiments. Dave, many thanks for always believing in me and being a friend. I am also grateful to Dagmar Drexler who showed me useful techniques and helped me with experiments.

I am grateful to my previous and current colleagues. Dear Jelena Katic, Nina Westphal, Agnieszka Kotarska, Gaston Castillo, Maria Girbes-Minguez and Patricia García-Jareño. Thank you for your support and friendship. Especially, I am thankful to Ute Bork for her technical assistance, her support and commitment in the lab.

Finally, I would like to thank my mother for believing in me, for teaching me how to work efficiently and for showing me to never give up. Thanks to my sisters for the huge support and constructive help. My special thanks go to my boyfriend, who was encouraging me and being always on my side during hard and good times.

Zentrum für Molekulare Neurobiologie Hamburg (ZMNH)
Institut für Synaptische Physiologie

Dr. Christine Gee
Institut für Synaptische Physiologie

ZMNH, Falkenried 94
20251 Hamburg

Telefon: +49 (0) 40 7410-57190
Fax: +49 (0) 40 7410-58364
christine.gee@zmnh.uni-hamburg.de

Universitätsklinikum Hamburg-Eppendorf | ZMNH | Institut für Synaptische Physiologie
Falkenried 94 | 20251 Hamburg

English Language Certification – Dissertation Kristina Kraus

Hamburg, 14.08.2017

As a native english speaker, I certify that the english in the thesis, "The functional role of the cell adhesion molecule L1 in mitochondrial metabolism and dynamics and the functional consequences of L1´s interaction with nuclear receptors in the murine central nervous system" by Kristina Kraus, is of a high quality and that the thesis is fully understandable.

Christine Gee HAMBURG, 14.08.2017

Christine Gee

Declaration on oath

I hereby declare, on oath, that I have written the present dissertation by my own and have not used other than the acknowledged resources and aids.

Hamburg, 17. August 2017 _____

signature